2004

Molecular speciation using pulsed glow discharge time -of -flight mass spectrometry

Lei Li
West Virginia University

Recommended Citation

Li, Lei, "Molecular speciation using pulsed glow discharge time -of -flight mass spectrometry" (2004). *Graduate Theses, Dissertations, and Problem Reports*. 2117.
https://researchrepository.wvu.edu/etd/2117

Molecular Speciation Using Pulsed Glow Discharge Time-of-Flight Mass Spectrometry

Lei Li

Dissertation submitted to the Eberly College of Arts and Sciences
at West Virginia University
in partial fulfillment of the requirements
for the degree of

Doctoral of Philosophy
in
Chemistry

Approved by

Fred L. King, Ph. D., Chair
Ronald B. Smart, Ph. D.
Aaron Timperman, Ph. D.
Bjorn Soderberg, Ph. D.
Earl Scime, Ph. D.

C. Eugene Bennett Department of Chemistry

Morgantown, West Virginia
2004

Keywords: Pulsed glow discharge, Mass spectrometry, Optical spectroscopy

ABSTRACT

Molecular Speciation Using Pulsed Glow Discharge Time-of-Flight Mass Spectrometry

Lei Li

Glow discharge mass spectrometry is a well-developed elemental analysis technique for solid samples. Pulsed glow discharges exhibit advantages over continuous power glow discharges. The brief, high-power pulse yields transient but intense analytical signals, increasing analytical sensitivities; meanwhile, the following power-off period allows samples to be sufficiently cooled to avoid plasma instability. In this work, pulsed glow discharge mass spectrometry has been successfully employed to determine bromine concentrations in a series of thermally labile plastic samples.

Of more analytical interest are the temporal variations in plasma chemistry within the pulsed glow discharges. A plasma perturbation method was employed to investigate the plasma processes after the power termination, i.e., the afterpeak regime. The experimental results strongly indicate that, after power termination, discharge gas ions recombine with thermalized electrons; subsequently, a large population of metastable argon atoms is yielded that plays a central role in excitation and ionization during the afterpeak regime.

Because the dominant ionization mechanisms alternate over a pulse cycle, plasma ionization is temporally dependent. The apparent plasma energy of a millisecond pulsed glow discharge was measured using tungsten hexcarbonyl as a "thermometer molecule". The semi-quantitative results reveal the plasma energies undergo significant temporal and spatial variations, thereby effecting both "soft" and "hard" ionization for a given molecular species. As a result, elemental, structural, and molecular information can be obtained with the same plasma ion source. Its analytical utilities were further demonstrated by analysis of a series of organic and organometallic compounds using pulsed glow discharge time-of-flight mass spectrometry.

To understand the fundamental plasma processes involving molecular species, nitrogen was introduced into pulsed argon and helium glow discharge plasmas as a probe molecule; its interactions with various plasma species were monitored using spectroscopic techniques. The study yielded insights into the excitation and ionization of molecular species in a pulsed glow discharge. The adverse effects of the admixed molecules on plasma ionization were also discussed. These data will be useful in future efforts to optimize the analytical performance of the pulsed glow discharge ion source.

To My Parents and Grandma

with Love

ACKNOWLEDGEMENTS

I am indebted to my advisor Dr. Fred L. King. His guidance has not only led me into the fascinating world of science, but also equipped me with the abilities, confidence, and honesty to explore the world as an independent researcher. I would like to take this opportunity to thank my mentor Dr. Douglas C. Duckworth and the staff of the Chemical and Isotope Mass Spectrometry group (CIMS) at Oak Ridge National Laboratory, where I witnessed how research was conceived, proposed, designed, performed, and concluded.

I am grateful to my committee members: Dr. Earl Scime, Dr. Ronald Smart, Dr. Bjorn Soderberg, and Dr. Aaron Timperman. I will always be thankful for their help and knowledge passed on to me over these years. I also wish to express my gratitude to Dr. Chris Barshick at GE Plastics for his collaborative support.

I wish to thank the entire King group at WVU for creating such a friendly and supportive environment. Special thanks to Dr. Cris Lewis. He recruited me into the group and helped me start my research. Thanks also go to his entire family, who have made me feel welcome in America. I am also extremely appreciative of Dr. Glen Jackson who gave me tremendous help while I was interning at ORNL. I wish to express my gratitude to Donald Feathers and Allen Burns for their professional skills and assistance in performing my experiments at WVU.

I wish to acknowledgement funding support from US Department of Energy, through grand DE-FG02-00ER45837, and under contract DE-AC05-00OR22725 with Oak Ridge National Laboratory, managed and operated by UT-Battelle, LLC. The Eberly College of Arts and Sciences at WVU and C. Eugene Bennett Chemistry Department at WVU are also greatly appreciated for their financial support. The support of GE Plastics through the donation of polymer samples and expendable supplies is gratefully acknowledged.

Foremost, I would like to express my appreciation to my parents and my grandma for their encouragement over the years. Without their love I would not be where I am today.

TABLE OF CONTENTS

LIST OF FIGURES

LIST OF TABLES

Chapter 1. Introduction

1.1. Glow Discharge Mass Spectrometry: a Historical Perspective

Mass spectrometry and glow discharge, two seemingly disparate topics in science, are in fact closely related. The close tie can be tracked back to the adolescent period of mass spectrometry about 100 years ago when J. J. Thomson first developed “Mass spectrograph” to study the “positive rays” (positive ion beams) generated in a low-pressure electric discharge.[1] The resultant mass spectra revealed the atomic masses and isotopic compositions of the elements present in the discharge. Thompson was quick to understand the far-reaching implication of his work and presciently pointed out the potential applications of the “mass spectrograph” for analytical science:[1]

> “… I have described at some length the applications of positive rays to chemical analysis; one of the main reasons for writing this book was the hope that it might induce others, and especially chemists, to try this method of analysis. I feel sure that there are many problems in chemistry which could be solved with far great ease by this than any other method. The method is surprisingly sensitive – more so even than that of spectrum analysis, requires an infinitesimal amount of material, and does not require this to be specially purified; the technique is not difficult if appliances for producing high vacua are available…”

Aston, Thomson’s assistant, went on to develop a more sophisticated mass spectrometer system in which a discharge bulb is used as an ion source.[2] With it, Aston established the existence of isotopes of the stable elements and measured their atomic masses. He also showed that molecular species could also be ionized in the discharge bulb. As an experimentalist, he made significant progress in instrument design and vacuum technology. In *Mass Spectra and Isotopes*, he described his personal experience with mass spectrometry from a practical perspective:

> “It behaves at times in the most capricious and unaccountable manner … when by good fortune all is well the arrangement is capable of good performances. Thus, after a favorable setting of the apparatus, six elements were successfully analyzed in as many working days. On the other hand, after dismantling became imperative and it had to be cleaned and rebuilt, exactly as before as one could tell, no results of any value were obtained during weeks of work.”

The remarks, combined with Thomson’s vision, yield a panoramic picture of mass spectrometry that many mass spectrometrists still agree with.

After World War II, mass spectrometry underwent rapid growth and quickly matured as an analytical technique.[3] Meanwhile discharge-type ion sources continued to evolve. The most widely known is the spark source that employs an energetic spark, a type of electric discharge, for the thermal atomization and ionization of sample material. The spark source was the ionization method of choice for direct solid analysis until the advent of glow discharge mass spectrometry (GDMS).

In early 1970's, materials industries started extensively employing glow discharges for thin film deposition, etching, and surface treatment.[4] Motivated by industrial needs, Coburn et al. [5, 6] employed mass spectrometry to study glow discharge plasmas. Meanwhile, they realized the unique ability of glow discharges to sputter atoms off the solid cathode; subsequently, the sputtered atoms could be ionized in the plasma, generating a mass spectrum that reflects the composition of the cathode material.[7, 8] The fundamental atomization, excitation, and ionization processes in glow discharge plasmas and their applications have been described previously.[9]

Shortly after Coburn's studies, Harrison et al. [10] reported glow discharge mass spectrometry (GDMS) as an analytical technique for direct solids analysis. Since then, GDMS has established its role as a leading elemental analysis method for solid samples.[11] GDMS outperforms SSMS in that glow discharge produces more stable and reproducible ion beams with much narrower ion kinetic energy distribution. As compared with the other common solid analysis techniques, such as secondary ion mass spectrometry (SIMS) and thermal ionization mass spectrometry (TIMS), glow discharge is free of excessive matrix effects because of the decoupling of atomization and ionization in glow discharges. Other advantages include depth profiling ability, design simplicity, and ease of use. Several review articles highlight the applications and recently developments in GDMS with different emphases.[11-14]

Like any other analytical technique, GDMS has shortfalls. Glow discharge is characterized by low energy sputtering and “cool” plasma ionization processes: the sputtered atom population accounts for less than 1% of overall species in the plasma [15] and, among them, only about 0.1-1% are ionized.[9] The low efficiencies directly limit the analytical performance of GDMS, particularly, detection limits. In contrast, “hot” plasmas offer much higher ionization efficiency. For example, the inductively coupled plasma (ICP) can readily achieve 90% or higher ionization for most of the elements.[16] Recently, laser-based sampling techniques have been successfully interfaced with ICP-MS, providing an alternative and more sensitive approach for solid sample analysis. These techniques have presented challenges to GDMS as the technique of choice for direct solid analysis.

These challenges, on the other hand, also provided incentives for further developments of GDMS. To compete with the “hot” plasmas, an obvious approach is to improve the atomization and ionization efficiency of glow discharges. This can be readily achieved by increasing discharge power input, which raises both discharge current and voltage. The intense discharge current directly results in a higher flux of incident ions striking the cathode surface;[17] the elevated discharge voltage further increases the average energy of each sputter event. Consequently, sputter yield is dramatically enhanced. Furthermore, the elevated power input also creates an intense plasma with a higher ionization efficiency. As the result, not only are more atoms sputtered, but also higher percentage of them are ionized, thereby yielding more intense ion signals.

The second approach is to realize the advantages of the “cold” glow discharge plasma and expand its analytical application. “Hot” plasmas, such as the ICP, are specifically designed and configured to maximize the production of atomic ions. The molecular analyte would be completely atomized and ionized, which automatically eliminates any possibility to obtain structural and molecular information from the same sample run. Therefore, different methods have to be employed for molecular information, inevitably increasing requirements for analysis duration and costs, operator skills, and sample sizes. In contrast, owing to its “cold” nature, the glow discharge can effect “soft” ionization and generate ions of molecular species. The resultant mass spectra reveal molecular and structural information of the analyte, providing a potential advantage over the “hot” plasma ion source.

Recently, pulsed GDMS has become a research area of great interest because it fully utilizes the advantages of a glow discharge ion source. A brief, high-power pulse can yield transient but intense analytical signals, increasing analytical sensitivities and lowering detection limits.[18, 19] More significantly, pulsed operation creates temporal variations in ionization characteristics; the plasma can be configured for “soft” and “hard” ionization within a transient pulse cycle. Using a time-gated detection method, the type of ionization can be readily selected at the operator’s discretion. Pulsed GDMS has been applied to discriminate against interfering background signals [20] and to achieve selective ionization and fragmentation of molecular species [21, 22].

1.2. Enhancement of Atomization and Ionization in Pulsed GD Plasmas

As explained previously, increasing discharge power greatly enhances atomization and ionization efficiency. However, in continuous power glow discharges, the heat generated by the high power input would accumulate and eventually lead to sample overheating and plasma instability; hence, the maximum power input is limited. Pulsed operation, on the other hand, affords a unique heat ameliorating mechanism: the heat generated during the brief power-on portion can efficiently dissipate during the following, usually much longer, power-off portion. In this manner, higher powers are accessible without compromising the sample integrity and plasma stability.

The high instantaneous power applied during the power-on period yields transient yet more intense analytical signals that translate into lower detection limits. Klingler et al. [23] examined a millisecond pulsed glow discharge operated at 50% duty cycle. Compared with its continuous counterpart of the same average current, the pulsed discharge enhanced the ion signal intensities by a factor of 2. Shorter pulses and reduced duty cycle allow application of much higher power input and produce more prominent enhancements. For example, using microsecond pulsed glow discharges, Hang [24] and Yang [25] applied instantaneous power of several hundred watts and enhanced the analyte signals by one order of magnitude.

1.3. Temporal Characteristics of Pulsed GD Plasmas

The original intention of the pulsed glow discharge was to produce transient but more intense analytical signals. The signals were expected to resemble closely the applied square-wave power pulse; thus, the most intense signals could be sampled during the plateau period of the pulse. However, studies [26, 27] revealed that ion signals exhibit "abnormal" temporal profiles. For the discharge gas species, i.e. argon and contaminants contained therein, the ion signals are maximized immediately after the power onset whereas the sputtered ion signals reach maxima shortly after power termination. The "abnormal" temporal profiles motivated further investigations into the plasma physicochemical processes associated with ion formation and led to analytical utilities beyond initial expectation.

1.3.1 Atomization and Mass Transport Processes

An ion signal profile reflects not only the temporal variation in ionization process but also the variation in the neutral precursor population in the plasma. This is especially true for the sputtered species. Before being ionized in the plasma, the atoms have to be released from the cathode surface via sputtering processes and subsequently transferred to the negative glow region.

The sputtering process is coupled closely with discharge power. As the power is applied and the discharge breaks down, positive ions are produced and accelerated toward the cathode, sputtering atoms off the cathode. After being release, the sputtered atoms undergo frequent collisions and quickly thermalize.[28] Diffusion and convection then drive the atom cloud to expand toward the surrounding regions. It has been shown that, under common discharge conditions, diffusion plays a major role in atom transport.[29, 30] Driven by random movements of atoms, diffusion spontaneously transports the atoms from one area to another of lower concentration. However, because of the passive nature, diffusional mass transfer is relatively slow and of low efficiency.

The discharge gas flow also can facilitate atom transport.[29] Using a computational model, Bogaerts predicted high discharge gas flows are able to effect a dominating convection force that can significantly enhance atom transport efficiency.[28] The higher transport efficiency directly leads to higher atom concentrations in the negative glow. Because the ion population is proportional to that of the precursor atom,[30] the higher atom concentration is translated into more intense ion signal. Realizing the potential analytical advantages, Oxley et al [31] implemented convection-assisted atom transfer into their glow discharge ion source design, achieving significant increases in the analyte signal.

Because of the sputtering and transport processes, the appearance of sputtered atoms in the plasma is delayed with respect to the power onset. The concentration of sputtered atoms rises until it reaches a steady state at ~1 ms into the pulse cycle, when the sputtering atomization rate is balanced by the loss rate via redeposition onto the discharge chamber walls. Upon the power termination, sputtering processes halt immediately; however, the sputtered atom population in the plasma will remain relatively stable because of the slow diffusion. After a dissipation period of a few milliseconds the population slowly decays toward zero.[32]

The populations of discharge gas species, including argon and the contaminant components, remain constant as the discharge gas is introduced continuously at a fixed pressure. The typical temporal profiles of discharge gas species and sputtered atoms are shown in Figure 1.1.

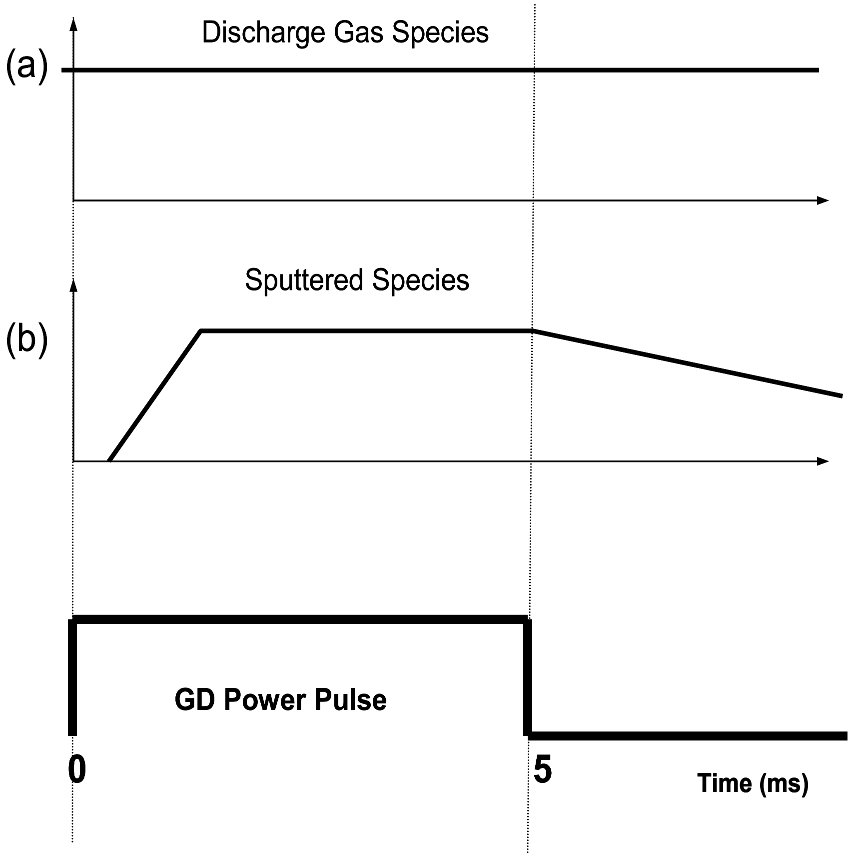

Figure 1.1. Schematic temporal profiles of (a) discharge gas species, such as argon and contaminant components, and (b) sputtered neutral species in a pulsed glow discharge.

1.3.2. Ionization Mechanisms

The major ionization mechanisms in a glow discharge include electron ionization, charge transfer, and Penning ionization.[9] In a continuous power glow discharge, these mechanisms take place concurrently and contribute to the total ionization, resulting in a steady-state ionization environment. In a pulsed discharge, the power is frequently switched on and off; the ionization mechanisms no longer remain steady and their responses to the power modulation become important. It is therefore essential to understand how and at what rate each ionization mechanism responds to the power onset and termination.

1.3.2.1. Electron Ionization

Among the active plasma species, electrons are the most sensitive to electric field changes and, hence, power modulations because of their light mass and high mobility. The applied electric power can be almost simultaneously coupled into the electrons.[33] The electrons gain sufficient energy and subsequently ionize the collision partners in inelastic collisions.

$$e^- \text{ (fast)} + R \rightarrow R^+ + 2\ e^- \text{ (slow)}$$

Upon ionization, an additional electron is released which can accelerate and cause ionization in the same manner. The exponential growth of ionizing electrons leads to discharge gas breakdown.[34] Electron ionization is expected to be solely responsible for ionization at the discharge breakdown period.

Electron ionization is a well developed ionization method.[35] In a standard EI source, a heated filament is used to generate an electron beam of ~0.1 mA; the electrons are accelerated to 70 eV and allowed to interact with the analyte species for ionization. In a pulsed glow discharge, the voltage applied across the electrodes can reach up to several thousand volts and the resultant current can be a few milliamps. This configuration creates an electron beam of much higher flux and average energy, giving rise to more efficient ionization.

Shortly after the discharge breaks down, the plasma forms its classic architecture; the electric field is compressed into the cathode dark space and the negative glow region becomes nearly field-free.[9] As a result, the electron energy distribution shifts to lower energies with the average energy between 2 and 4 eV; only a small fraction (<1%) of electron population is actually capable of ionization. Hence, electron ionization efficiency declines.

Immediately after the power termination, the energetic electrons in the plasma quickly diffuse away or become thermalized through collisions.[36] The energetic electron population is no longer replenished because of the disappearance of the electric field. Thus, electron ionization extinguishes immediately after the power termination.

1.3.2.2. Charge Transfer

The discharge species can be ionized via charge transfer process by the ions of the discharge gas, Ar^+.

$$Ar^+ + R \rightarrow Ar + R^{+*} + \Delta E$$

The process is most likely when there is energy resonance, i.e., ΔE is between +0.2 eV and -0.02 eV.[37] It requires that the potential energy of R^+ or, most likely, an excited state R^{+*}, closely matches the ionization potential of argon (15.67 eV); hence, it is a highly selective ionization process. Charge transfer initiates as argon ions are produced at the discharge breakdown. After ~1ms, the argon ion population reaches a plateau value and remains steady till the power termination. When the discharge power is terminated, argon ions quickly disappear,[23, 38] minimizing charge transfer as a major ionization mechanism.

1.3.2.3. Penning Ionization

Long-lived metastable argon atoms can also result in ionization, which is commonly referred to as Penning ionization.

$$Ar^m + R \rightarrow Ar + R^+ + e^-$$

In order for the discharge species to be Penning ionized, its ionization potential must lie below the metastable energies of argon (11.55 and 11.72 eV). For these species, Penning ionization accounts for 40-80% of the total ionization in a continuous power glow discharge.[39] In a pulsed glow discharge, as the metastable atoms are time-dependent, the contribution from Penning ionization varies.

Combining spectroscopy and mass spectrometry techniques, the King group [27, 32, 40, 41] has studied the temporal variations in metastable argon atom population over a pulse cycle and the corresponding Penning ionization. Atomic absorption measurements showed that metastable argon atoms appear after discharge breakdown. Gradually their population reaches a plateau value at ~ 1ms into the pulse cycle. After power termination, the metastable population increases and reaches a maximum value, instead of decreasing as one might expect. The population upsurge originates from the sudden “cooling” of electrons owing to the disappearance of electric field, establishing the prerequisite condition for ion-electron recombination. The recombination of argon ions and electrons, followed by radiative decay, produces a large population of metastable argon atoms; consequently, Penning ionization is greatly enhanced. Meanwhile, the other energetic species, i.e. ionizing electrons and argon ions, quickly disappear. Thus, Penning ionization becomes the dominant ionization mechanism after power termination.

Figure 1.2 schematically summarizes the temporal characteristics of various plasma species capable of ionizing analytes, i.e., ionizing electrons, argon ions, metastable argon atoms. Note that the pulse glow discharge creates a temporal separation among the ionization mechanisms, as illustrated in Figure 1.2d.

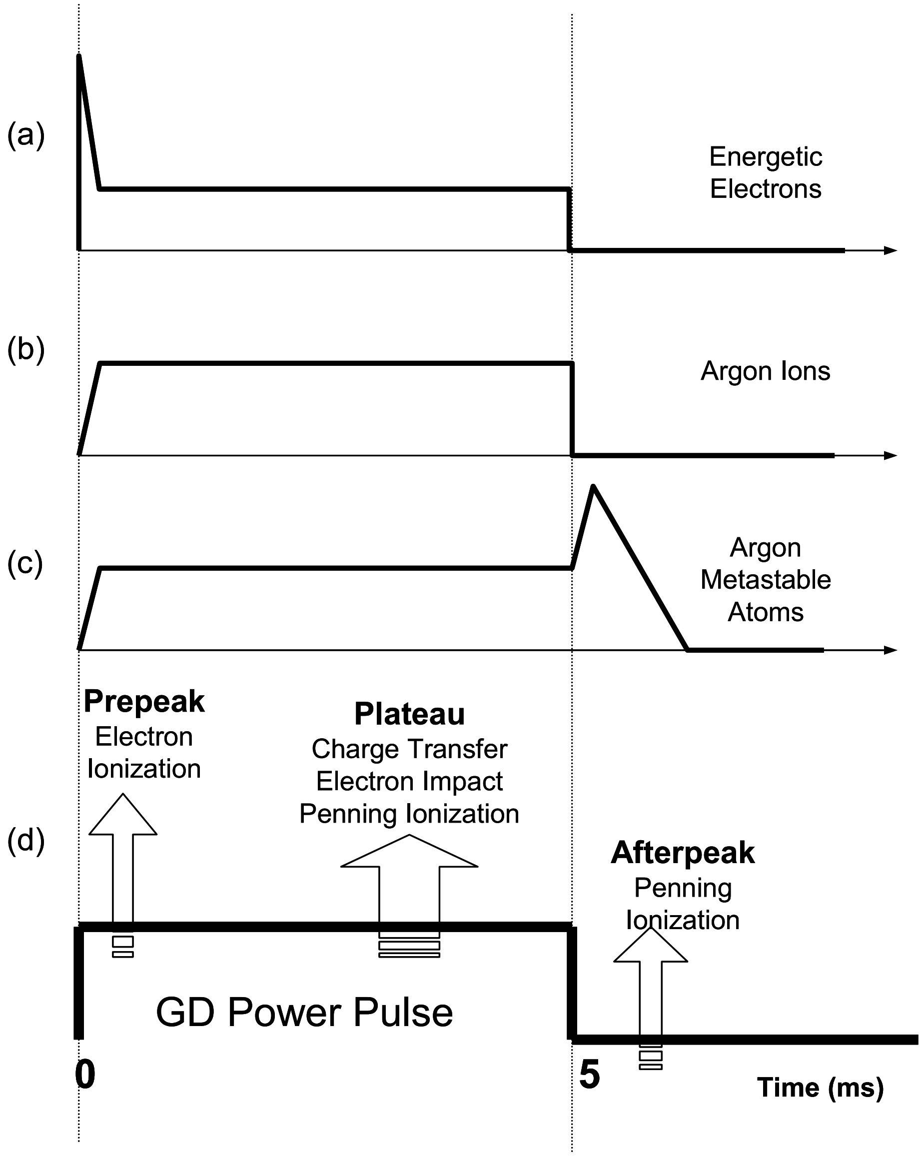

Figure 1.2. Schematic temporal profiles of (a) energetic electrons, (b) argon ions, (c) metastable argon atoms, and d) overall ionization processes in a pulsed glow discharge.

1.3.3. Time-resolved Mass Spectra

The population of ion species in a plasma is directly determined by 1) the population of the neutral precursor and 2) the corresponding ionization processes. In pulsed glow discharges, both factors exhibit temporal variation over a pulse cycle; hence, ion population varies, yielding a series of time-dependent mass spectra. Among them, distinct mass spectra can be obtained at the onset, plateau, and post-pulse period of a pulse cycle.[26, 27]

Pulse Onset. At the power onset and discharge breakdown period (0.1-0.5 ms), electron ionization is the dominant ionization mechanism. The surge of energetic electrons results in efficient ionization of discharge gas species such as Ar and H_2O. The discharge gas ion signals reach maxima at the discharge breakdown; this period is hence termed as the prepeak regime. Note the ions of sputtered species were not present because the sputtered atoms had not yet been transported to the negative glow region.[23, 26, 27]

Shortly after the discharge breakdown, the ions of the sputtered species are detected as the sputtered atoms reach the negative glow region and are ionized therein. Meanwhile, discharge gas ions and metastable discharge atoms are produced in the plasma, initiating charge exchange and Penning ionization.

Plateau Period. At ~1ms into the pulse cycle, the plasma reaches a quasi-steady state. The concentrations of the sputtered atoms and gas species reach steady values;

the stable neutral populations are ionized by the quasi-steady state plasma through electron ionization, charge transfer, and Penning ionization. Both discharge gas and sputtered species can be observed and their intensities remain essentially unchanged until power termination. This plasma configuration is equivalent to its continuous power counterpart. Indeed, the plateau regime mass spectra were found to closely resemble continuous power glow discharge spectrum obtained at approximately the same voltage.[26]

Post-Pulse Period. Upon the termination of discharge power, the populations of neutral species remain relatively stable. However, the plasma ionization environment undergoes dramatic changes: electron ionization and charge transfer halt while Penning ionization enhances. Keep in mind that Penning ionization is associated with lower ionization energetics, at 11.72 eV for metastable argon atoms, and effects selective ionization. The major discharge gas species have high ionization potentials, such as 15.67 eV for argon, 15.62 eV for N_2, and 16 eV for H_2O, and cannot be ionized by metastable argon atoms; therefore, their ion signals rapidly decline to the spectral baseline. Meanwhile, the sputtered species, especially metal atoms, are efficiently Penning ionized, yielding intense signals. Thus, the afterpeak spectra are characterized by intense analyte signal without severe discharge background interferences, i.e., an analytically clean spectrum.[23, 26, 27, 40]

In summary, a pulse glow discharge affords a series of temporal regimes featuring distinct ionization characteristics. Of special interest is the afterpeak regime that provides selective and efficient ionization of the sputtered analyte species and, hence, permits discrimination of analytical signals against the interferences. This analytical utility was demonstrated by the determination of calcium,[20] a task impractical for continuous plasmas because of the isobaric interference of $^{40}Ar^+$. However, in the afterpeak regime, Penning ionization efficiently ionizes calcium but not argon; Ca^+ signal remains intense without the presence of Ar^+. Consequently, quantitative analysis of calcium was readily accomplished. Using microsecond pulsed glow discharge, Harrison's group combined the selective temporal ionization with enhanced atomization/ionization for improvement of analytical performances;[31, 42] detection limits of sub-ppm level were routinely achieved.[24, 25]

1.4. Pulsed Glow Discharges for Molecular Chemical Speciation

Although glow discharges were originally and are most commonly used for elemental analysis of solid samples, its relatively "cool" ionization environment has led researchers to explore the potential application as an ion source for molecular species. In the early 20th century, Aston noticed that molecular ions survived in his discharge ion source.[2] Recently, Carazzato and Bertrand [43] and Mason and Milton [44] introduced organic compound vapors into continuous glow discharge plasmas for ionization. The resultant mass spectra presented a large variety of ions originating from the analyte molecules, ranging from quasi-molecular ions formed through proton transfer to extensive fragment ions yielded by high-energy ionization processes such as electron ionization and charge transfer. The authors realized the simultaneous occurrence of high and low energy ionization mechanisms yielded a great diversity of ion species;

therefore, rich information can be obtained regarding the analyte molecules. On the other hand, these ions, along with discharge background ions, compose a convoluted and complex mass spectrum, hindering spectral interpretation.

To de-convolute the complex plasma spectrum, it is favorable to disperse the spectrum over an additional dimension according to the respective ionization mechanisms. Realizing the temporal separation of ionization mechanisms, Steiner et al. [21] proposed the use of pulsed glow discharges for molecular chemical speciation. The pulsed glow discharge affords discrete temporal regimes featuring distinct ionization mechanisms; each regime, based on the respective ionization characteristic, can provide a simple spectrum with the molecular, structural, or elemental information. The information can then be pieced together to yield a complete picture of the given analyte.

Prepeak Regime. Electron ionization dominates the prepeak regime. The high-flux energetic electron beam not only ionizes the analyte molecules but also decomposes them to small fragments and even atomic constituents. Thus, the prepeak spectra feature abundant small fragments and atomic ions, from which elemental information is readily available.

Plateau Regime. Various ionization mechanisms take place concurrently during the plateau regime, including Penning ionization, charge transfer, along with electron ionization. Charge transfer involves a resonant energy transfer of 15.76 eV (or higher for excited argon ions); the energy is much greater than the typical ionization potentials of organic compounds, usually resulting in intensive fragmentation. On the other hand, Penning ionization is a low-energy process, leading to production of molecular ions. The concurrence of various ionization yields a large variety of ions, revealing rich structural information.

Afterpeak Regime. Penning ionization exclusively dominates the afterpeak regime. Since the energies of metastable argon atoms (11.55 and 11.72 eV) lie slightly above the ionization potentials (~9 eV) of most organic compounds, the molecules can be efficiently ionized with small amount of surplus energy. Furthermore, the surplus energy can be carried away by the ejected electron upon ionization. Therefore, Penning ionization by metastable argon atoms usually promises soft ionization and predominantly yields molecular ions.[45] Hence, molecular weight can be readily measured.

Shortly after the proposal of this methodology, Majidi et al. [22] demonstrated the analytical utility using numerous organic and organometallic compounds. The time-resolved spectra were acquired at each regime sequentially in an almost simultaneous fashion; the elemental, structural, and molecular information of a given analyte were obtained. The fast data acquisition rate makes it a promising technique for molecular chemical speciation. The unique temporal variation of a pulsed glow discharge proves to be most advantageous for molecular mass spectrometry.

To make the pulsed GDMS viable, reliable, and robust, a better understanding of the fundamental plasma processes involving ionization of molecular species is essential. From a practical stand point, the plasma energetics needs to be characterized to optimize analytical performance. These studies would provide valuable theoretical guidance for both method development and instrument design.

This work focuses on analytical applications and theoretical studies of pulsed glow discharge mass spectrometry. Chapter 2 employs spectroscopic methods to study the excitation and ionization mechanisms taking place in the afterpeak regime. The data support the formation of metastable atoms via ion-electron recombination-decay processes. The results suggest that the apparent plasma energy varies as the dominant ionization mechanisms alternate over a pulse cycle. In Chapter 3, the internal energy distributions, P(ε), of a pulsed glow discharge plasma were investigated using tungsten hexcarbonyl $W(CO)_6$ as a “thermometer molecule”. The results indicate the pulsed glow discharge affords excellent energy tunability that can be used to perform selective ionization and fragmentation for molecular, structural, and elemental information. Using some organic and organometallic compounds, we further demonstrated the analytical utility of pulsed GDMS for molecular speciation (Chapter 4). The time- and space-resolved spectra explicitly exhibited the flexibility and tunability of the pulsed glow discharge. Chapter 5 concentrates on the fundamental plasma processes involving molecular species. A probe molecule, N_2, is introduced into pulsed glow discharge plasmas; the N_2 and N_2^+ at various excited energy states were monitored using spectroscopic methods. The study reveals that molecular species are excited and ionized by various plasma species, such as electrons, argon ions and metastable atoms, and sputtered atoms. Finally, Chapter 6 demonstrates the applicability of pulsed GDMS to the quantitative determination of elements in commercial polymers. The pulsed operation exhibits advantages over its continuous operation counterpart in that no additional sample cooling equipment is required for the thermally labile samples.

1.5. References

(1) Thomson, J. J. *Rays of Positive Electricity and their Application to Chemical Analysis*; Longmans Green: London, 1913.
(2) Aston, F. W. *Isotops*; Longmans: New York, 1924.
(3) Svec, H. J., *Int. J. Mass Spectrom Ion Processes* 1985**, 66,** 3-29.
(4) Bogaerts, A.; Neyts, E.; Gijbels, R.; van der Mullen, J., *Spectrochim. Acta B* 2002**, 57,** 609-658.
(5) Coburn, J. W., *Rev. Sci. Instrum.* 1970**, 41,** 1219-1223.
(6) Coburn, J. W.; Eckstein, E. W.; Kay, E., *J. Vac. Sci. Technol.* 1975**, 12,** 151-154.
(7) Coburn, J. W.; Kay, E., *App. Phys. Lett.* 1971**, 19,** 350-352.
(8) Coburn, J. W.; Taglauer, E.; Kay, E., *Journal of Applied Phyiscs* 1974**, 45,** 1779-1786.
(9) Chapman, B. N. *Glow Discharge Processes*; John Wiley and Sons: New York, 1980.
(10) Harrison, W. W.; Magee, C. W., *Anal. Chem.* 1974**, 46,** 461-464.
(11) King, F. L.; Teng, J.; Steiner, R. E., *J. Mass Spectrom.* 1995**, 30,** 1061-1075.
(12) Harrison, W. W.; Hess, K. R.; Marcus, R. K.; King, F. L., *Anal. Chem.* 1986**, 58,** 341A-350A.
(13) King, F. L.; Harrison, W. W., *Mass Spectrom. Rev.* 1990**, 9,** 285-317.
(14) Marcus, R. K., *J. Anan. At. Spectrom.* 1993**, 8,** 935-943.
(15) Vieth, W.; Huneke, J. C., *Spectrochim. Acta* 1990**, 45B,** 941-949.
(16) Houk, R. S., *Anal. Chem.* 1986**, 58,** 97A-105A.
(17) Tong, S. L.; Harrison, W. W., *Anal. Chem.* 1984**, 56,** 2028-2033.
(18) Pollmann, D.; Ingeneri, K.; Harrison, W. W., *J. Anal. At. Spectrom.* 1996**, 11,** 849-853.
(19) Hang, W.; Walden, W. O.; Harrison, W. W., *Anal. Chem.* 1996**, 68,** 1148-1152.
(20) Lewis, C. L.; Oxley, E. S.; Pan, C.; King, F. L., *Anal. Chem.* 1999**, 71,** 230-234.

(21) Steiner, R. E.; Lewis, C. L.; Majidi, V., *J. Anal. At. Spectrom.* 1999**, 14*,*** 1537-1541.
(22) Majidi, V.; Moser, M.; Lewis, C.; Hang, W.; King, F. L., *J. Anal. At. Spectrom.* 2000**, 15*,*** 19-25.
(23) Klingler, J. A.; Barshick, C. M.; Harrison, W. W., *Anal. Chem.* 1991**, 63*,*** 2571-2576.
(24) Hang, W.; Baker, C.; Smith, B. W.; Winefordner, J. D.; Harrison, W. W., *J. Anal. At. Spectrom.* 1997**, 12*,*** 143-149.
(25) Yang, C.; Mohill, M.; Harrison, W. W., *J. Anal. At. Spectrom.* 2000**, 15*,*** 1255-1260.
(26) Klingler, J. A.; Savickas, P. J.; Harrison, W. W., *J. Am. Soc. Mass Spectrom.* 1990**, 1*,*** 138-143.
(27) King, F. L.; Pan, C., *Anal. Chem.* 1993**, 65*,*** 735-739.
(28) Bogaerts, B.; Okhrimovskyy, A.; Gijbels, R., *J. Aanl. At. Spectrom.* 2002**, 17*,*** 1076-1782.
(29) Hang, W.; Harrison, W. W., *Anal. Chem.* 1997**, 69*,*** 4957-4962.
(30) Loving, T. J.; Harrison, W. W., *Anal. Chem.* 1983**, 94*,*** 1523-1526.
(31) Oxley, E.; Yang, C.; Jian, L.; Harrison, W. W., *Anal. Chem.* 2003**, 75*,*** 8478-6484.
(32) Lewis, C. L.; Jackson, G. P.; Doorn, S. K.; Majidi, V.; King, F. L., *Spectrochim. Acta* 2001**, 56B*,*** 487-501.
(33) Fey, F. H. A. G.; Stoffels, W. W.; van der Mullen, J. A. M., *Spectrochim. Acta* 1991**, 46B*,*** 885-900.
(34) Townsend, J. S., *Nature* 1900**, 62*,*** 340-341.
(35) Field, F. H.; Franklin, J. L. In *Pure and Applied Physics*; Massey, H. S. W., Ed.; Acedamic Press: New York, 1957; Vol. 1.
(36) Golubovskii, Y. B.; Lange, H.; Maiorov, V. A.; Porokhova, I. A.; Sushkov, V. P., *J. Phys. D* 2003**, 36*,*** 694-703.
(37) Steers, E. B. M.; Fielding, R. J., *J. Anal. At. Spectrom.* 1987**, 2*,*** 239-244.
(38) Jackson, G. P.; King, F. L., *Spectrochim. Acta* 2003**, 58B*,*** 185-209.
(39) Smith, R. L.; Serxner, D.; Hess, K. R., *Anal. Chem.* 1989**, 61*,*** 1103-1108.
(40) Pan, C.; King, F. L., *J Am Soc Mass Spectrom* 1993**, 4*,*** 727-732.
(41) Jackson, G. P.; Lewis, C. L.; Doorn, S. K.; Majidi, V.; King, F. L., *Spectrochim. Acta* 2001**, 56B*,*** 2449-2464.
(42) Pisonero, J.; Turney, K.; Bordel, N.; A., S.-M.; Harrison, W. W., *J. Anal. At. Spectrom.* 2003**, 18*,*** 624-628.
(43) Carazzato, D.; Bertrand, M. J., *J. Am. Soc. Mass Spectrom.* 1994**, 5*,*** 305-315.
(44) Mason, R.; Milton, D., *Int. J. Mass Spectrom. Ion Processes* 1989**, 91*,*** 209-225.
(45) Anderson, D. R.; Bierbaum, V. M.; Depuy, C. H.; Grabowski, J. J., *Int. J. Mass Spectrom. Ion Phys.* 1983**, 52*,*** 65-94.

Chapter 2: Excitation and Ionization in the Afterpeak Regime of a Pulsed Glow Discharge Plasma

2.1. Introduction

Glow discharges are widely used as atomization, excitation, and ionization sources for various analytical spectrometries.[1] The inherent sputtering process affords the ability to generate gas phase atoms directly from solid samples, providing a ground state atom population for atomic absorption [2] and fluorescence.[3] The rich excitation and ionization environment further yields excited-state atoms for atomic emission,[4] and ions for mass spectrometry.[5]

Most analytical glow discharges operate in continuous mode, yielding essentially steady-state analytical signals. Pulsed glow discharges have been explored as an effective alternate to enhance sputtering, excitation, and ionization while alleviating sample overheating problems. The short-term "on-period" with much higher instantaneous power promises intense analytical signals, which can be readily acquired using time-gated techniques;[6] the following long "off-period" allows for efficient sample cooling. A 100-fold increase in intensity for a pulsed discharge has been reported as compared to a continuous discharge of the same average power input. However, recent attention has been focused on the period immediately following the discharge power termination because of the unique plasma chemistry therein.

While studying a high pressure (10-20 Torr) pulsed helium microwave discharge plasma, Johnson et al. [7] observed that the total light intensity of the plasma started to rise and reached the maximum at 0.05-1 ms after the power termination. The intensity increase was thus termed “afterglow”. The temporal position of the maximum, as well as its temporal span (broadness), was found to be dependent on the discharge conditions, especially the initial ion density before the discharge was terminated. Base on these observations, the authors attributed the “afterglow” to the excited He_2 species arising from recombination of He_2^+ ions and electrons.

The similar “afterglow” phenomenon was also observed in a low-pressure glow discharge plasma by Strauss and coworkers.[8] The atomic emissions of the sputtered atoms were found to persist for a few milliseconds after the power termination, much longer than the known lifetimes of the excited atoms. Because the persisting emissions severely interfered with fluorescence measurements, great effort was expended to study their origins. The authors ascribed the excitation after the power termination to the enegetic electrons released during the energy pooling (ionization) process of two metastable argon atoms.

Harrison and coworkers [9, 10] investigated the ion species in a pulsed glow discharge plasma and observed that a large number of sputtered copper atoms were ionized after the termination of discharge power, in the so-called “afterpeak” regime. Combining mass spectrometry with spectroscopic methods, the King group [11-14] further studied ion formation mechanisms within the afterpeak regime. The studies confirmed the metastable argon atom population increases after the power termination, presumably arising from ion-electron recombination.[15-17] The metastable atoms efficiently Penning ionize the plasma species of lower ionization potentials. Subsequently, the ions recombine with electrons and form highly excited atoms; the excited species radiatively decay, giving rise to the emission intensity upsurge.

The “afterpeak” of a pulsed glow discharge provides significant analytical opportunities. Note the dominant Penning ionization is limited by the potential energies of metastable argon atoms at 11.55 and 11.72 eV; therefore, the afterpeak regime affords selective ionization. For elemental analysis, the selective ionization permits discrimination of analytical signals against interferences. The metastable argon atoms can efficiently ionize the sputtered atoms, but not the background interfering species, such as Ar, N_2 and H_2O, because of their higher ionization potentials. This analytical utility was demonstrated by the determination of calcium [18]with argon as the discharge support gas, a task impractical for continuous plasmas because of the isobaric interference of $^{40}Ar^+$. However, in the afterpeak, Penning ionization only efficiently ionizes calcium but not argon. The Ca^+ signal remained intense without the presence of Ar^+ to yield a “clean” mass spectrum; consequently, quantitative analysis of calcium was readily achieved. Recently, the afterpeak regime was further employed for molecular mass spectrometry. The “soft” Penning ionization produced molecular ions and molecular weight information was readily obtained [19, 20] (also Chapter 3 and 4 of this document).

Even now there remains a debate as to the origin of the afterpeak phenomenon with focus on the ion-electron recombination process. The argon ion-electron recombination has long been known as a low-probability process.[21, 22] Theoretical modeling study by Bogaerts [23] showed that the increase in metastable atom population requires a 100-fold increase in thermalized electron density after power termination. The two orders of magnitude increase, although expected to be readily detected, has not yet been experimentally observed. Because ion-electron recombination is critical to the production of metastable argon atoms and, consequently, the analytical utilities of a pulsed glow discharge ion source, the fundamental plasma processes during the afterpeak regime deserve further investigation.

This work employed a perturbation method [24, 25] to examine the energy transfer processes within the afterpeak regime in a pulsed glow discharge plasma. A brief power pulse was applied during the afterpeak regime to disturb the plasma environment, especially electron energies. The responses of various plasma species to the perturbation pulse were measured using atomic emission or absorption spectroscopy. The data provided insight into the physicochemical plasma processes within the afterpeak regime and evidence of ion-electron recombination. Furthermore, the kinetic information of these processes can be deduced from the corresponding response time.

2.2. Experimental Section

Glow Discharge Device. A stainless steel six-way cross (MDC, Hayward, CA), equipped with two Suprasil optical view ports (Heraeus Quartz, Duluth, GA), served as the glow discharge chamber (Figure 2.1). The chamber was evacuated by a turbo molecular pump (Pfeiffer TPH50, Nashua, NH) and a mechanical pump. Prior to experiments, a base pressure lower than 1 mTorr was achieved. The argon discharge support gas (ultra pure, Airgas, Randor, PA) was introduced through a metering valve. The pressures were monitored by a thermocouple pressure gauge (Varian 801, Lexington, MA). A copper disk cathode (NIST SRM 495, Gaithersburg, MD), 5 mm in diameter and 2 mm in thickness, was mounted on a direct insertion probe (DIP) and introduced into the discharge chamber via a ball valve interlock.

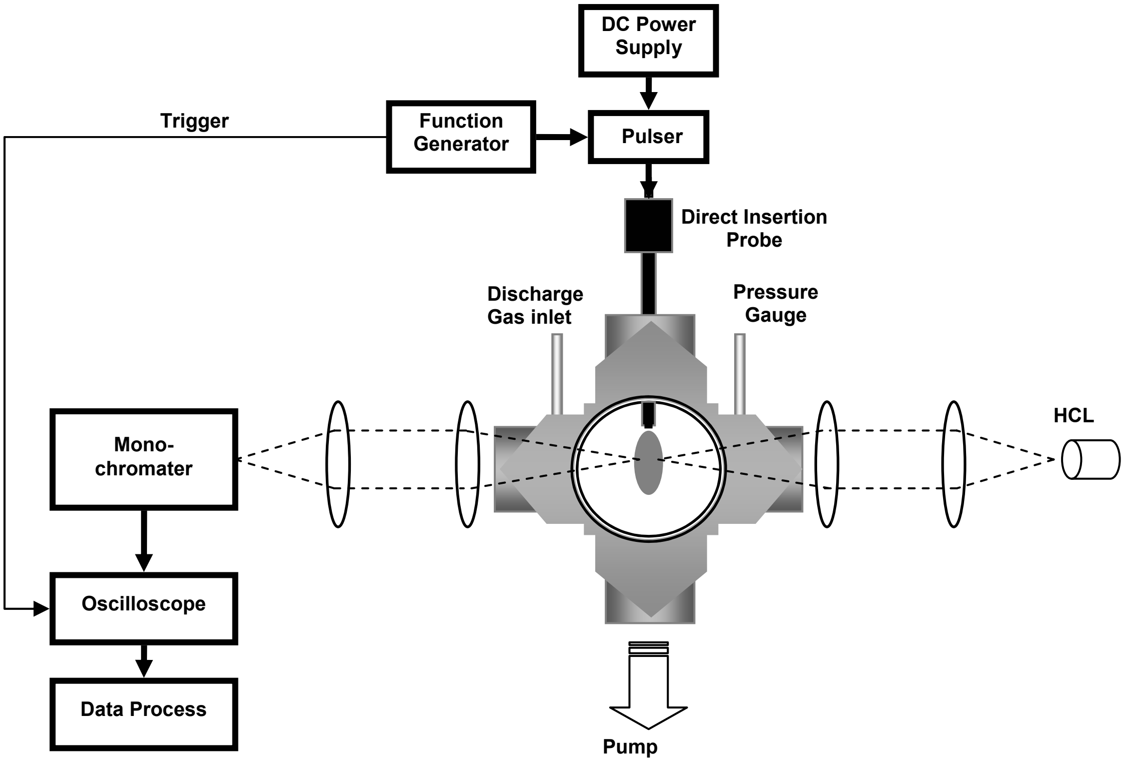

Figure 2.1. Schematic of the optical spectroscopic measurement system.

The previously used home-built power pulser [13] was substituted by a pulsed DC power supply system. The new system consists of a function generator (DS345, Stanford Research Systems, Sunnyvale, CA 94089), an electronic high voltage pulser (GRX-H, Directed Energy, Fort Collins, CO), and a power supply (Kepco OPS 2000M, Flushing, NY). The function generator was programmed to produce the desired waveforms, which in turn triggered the pulser to gate the high voltage output from the power supply. The waveform also provided triggers to synchronize the signal detection system. The resultant pulse train was monitored using an oscilloscope (Tektronix 2232, Beaverton, NY) through a high voltage probe (Tektronix P6015, Beaverton, NY).

Atomic Emission Measurements. Two plano-convex lenses were used to project the GD plasma image on the entrance of a Czerny-Turner monochromator (ISA HR-640, Edison, NJ) at 1:1 ratio. The monochromator entry and exit orifice were both set at 50 μm wide and 1 mm high. Throughout this study, the lateral center of the plasma image was carefully aligned with the entrance and then fixed. The plasma was monitored at different distances along the plasma axial direction by careful positioning of the transportable DIP to vary the vertical position of the plasma image. The vertical zero position was determined when the copper cathode surface image is located at the vertical center of the entry orifice.

The signals were detected by a photomultiplier tube (Hamamatsu R928, Bridgewater, NJ) and subsequently fed into an oscilloscope (LeCroy LT342, Chestnut Ridge, NY) to generate emission temporal profiles. The profiles were digitized using 2500 data point and averaged for 100 sweeps in the oscilloscope. The resultant data were then transferred to a computer through a GPIB interface. A spreadsheet program (Excel, Microsoft, Seattle, WA) was used to further process and plot the data.

Atomic absorption Measurements. The population of the metastable argon atom and ground copper atom was measured using an atomic absorption technique. A boron-argon and a copper-neon hollow cathode lamp (HCL) operated at 15 mA current were used as the light sources. The incident light was first focused into the discharge chamber above the center of the cathode by two plano-convex lenses. The transmitted light was then collected into the monochromator entry orifice by the same optical lenses used in the emission measurements. The detailed procedure of atomic absorbance measurements are given in section 2.3.3.

2.3. Results and Discussion

2.3.1. Perturbation of the Plasma by Power Modulation

The pulsed GD plasma was operated under a fixed pressure at 0.8 Torr. Under the normal pulse mode, the discharge power is kept on for 5 ms and turned off for 15 ms, giving 50 Hz pulsing rate with 25% duty cycle (Figure 2.2a). The pulse voltage was set at 800 V and the peak current was measured to be 3.2 mA, resulting in a 0.64 Watt average power.

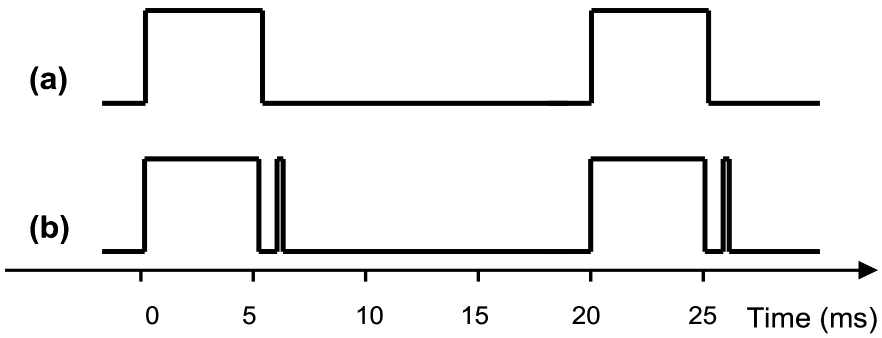

Figure 2.2. Glow discharge power profiles for (a) the normal pulsed glow discharge, and (b) the pulsed glow discharge with the perturbation pulse applied during the afterpeak regime.

In order to explore the plasma processes within the afterpeak regime, a brief power pulse was applied shortly after the termination of the main power pulse to perturb the plasma (Figure 2.2b); the brief pulse is therefore termed a “perturbation pulse”. The duration of the perturbation pulse is set for 0.1 ms and positioned at 0.05 ms, 0.1 ms and 0.2 ms after the discharge power termination. Similar responses were observed for these positions and only one position will be discussed in detail.

The applied power pulse imposes an electric field across the electrodes. Among the plasma species, electrons are most sensitive to the power perturbation. The electric field immediately energizes free electrons because of their light mass and high mobility. Subsequently the energetic electrons can excite or ionize the heavy particles, i.e., atoms and molecules. These plasma species can further dissipate their energies to the surrounding environment; one of the energy dissipation processes is emission of photons. The energy transfer chain can be schematically presented as following:

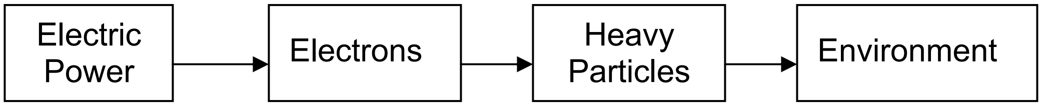

When the power is terminated, Highly energetic electrons disappear from the plasma almost immediately after the power termination, suspending electron excitation and ionization. After disappearance of the electric field, electrons will slow down through elastic collisions and eventually become thermalized.[26] However, it takes relatively long period for electrons to completely thermalize. The electron thermalization time in an ICP plasma is measured at the order of microsecond.[24]

Power modulations cause electron energy changes and will further affect excitation of heavy particles. The changes will eventually lead to variations in the respective spectroscopic signals. Therefore, the spectroscopic studies afford rich insight into the energy transfer processes in the plasma. Furthermore, the temporal signal profiles provide kinetic information for the corresponding energy transfer process. For example, the energy transfer directly involving electrons is expected to exhibit fast response rate.

In this study, the spectroscopic responses of discharge gas and sputtered species to power modulations were monitored. The transitions explored are listed in Table 2.1; of each group, a representative transition will be discussed in detail.

Table 2.1. Selected spectral lines and the respective transitions.

Group	Wavelength (nm)	Transition
Argon atom	**Ar I 811.5**	4p2 – 4s $^3P_2$
	Ar I 794.8	4p7 – 4s $^3P_0$
	Ar I 415.8	5p5 – 4s $^3P_2$
	Ar I 420.0	5p2 – 4s $^3P_2$
	Ar I 810.3	4p4 – 4s $^3P_1$
	Ar I 750.3	4p10 – 4s $^1P_1$
Argon ion	**Ar II 476.5**	4p $^2P_{3/2}$ – 4s $^2P_{1/2}$
	Ar II 427.7	4p' $^3P_{3/2}$ – 4s $^2D_{5/2}$
	Ar II 410.3	5s $^4P_{5/2}$ – 4p $^4D_{7/2}$
	Ar II 413.1	3d' $^2D_{3/2}$ – 4s' $^2D_{3/2}$
Copper atom	Cu I 324.7	4p $^2P_{1/2}$ – 4s $^2S_{1/2}$
	Cu I 327.4	4p $^3P_{3/2}$ – 4s $^2P_{1/2}$
	Cu I 809.3	5s $^2S_{1/2}$ – 4p $^2P_{3/2}$
	Cu I 368.7	6d $^2D_{5/2}$ – 4p $^2P_{3/2}$
	Cu I 515.3	4d $^2D_{3/2}$ – 4p $^2P_{1/2}$

Note: The transitions in bold are discussed in detail as the representative for each group.

2.3.2. Temporal Accuracy of the Measurements

The typical 10% - 90% rise/fall times of the discharge power pulse were found to be less than 5 μs. The rapid power modulation results in fast signal responses that are expected to take place on the order of microseconds. To accurately measure the fast-changing signals, the detection system must be carefully arranged to ensure a quick response time and a wide bandwidth.

Figure 2.3a shows an equivalent circuit schematic of the detection system in use. The transient emission signals were detected by a photomultiplier tube with a typical response time of 22 ns. The bandwidth of the oscilloscope used in this study is 500

MHz. Both devices satisfy the requirements for measuring the fast signals. However, the maximum bandwidth of the detection system is limited by the RC constant of the output circuit. The capacitance (C) is the total capacitance of the photomultiplier tube anode to all other electrode including stray capacitance such as wiring capacitance. The effective load resistance (R) is determined by the load resistance (R_{Load}= 1MΩ) and the input coupling of the oscilloscope (R) which can be set at 1MΩ or 50Ω.

$$R = \frac{R_{Load} \times Ro}{R_{Load} + Ro}$$

The effective load resistant is 0.5M Ω when 1M Ω input coupling is selected and ~50 Ω when 50 Ω input coupling is in use. The resultant cutoff frequency (f) of the output circuit can be expressed by the following relationship.

$$f = 1/(2\pi CR)$$

Since high effective load gives low cutoff frequency, the 1M Ω input coupling is expected to cause considerable distortion to the signals.

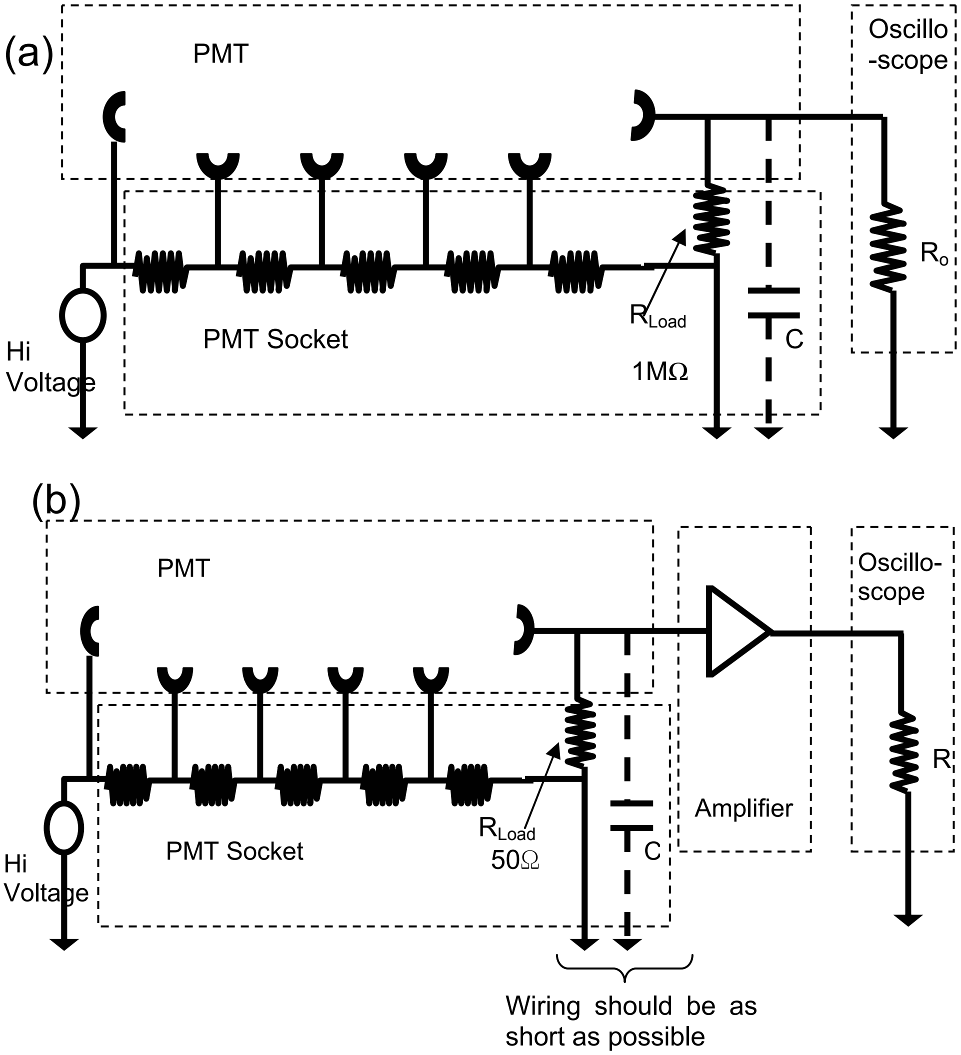

Figure 2.3. Circuit diagrams of (a) standard signal detection system; and (b) modified detection system for improved temporal accuracy.

In order to examine the expected distortion, Cu 324.7 nm emission was measured using 1 MΩ and 50Ω input coupling and the profiles are shown in Figure 2.4a. The signal distortion associated with 1MΩ can be clearly seen: the afterpeak is less pronounced and broadened, presumably because the low bandwidth cuts off the signal components of higher frequencies. Indeed, when the profiles were further converted into the frequency domain (Figure 2.4b), the comparison explicitly shows that the signal components over 200 Hz are severely attenuated or eliminated when 1MΩ input coupling is used.

The result indicates that 50Ω coupling should be used for accurate measurement of the signal temporal profiles. Unfortunately, 50Ω coupling gives lower voltage drops and, hence, lower signal intensities. The lower signal is mirrored by the high noise level in Figure 2.4a in which the data are normalized. In order to reduce the noise, a digital filter is set at 10 KHz to screen the high-frequency noises. The filtered data are then converted into the time domain signal using an inverse FFT procedure. The improvement can be seen in Figure 2.5: the noise is significantly suppressed without compromising the temporal fidelity. However, considerable noise does still exist. Because most emission signals of interest are much weaker than this example emission, the approach would not provide meaningful results for weak emissions.

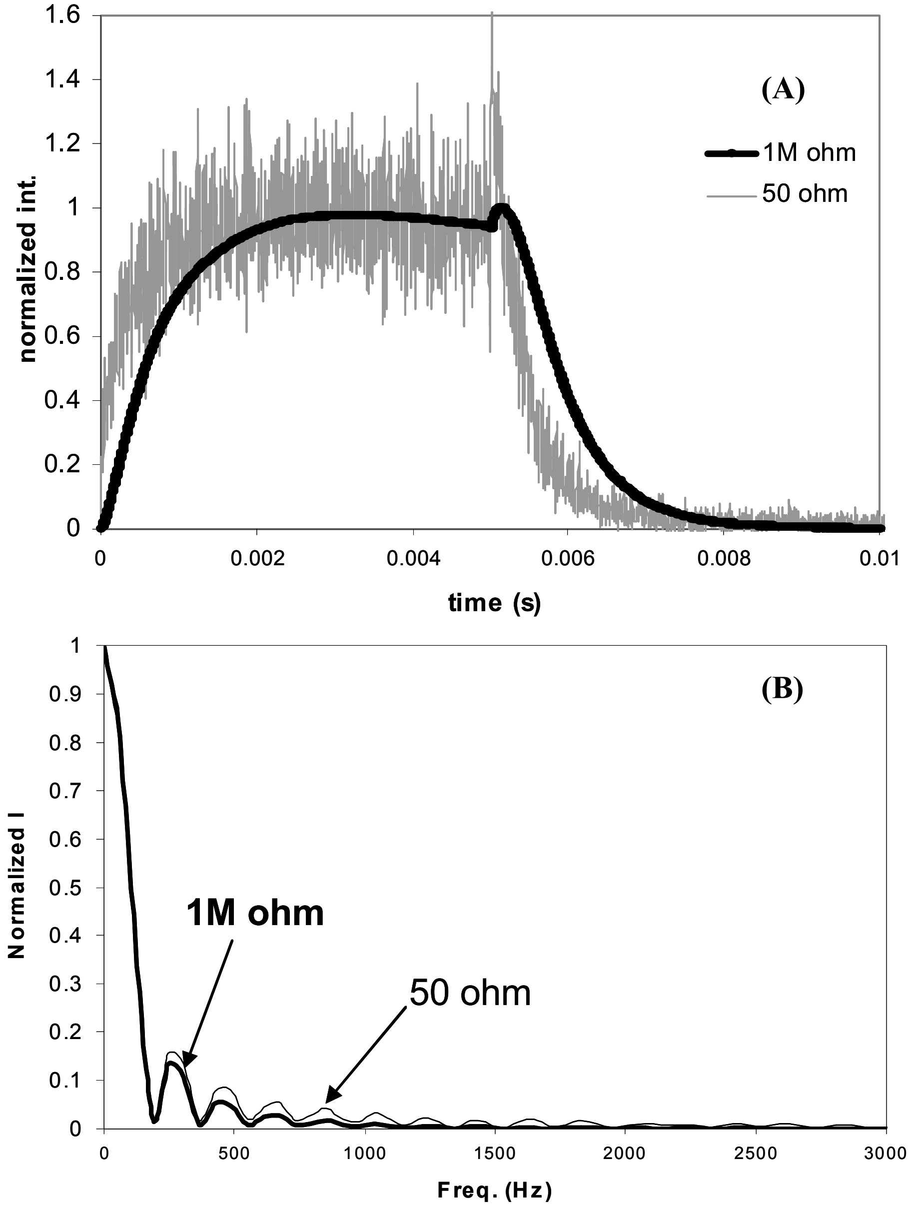

Figure 2.4. Temporal emission profiles of Cu I 324.7 nm line measured using 1M Ω and 50 Ω input coupling (a) and the respective frequency domain spectra (b).

Clearly, further improvements of the detection system are required to acquire the fast signals with both temporal accuracy and sufficient intensity. First, both load resistor and oscilloscope input coupling should be set at 50Ω to reduce the RC constant of the output circuit and increase its bandwidth. Then, a high-speed wide-bandwidth operational amplifier can be employed to amplify the resultant weak signals before the oscilloscope input (Figure 2.3B). Alternatively, it is highly recommended to use the PMT socket with a built-in amplifier (available from Hamamatsu), which promises both sensitivity and wide bandwidth. However, these devices were not available to us when the work was conducted. Throughout this work, 1MΩ input coupling and load resistor were used to allow for measurement of weak emissions. Realizing the associated distortions in the measurements, we only seek here to demonstrate the applicability of perturbation methods to glow discharge diagnosis. All the data contained herein should be treated as relative in terms of temporal accuracy.

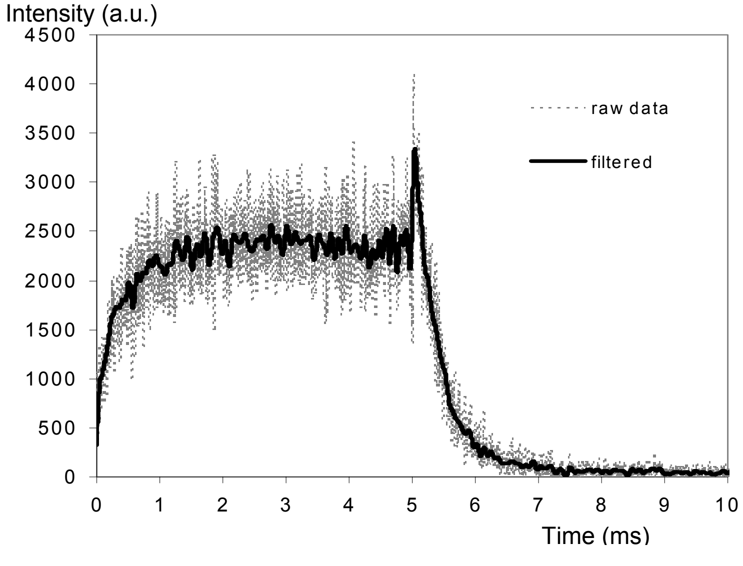

Figure 2.5. Temporal emission profiles of Cu I 324.7 nm line before and after digital noise filtration.

2.3.3. Atomic Absorption Measurement

The populations of metastable argon atoms and ground state copper atoms were measured using atomic absorption spectrometry. The commonly used method for absorption measurements employs a modulated incident light to produce an absorption signal of the same periodical variation, which can then be demodulated and amplified by a lock-in amplifier. However, this method is not suitable for profiling the fast-changing signals generated by the millisecond pulsed glow discharge because the relatively large RC constant associated with the lock-in amplifier distorts the signal temporal profile. [13]

In this study, an alternate approach was taken to eliminate the use of a lock-in amplifier. The adopted method takes a three-step measurement followed by an absorbance calculation (Figure 2.6). First, the HCL is ignited and its emission intensity profile was measured (I_{HCL}). Then, the GD plasma is turned on and the total signal (I_{total}) was measured, which consists of the emission from the GD plasma (I_{plasma}) and the transmitted light from the HCL after being absorbed by the plasma (I_{trans}). Finally, the HCL light source is blocked and only the emission from the plasma was measured (I_{plasma}). The differences between the total signal and the plasma emission signal were calculated, giving the transmitted light intensity (I_{trans}). The absorbance was then calculated based on Equation 1.

$$A= \log [I_{HCL}/I_{trans}] = \log [I_{HCL}/(I_{total}-I_{plasma})] \qquad \text{(Equation1)}$$

Where: I_{HCL} = emission intensity of the HCL.

I_{trans} = intensity of transmitted light.

I_{plasma} = emission intensity of the plasma only.

I_{total} = total intensity of both transmitted light and plasma emission.

Note that the absorbance profiles were calculated from emission signals. The resultant absorbance profiles can hence be directly compared with the emission profiles in terms of temporal characteristics.

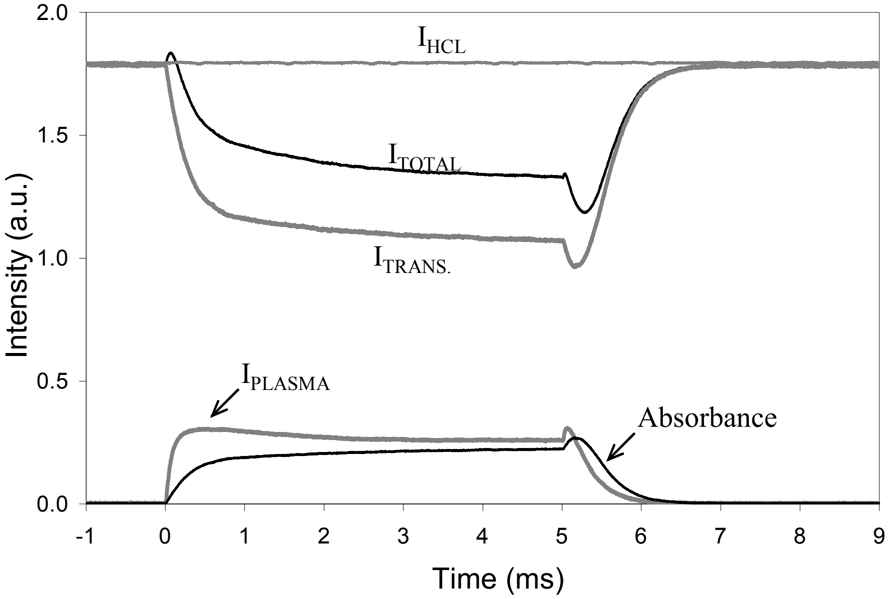

Figure 2.6. Temporal profiles of HCL emission intensity (I_{HCL}), plasma emission intensity (I_{PLASMA}), total emission intensity (I_{TOTAL}); and the calculated transmitted light intensity (I_{TRANS}) and absorbance.

2.3.4. Argon Ion Emission Measurements

All the argon ion emissions exhibit similar responses. The 476.5 nm emission, corresponding to the transition from 4p $^2P_{3/2}$ (19.87 eV) to 4s $^2P_{1/2}$ (17.26 eV), is discussed in detail. Because of the high excitation energies, the excited argon ions are most likely produced by a two-step process: electron ionization of argon followed by electron excitation. [14]

1) electron ionization: $Ar + e^-(fast) \rightarrow Ar^+ + 2\ e^-\ (slow)$

2) electron excitation $Ar^+ + e^-\ (fast) \rightarrow Ar^+\ (excited) + e^-\ (slow)$

Both steps directly involve energetic electrons; therefore, the emission is expected to exhibit immediate responses to power modulation. Indeed, the spontaneous responses can be readily recognized in Figure 2.7a: the emission intensities quickly decay as soon as the power is turned off. As explained earlier, energetic electrons disappear immediately after the power termination and both ionization and excitation halt; therefore, the excited argon ion state is no longer populated. Consequently, the emission undergoes a sharp decrease. Following the same argument, the application of the perturbation pulse will reverse the processes and the intensities will instantaneously increase (Figure 2.7b).

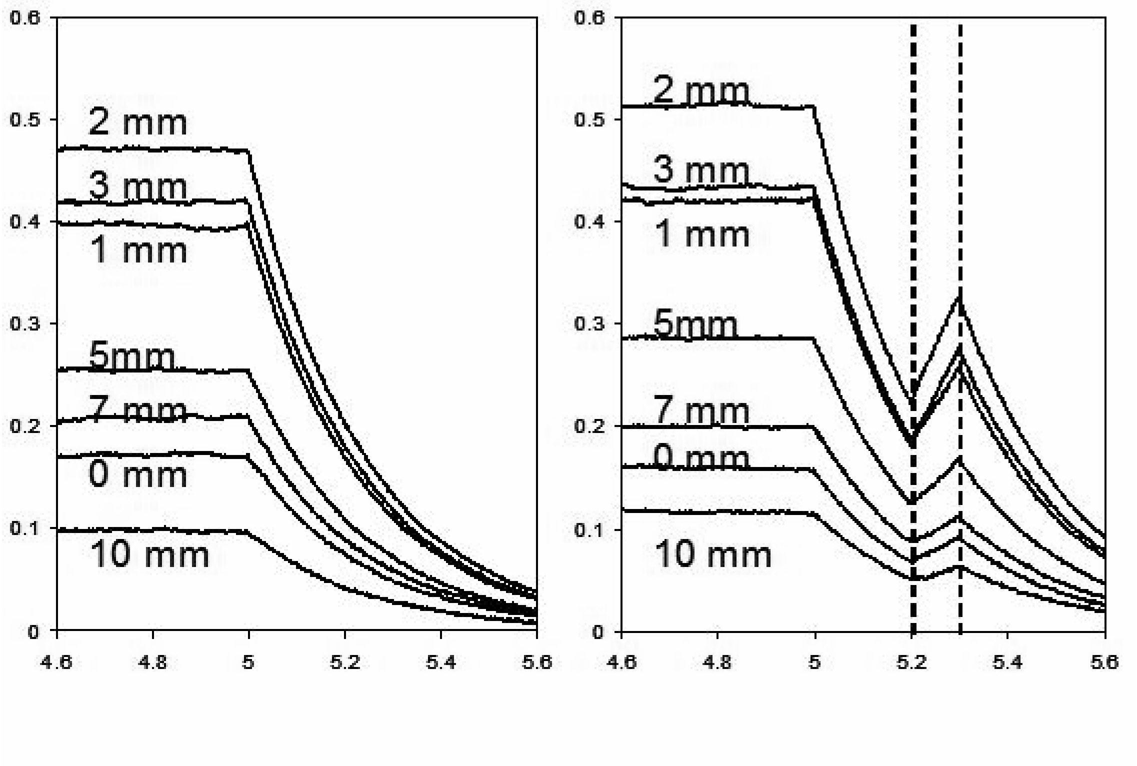

Figure 2.7. Temporal emission profiles of Ar II 476.5 nm line at various distances for (a) the normal pulsed glow discharge, and (b) the pulsed glow discharge with the perturbation pulse applied between 5.2 ms and 5.3 ms.

2.3.5. Argon Atom Emission Measurements

Excited argon atoms can be produced through various mechanisms in a glow discharge. Within the cathode dark space (0-2 mm), fast atom excitation is the dominant excitation mechanism [27]because of the presence of the strong electric field.

1) Energy coupling into argon ion: Electric Field + Ar^+ (slow) → Ar^+ (fast)

2) Charge exchange yielding fast atoms:

Ar^+ (fast) + Ar (slow) → Ar^+ (slow) +Ar (fast)

3) Fast atom excitation: Ar (fast) + Ar → Ar (slow) +Ar^* (excited)

In the negative glow region (3-10 mm), the major excitation mechanisms are electron excitation and ion-electron recombination.

Electron excitation: e^- (fast) + Ar (ground) → e^- (slow) +Ar* (excited)

Ion-electron recombination-decay: $Ar^+ + e^-$ (slow) → Ar** (highly excited).

The highly excited argon states lie close to the ionization continuum; once formed, they undergo radiative decay to lower excited states: Ar** → Ar* + photon.

Figure 2.8 shows the temporal profiles of argon atom emission at 811.5 nm. This emission corresponds to the transition from 4p $^3D_3$ (13.08 eV) to the 4s $^3P_2$ metastable state (11.55 eV). It is evident that the temporal profiles are spatially dependent. In the close proximity of the cathode surface (0-1 mm), the emissions quickly decay after the power termination; no afterpeak is observed. However, the intensities start to enhance as soon as the perturbation pulse is applied. These observations are consistent with the proposed fast atom excitation mechanism. Note that the mechanism is coupled closely with the electric field that is essential for the production of fast atoms. The power termination, i.e., disappearance of the electric field, immediately suspends this mechanism. Hence, the cessation of the power would almost instantaneously halt fast atom excitation and result in an immediate intensity attenuation. When the perturbation pulse is switched on, the electric field is re-established; fast atom excitation is re-initiated and, therefore, the emission signals increase (Figure 2.8b).

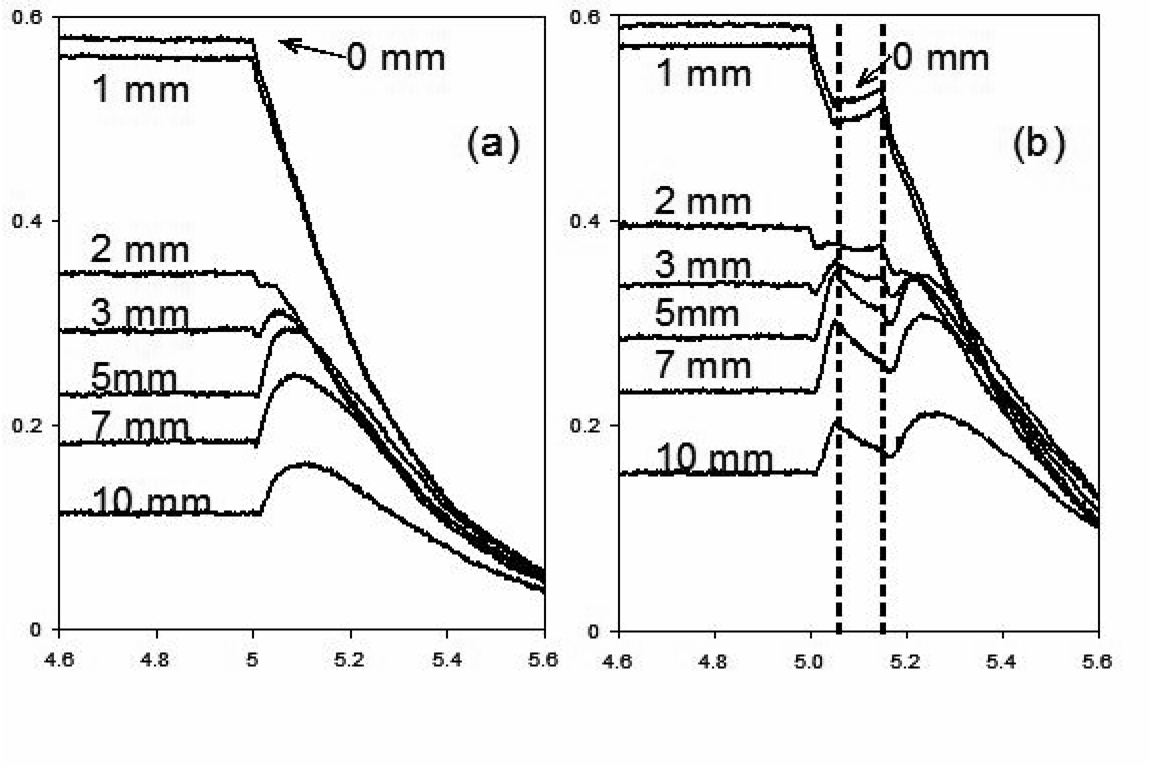

Figure 2.8. Temporal emission profiles of Ar I 811.5 nm line at various distances for (a) the normal pulsed glow discharge, and (b) the pulsed glow discharge with the perturbation pulse applied between 5.05 ms and 5.15 ms.

At distances between 3 to 10 mm, the emission exhibits a completely different response. The intensities increase after the power termination and form the so-called “afterpeak”. The intensity upsurges, or the increases in excited argon atom population, arise from either electron excitation or ion-electron recombination-decay.

The plasma perturbation allows one to determine which the dominant excitation mechanism is because electron excitation and ion-electron recombination have completely opposite responses to plasma perturbation. The power application almost simultaneously increases the average electron energy, further enhancing electron excitation. On the other hand, as the electrons are accelerated, the thermalized electron population diminishes and the probability of ion-electron recombination is lowered. Therefore, if electron excitation is the dominant mechanism, the 811.5 nm emission intensity would exhibit a positive response to the applied perturbation pulse; that is, the intensity would increase at the onset of the perturbation pulse. Otherwise, a negative response would strongly suggest ion-electron recombination-decay be the dominant excitation mechanism.

The experimental results, shown in Figure 2.8b, clearly show that the intensities undergo apparent decrease upon the onset of the perturbation pulse. Therefore, ion-electron recombination-decay is the predominant mechanism populating argon excited states during the afterpeak regime. As expected, the intensity increases after the perturbation pulse is terminated and ion-electron recombination is re-established. It is evident that the intensity increases are significantly delayed with respect to power termination, which can be presumably ascribed to the processes required for ion-electron recombination, i.e., electric field dissipation and electron thermalization. In this study, the delay period is found to be ~25 μs; however the accurate value can not be explicitly determined because of the signal distortion.

2.3.6. Metastable Argon Atomic Absorption Measurements

The metastable atoms of the discharge gas play very important roles in excitation and ionization; therefore, the population of metastable atoms and its production mechanism are of special interest. In this study, the population of the argon $^3P_2$ metastable state was monitored by measuring the absorbance at 811.5 nm and the results are shown in Figure 2.9.

The temporal responses of metastable argon atom $^3P_2$ population are found to be correlated with the respective argon atom emission profiles. Within the cathode dark space (0-1 mm, Figure 2.9a, b), the metastable population decreases as the discharge power pulse is turned off and then immediately increases at the onset of the perturbation pulse. These observations suggest that, as are the other excited states, the metastable state is populated predominantly by fast atom excitation inside the cathode dark space.

The afterpeaks were observed at distances of 3-10 mm (Figure 2.9c), indicating metastable argon atoms continue to form after power termination. As discussed earlier, the dominant excitation mechanism is ion-electron recombination followed by radiative decay. When the perturbation pulse is applied, electrons are energized and ion-electron recombination is suppressed. In addition, the energetic electrons depopulate metastable atoms via electron ionization and excitation (Figure 2.9d).

After the termination of the perturbation pulse, the metastable argon atom population recovers. The recovery is delayed with respect to the perturbation pulse termination. Note that the delay closely matches the emission signal delay observed in Figure 2.8b. That is, the metastable argon atom population starts to increase as soon as argon ion-electron recombination-decay re-initiates. The strong correlation provides additional evidence for the conclusion that recombination-decay mechanism is responsible for metastable atom formation in these plasmas.

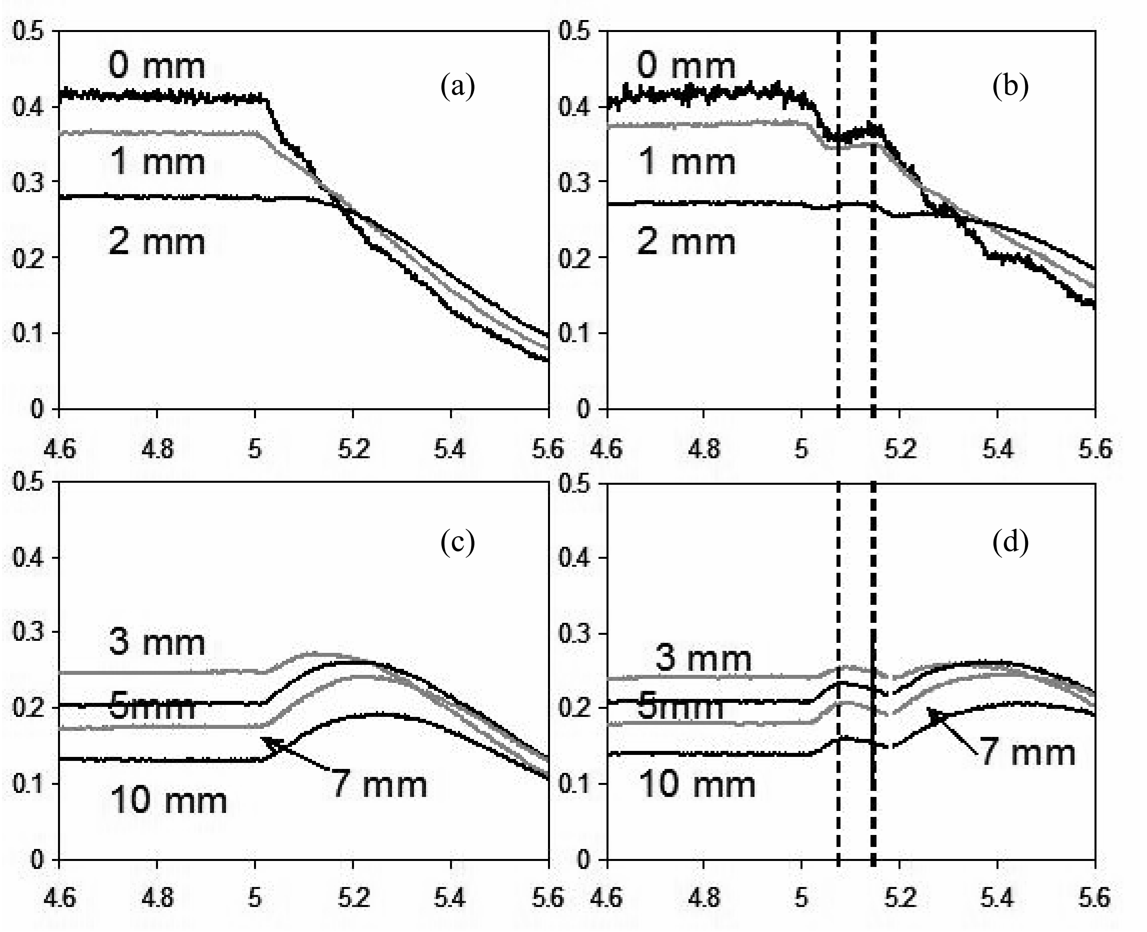

Figure 2.9. Temporal absorbance profiles of metastable argon atom at 811.5 nm for the normal pulsed glow discharge (a and c), and the pulsed glow discharge with the perturbation pulse applied between 5.05 ms and 5.15 ms (b and d).

2.3.7. Copper Atom Emission Measurement

The excited Cu atom group is represented by the emission at 368.7 nm which originates from 6d $^2D_{5/2}$ state (7.18 eV). Significant afterpeaks were found throughout the plasma after the power was terminated (Figure 2.10a). Atomic absorption measurements of copper revealed that the copper atom population in the plasma remains relatively stable during the same period because of the slow diffusion processes (Figure 2.11). Therefore, the afterpeaks can be readily attributed to the corresponding excitation mechanisms of copper.

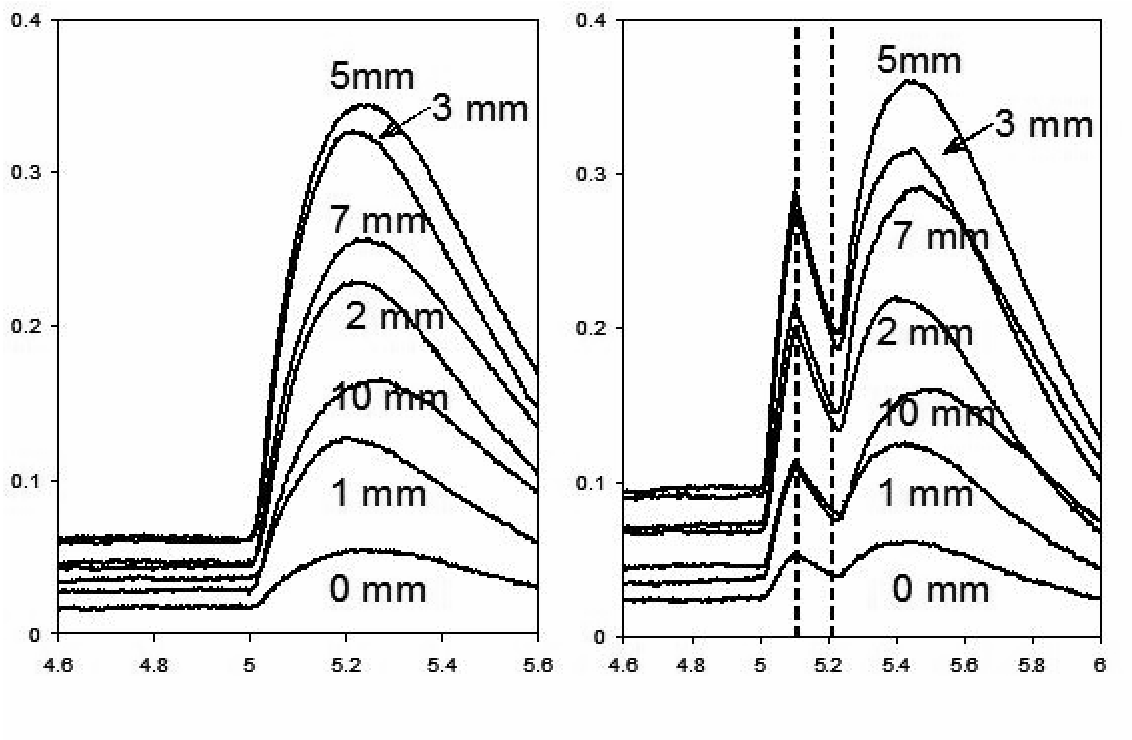

Figure 2.10. Temporal emission profiles of Cu I 368.7 nm line at various distances for (a) the normal pulsed glow discharge, and (b) the pulsed glow discharge with the perturbation pulse applied between 5.1 ms and 5.2 ms.

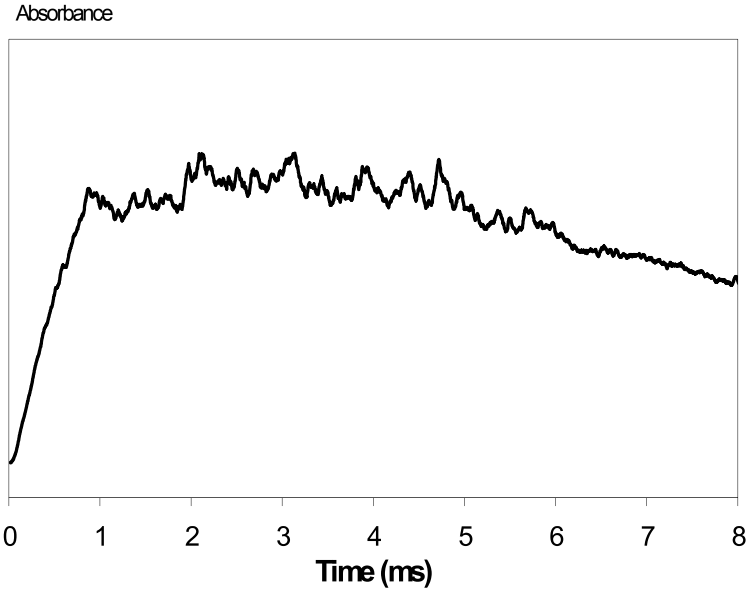

Figure 2.11. Typical temporal absorbance profile of copper atom at 324.7 nm in the normal pulsed glow discharge (sampling distance: 4mm).

Strauss et al. [8] also observed similar intensity increases and ascribed the increases to electron excitation. The energy pooling of a pair of metastable argon atoms can yield an electron carrying the extra energy of ~7 eV; the energetic electrons can subsequently excite copper atoms.

$Ar^m + Ar^m \rightarrow Ar^0 + Ar^+ + e^- + \Delta E$ where $\Delta E = 7.48$ eV

e^- (fast) + Cu^0 (ground) → Cu^* (Excited)

An alternative mechanism is similar to the recombination-decay of argon.[14] The increasing metastable argon atoms Penning ionize copper atoms directly, resulting in an upsurge of copper ions after power termination.[10, 12] The resultant copper ions recombine with thermalized electrons and subsequently populate the excited states of copper atom through radiative cascade decay.

$Ar^m + Cu^0 \rightarrow Ar + Cu^+$

$Cu^+ + e^-$ (slow) $\rightarrow Cu^*$ (excited)

Again, the dominant excitation mechanism can be determined by applying the perturbation method. Figure 2.10b shows the responses of the copper emission to the applied perturbation pulse. The onset of the perturbation pulse caused sudden and significant decreases in the intensities at various distances; the intensities start to increase after the pulse is terminated. However, unlike the argon excitation emissions, no spatial differences were observed. The negative responses strongly suggest that copper atoms are predominantly excited through ion-electron recombination-decay mechanism throughout the plasma. Shortly after the perturbation pulse is terminated, the copper emission intensities increase again. As has been observed in argon excited atom emissions, characteristic delays of ~25 μs can be observed for the re-increases with respect to the perturbation pulse termination.

Close examination reveals that the copper emission afterpeaks maximize at ~5.2 ms. As compared to the argon emissions, the maxima are delayed for ~0.1 ms, suggesting that the copper ion-electron recombination follows argon ion-electron recombination in time. Furthermore, the maximum positions and the breadths of the copper afterpeaks closely match those of the metastable argon atom population afterpeaks shown in Figure 2.9b. The close match suggests that the excited copper atoms are associated with metastable argon atoms: the copper ion population that undergoes further recombination-decay arises from Penning ionization during the afterpeak regime, rather than the residual copper ions from the plateau regime. [10, 12]

2.4. Conclusions

This study employed a peturbation method to probe the ionization and excitation processes within the afterpeak regime of a pulsed glow discharge plasma. The responses of various plasma species to the perturbation were measured using spectroscopic techniques. The experiments strongly suggest the following processes take place in sequence after the power termination.

1) electron thermalization;

2) argon ion-electron recombination-decay forming metastable argon atoms;

3) Penning ionization of copper atoms yielding copper ions;

4) copper ion-electron recombination-decay forming excited copper atoms.

During the chain of events, the plasma energy cascades from the argon ion (>15 eV) to the argon metastable state (>11.55 eV), to the copper ion (7.7 eV), and then to the excited copper atom. The downward energy flow arises from the plasma decay after power input is halted. Because radiative decay of metastable states is forbidden, these states serve as energy reservoirs; their populations undergo temporary increases during the decay process. Consequently, the energetic (11.55 and 11.72 eV) metastable atoms play a central role for ionization and excitation during the afterpeak regime.

The experiments also revealed valuable information regarding kinetics of the associated plasma processes, such as electron thermalization time. However, the signal distortion associated with the detection system prevents accurate measurements of these values. Future work will update the signal detection system to make accurate measurements possible.

2.5. References

(1) Harrison, W. W.; Barshick, C. M.; Kingler, J. A.; Ratliff, P. H.; Mei, Y., *Anal. Chem.* 1990**, 62*,*** 943A-949A.

(2) Chakrabarti, C. L.; Headrick, K. L.; Hutton, J. C.; Bicheng, Z.; Bertels, P. C.; Back, M. H., *Anal. Chem.* 1990**, 62*,*** 157-161.

(3) Walden, W. O.; Harrison, W. W.; Smith, B. W.; Winefordner, J. D., *J. Anal. At. Spectrom.* 1994**, 9*,*** 1039-1043.

(4) Pan, C.; King, F. L., *Appl. Spectrosc.* 1993**, 47*,*** 2096-2101.

(5) King, F. L.; Harrison, W. W., *Mass Spectrom. Rev.* 1990**, 9*,*** 285-317.

(6) Steiner, R. E.; Lewis, C. L.; King, F. L., *Anal. Chem.* 1997**, 69*,*** 1715-1721.

(7) Johnson, R. A.; McClure, B. T.; Holt, R. B., *Phys. Rev.* 1950**, 80*,*** 376-379.

(8) Strauss, J. A.; Ferreira, N. P.; Human, H. G. C., *Spectrochim. Acta.* 1982**, 37B*,*** 947-954.

(9) Klingler, J. A.; Savickas, P. J.; Harrison, W. W., *J. Am. Soc. Mass Spectrom.* 1990**, 1*,*** 138-143.

(10) Klingler, J. A.; Barshick, C. M.; Harrison, W. W., *Anal. Chem.* 1991**, 63*,*** 2571-2576.

(11) King, F. L.; Pan, C., *Anal. Chem.* 1993**, 65*,*** 735-739.

(12) Pan, C.; King, F. L., *J Am Soc Mass Spectrom* 1993**, 4*,*** 727-732.

(13) Jackson, G. P.; Lewis, C. L.; Doorn, S. K.; Majidi, V.; King, F. L., *Spectrochim. Acta* 2001**, 56B*,*** 2449-2464.

(14) Lewis, C. L.; Jackson, G. P.; Doorn, S. K.; Majidi, V.; King, F. L., *Spectrochim. Acta* 2001**, 56B*,*** 487-501.

(15) Biondi, M. A., *Phys. Rev.* 1951**, 83*,*** 1078-1080.

(16) Biondi, M. A., *Phys. Rev.* 1952**, 88*,*** 660.

(17) Biondi, M. A., *Physical Review* 1963**, 129*,*** 118-1188.

(18) Lewis, C. L.; Oxley, E. S.; Pan, C.; King, F. L., *Anal. Chem.* 1999**, 71*,*** 230-234.

(19) Majidi, V.; Moser, M.; Lewis, C.; Hang, W.; King, F. L., *J. Anal. At. Spectrom.* 2000**, 15*,*** 19-25.

(20) Steiner, R. E.; Lewis, C. L.; Majidi, V., *J. Anal. At. Spectrom.* 1999**, 14*,*** 1537-1541.

(21) Bates, D. R., *Phys. Rev.* 1950**, 78*,*** 492-493.

(22) Bates, D. R., *Phys. Rev.* 1950**, 77*,*** 718-719.

(23) Bogaerts, A.; Gijbels, R.; Jackson, G. P., *J. At. Anal. Spectrom.* 2003**, 18*,*** 533-548.

(24) Bydder, E. L.; Miller, G. P., *Spectrochim. Acta.* 1988**, 43B*,*** 819-829.

(25) Fey, F. H. A. G.; Stoffels, W. W.; van der Mullen, J. A. M., *Spectrochim. Acta* 1991**, 46B*,*** 885-900.

(26) Golubovskii, Y. B.; Lange, H.; Maiorov, V. A.; Porokhova, I. A.; Sushkov, V. P., *J. Phys. D* 2003**, 36*,*** 694-703.

(27) Scott, D. A.; V., P. A., *Physical Review A* 1991**, 43*,*** 3043-3056.

CHAPTER 3: Temporal and Spatial Variations in Molecular Energetics for $W(CO)_6$ in Pulsed Glow Discharge

3.1. Introduction

Chemical analyses in many fields demand a “multi-dimensional” knowledge of a given sample – the constituent components and the identity, structure, and elemental composition of each component. This need has been the driving force behind the development of methods for elemental speciation, i.e., the identification of elements and the chemical environment in a given sample.[1] The most popular approach to elemental speciation is to utilize chemical separation methods coupled with elemental or molecular characterization techniques for each constituent composition.[2] Mass spectrometry (MS) techniques are often the best choice for such characterization because they afford both the selectivity and sensitivity needed to achieve molecular identification, structural elucidation, or elemental determination. However, the kind of information provided by MS is critically dependent on the ionization method in use: “hard” ionization methods for elemental composition or molecular fragmentation, and “soft” ionization methods for molecular ion detection.

For purposes of chemical speciation, the choice between a “hard” ionization method, particularly one capable of producing atomic spectra, and a “soft” ionization method is one of ion source hardware that is not readily interchangeable. For example, the inductively coupled plasma (ICP) is a “hard” ionization method capable of providing sensitive and accurate elemental detection. This advantage arises from its ability to completely fragment analyte molecules to provide abundant atomic species.[3] Unfortunately, the destruction of molecular species automatically eliminates any possibility to obtain structural and molecular information from the same sample run. The determination of intact molecular ions is readily available using “soft” ionization methods such as electrospray ionization; but no structural and elemental information can be obtained directly with such “soft” ionization sources. Therefore, various methods have to be employed and the results have to be judiciously pieced together to achieve a complete characterization of a given sample. This inevitably increases requirements for analysis duration and costs, operator skills, and sample sizes. Furthermore, great difficulties arise from interfacing multiple detection techniques to chemical separation methods. These considerations have led us to explore a tunable ionization method that is capable of yielding molecular, structural, and elemental information.

The development of a tunable ionization method requires the ability to control the internal energy deposited into the analyte molecules. The quasi-equilibrium theory of unimolecular reactions [4] makes clear the role of the internal energy in ionization and fragmentation of molecular species. Excitation energy, in addition to any thermal energy present before ionization, can be transferred into the molecule during the ionization process or after the formation of the parent ion. The internal energy left in the parent ion can drive it to undergo further fragmentation through a series of competing and consecutive unimolecular reactions and exert a controlling influence on both the thermodynamics and kinetics of these reactions. The final product ions are determined by the molecular internal energy distribution, P(ε), of a population of the molecular species. Hence, tuning the internal molecular energy allows control of the degree of fragmentation, thereby optimizing the desired ion abundance for molecular, fragment, or elemental detection.

Internal energy deposition is determined by both the energy transfer process and the energetic species involved. A straightforward approach to tune the internal energy deposition is to switch energetic species. Faubert et al. [5] utilized metastable atoms of different inert gases for selective ionization and fragmentation. Hard ionization was achieved using the helium metastable atoms with high potential energies, around 20 eV, while soft ionization was achieved using krypton metastable atoms with lower potential energies, around 10 eV. O'Connor and co-workers [6] tuned a helium plasma by introducing isobutane as the chemical ionization reagent. Whereas the pure helium plasma provided atomic ions through hard ionization; it could be "softened" by the introduction of isobutene as a chemical ionization reagent owing to the predominance of ion-molecule reactions with analyte species. Electron ionization type spectra were obtained by carefully lowering the isobutene introduction rate. Unfortunately, this approach suffers from slow tuning speed and, hence, is not suitable for on-line detection for chemical separation methods.

Pulsed glow discharge (GD) plasmas may provide rapid energy tunability through temporal control of their plasma chemistry. Numerous energetic species, such as fast electrons, excited atoms, especially the long-lived metastable atoms, and ions generated in plasma sustaining processes, can transfer energy to analyte molecules through various processes including electron ionization, Penning ionization, and ion-molecule chemical reactions.[7] Each type of energetic species, associated with the corresponding energy transfer process, can excite the analyte molecules to a certain energy range, generating a characteristic internal energy distribution. In continuous GD plasmas, the internal energy distributions resulting from different energy transfer processes convolute together and present a quasi-steady state overall $P(\varepsilon)$. However, pulsed operation of the glow discharge affords the ability to separate these processes in temporal sequence: a prepeak regime dominated by electron ionization, an afterpeak regime dominated by Penning ionization, and a plateau regime resembling the continuous glow discharge.[8, 9] The temporal alternation of energy transfer processes results in a time-dependent $P(\varepsilon)$ that varies over a wide energy range. The consequence of this variation is a series of transient ionization periods for analyte molecules that range from “hard” to “soft” within each pulse cycle. Time-of-Flight (ToF) mass spectrometry allows for acquisition of resultant transient mass spectra in a quasi-simultaneous fashion, sometimes referred to as gated detection.[10] It is important to note that the plasmas can be easily pulsed at high frequencies, typically from 10 to 10^3 Hz, corresponding to data acquisition rates of 10-1000 spectra per second. The advantage in speed makes the pulsed GD ion source ideal for direct coupling to chemical separation methods.

Heterogeneous GD plasmas also exhibit spatial variations in P(ε). The population of each energetic species and the corresponding ionization process vary with location in the plasma.[11,12] Analyte molecules at each location are subject to a specific convolution of energy transfer processes, resulting in a unique P(ε). Moreover, the discharge operating parameters, especially the discharge gas pressure and operating power, can be used to selectively enhance or reduce a specific energy transfer mechanism and, consequently, to further adjust the P(ε) of the analyte molecules. The energy tunability signals significant analytical potential for the pulsed GD plasma as a tunable ion source.

The energy tunability of the pulsed GD plasma has been employed in elemental mass spectrometry to selectively ionize the analyte atom of interest while eliminating background and interfering ions. This analytical advantage was demonstrated by determination of calcium with argon as discharge support gas.[13] The tuanability of the pulsed glow discharge is also useful for molecular mass spectrometry where elemental, structural, and molecular information can be acquired in rapid succession. Microsecond[14] and millisecond[15] pulsed GD plasmas have exhibited their utility for chemical speciation when coupled with ToF-MS. The extent of fragmentation can be easily controlled at the discretion of the user by positioning the detection gate at the desired temporal regime. Lewis et al. [15] demonstrated the ability to couple a millisecond pulsed GD-ToF to a gas chromatography (GC) system for real-time chemical speciation. After GC separation, each constituent was introduced into the pulsed GD plasma, yielding analyte ions therein for mass spectrometric detection. Three time-gated data acquisition systems were used to obtain the spectra at the prepeak, plateau, and afterpeak regime within a pulse cycle, respectively providing elemental, structural, and molecular information in a nearly concurrent fashion. This system was successfully employed for chemical speciation of a sample containing a series of aromatic and halogenated compounds.

A systematic measurement of P(ε) is essential to understand the energetics that shape the tunability and utility of pulsed GD plasmas. Because P(ε) is a reflection of energy flow within the plasma, the measurement of P(ε) should afford additional insight into the ionization and excitation mechanisms taking place in the plasma. Furthermore, P(ε) measurements allow evaluation of the effect of GD parameters on plasma energetics in great detail and, consequently, optimization of analytical performance. Experimentally, P(ε) may be approximated using "thermometer molecules", such as $W(CO)_6$, as a probe.[16] $W(CO)_6$ molecules introduced into the plasma undergo ionization and subsequent dissociations of W-CO bonds. The consecutive losses of CO groups follow almost identical pathways without significant competing side reactions. The population of molecules with a certain internal energy prior to fragmentation is mirrored by the abundance of the respective product ion. Hence, the ion abundances of $W(CO)_n^+$ (n=0-6), which can be directly determined through mass spectrometric measurements, can be used to calculate the internal energy distribution of $W(CO)_6$

molecules. This method has been used to examine the molecular internal energy distributions in various ion sources.[17]

The studies reported here employ $W(CO)_6$ molecules to examine the temporal and spatial molecular internal energy distributions in a millisecond pulsed GD plasma. ToF-MS permits the monitoring of ions generated at a specific time, providing $P(\varepsilon)$ information for any instant during the pulse cycle. The spatially resolved $P(\varepsilon)$ were obtained from the mass spectra acquired at different distances along the plasma axial direction. Both temporal and spatial variations in $P(\varepsilon)$ were observed and correlated to the alternations of dominant energy transfer processes in the plasma. The effects of discharge pressure and operating power on $P(\varepsilon)$ were evaluated and attributed to the parametric influences on the respective fundamental energy transfer processes. The observations suggest that the pulsed GD plasma affords fast and facile energy-tunability that can be used to perform selective ionization and fragmentation for molecular, structural, and elemental information.

3.2. Experimental Section

Pulsed Glow Discharge Plasma Device. The GD plasma was powered by a 13.56 MHz radio frequency (rf) generator equipped with an automatic matching network (RF Plasma Product Inc., Marlton, NJ, USA). The power supply system was used under power-control pulsing mode that permits control of applied power, pulse width, and duty cycle. Throughout the experiments, the rf pulse width was set at 5 ms with

25% duty cycle while the operating power was varied. The argon discharge support gas (ultra pure, Airgas, Randor, PA) was introduced through a metering valve to control the gas pressure. The pressures were monitored by a thermocouple pressure gauge (Varian, Lexington, MA).

Tungsten Hexcarbonyl Introduction. Tungsten hexcarbonyl (99.9%, Aldrich, Milwaukee, WI) was used to probe the molecular internal energy distribution in the pulsed plasma. It was first vaporized in a glass vial immersed in a water bath held at 45 ^{o}C to maintain a constant vaporization rate as well as to ensure the identical initial molecular thermal energy for each run. The chemical vapors were then introduced into the GD chamber through a stainless steel tubing with 0.2 mm inner diameter to the point right in front of the sampling orifice (Figure 3.1). The introduction tubing and GD chamber were heated to 50 ^{0}C using heat tape to prevent the $W(CO)_6$ vapor from condensing. The flow rate of $W(CO)_6$ was regulated by a metering valve to keep the partial pressures of chemical vapors lower than 10 mTorr. This design was aimed to introduce a small amount of chemical vapor, minimizing perturbation of the plasma environment while ensuring abundant ion signals. The minimum perturbations were further confirmed from the resultant mass spectra as will be discussed in the next section.

ToF Mass Spectrometer. The ToF mass spectrometer (R. M. Jordan Company, Grass Valley, CA) has been described in detail previously [10] and is briefly introduced here. A high vacuum bellows (MDC Vacuum Products Co., Hayward, CA) served as the GD chamber. A copper disk cathode with a 5 mm diameter and 2 mm thickness, mounted on a direct insertion probe (DIP), was introduced into the discharge chamber to generate plasmas. The transportable DIP allows adjustment of the distance of the copper cathode from the ToF sampling orifice and the plasma can thereby be sampled at different distances along the axial direction (Figure 3.1).

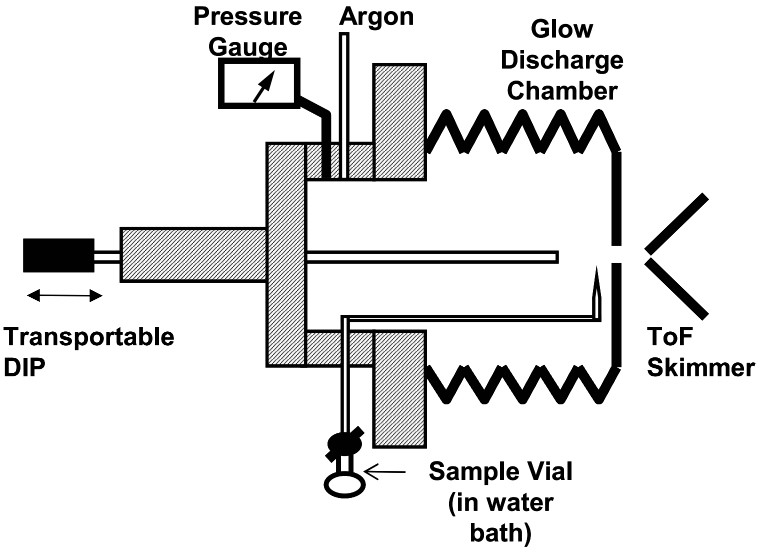

Figure 3.1. Schematic of the glow discharge ion source and the sample introduction system.

The orthogonal flight tube design of the ToF permits ion extraction from the GD source by pulsing the ToF repeller. A digital delay generator (EG&G Princeton Applied Research, Princeton, NJ), synchronized with the rf power pulse, subsequently triggers the application of an 1 μs ion extraction pulse to the ToF repeller as well as the initiation of the signal detection system. This timing scheme (Figure 3.2) allows for setting a detection gate to monitor the ions formed at a specific time within the power pulse sequence and its temporal position can be easily adjusted on the digital delay generator.

General operating conditions for the ToF mass spectrometer are presented in Table 3.1. The conditions were optimized to yield maximum signal for the $W(CO)_6$ species. The mass spectrometric signal was amplified and fed to a 1-GHz oscilloscope (LeCroy 9370M, Chestnut Ridge, NY), digitized and averaged for 150 sweeps. Through a GPIB interface, the averaged mass spectral data were imported into a Microsoft Excel 97 spreadsheet program (Microsoft, Redmond, WA) for construction of mass spectra. The mass spectra of $W(CO)_6$ were then converted to molecular internal energy distribution plots.

Table 3.1. Typical operating parameters used for the pulsed GD ToF-MS experiments.

Glow discharge	
Pressure	0.2 - 0.8 torr
Operating power	60 - 120 W
Pulse duration	5 ms
Duty cycle	25%
Sampling distance	3 – 40 mm
ToF	
Flight path length	1 m
Ion lenses potential	
Skimmer	-900 V
Extractor	0 V
Accelrator/flight tube	-2100 V
Deflector (X)	-2200 V
Deflector (Y)	-2100 V
Repeller	+200V; 1μs
Detector	-1800 V
Vacuum conditions	
Intermediate stage	10^{-5} Torr
Flight tube	10^{-6} Torr

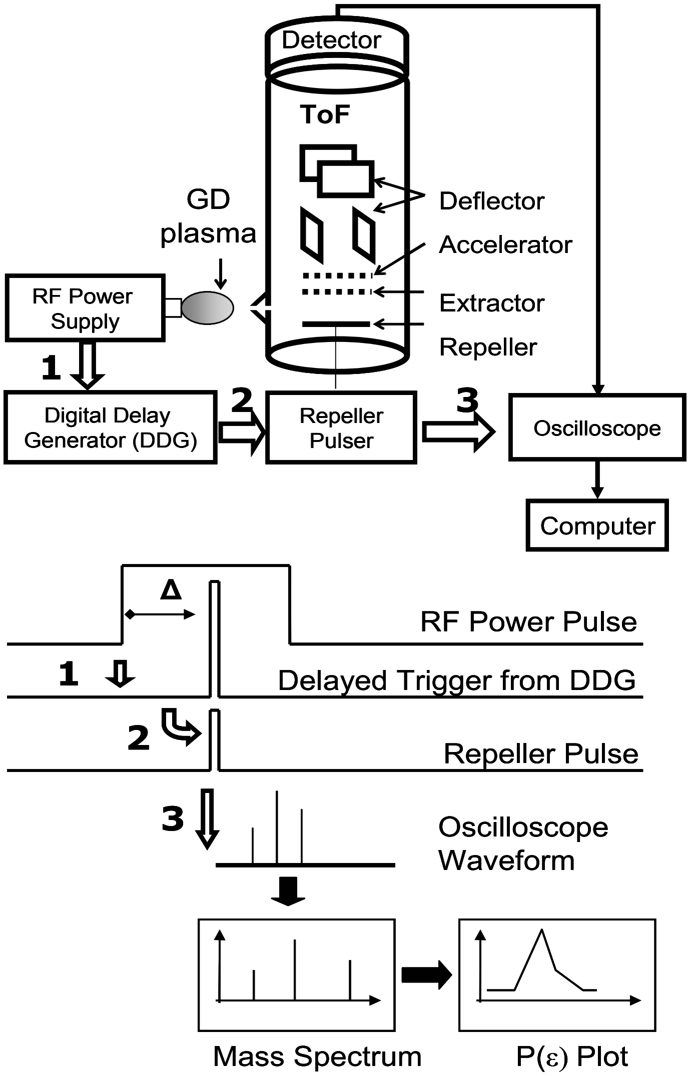

Figure 3.2. Schematics of the ToF mass spectrometer and the setup for time-gated detection. Hollow arrows represent the trigger sequence. The delay time (Δ) relative to the rf power onset can be adjusted on the digital delay generator.

3.3. Results and Discussion

3.3.1. Appearance of $W(CO)_6$ Mass Spectra and Calculation of P(ε).

A typical $W(CO)_6$ mass spectrum is presented in Figure 3.3a. The discharge gas species, such as Ar^+, $Ar^{2+}$and Ar_2^+ predominate the spectrum. Note that the Ar^+ intensity is about two orders of magnitude higher than the ion intensities of $W(CO)_n^+$ (n=0-6) species. The absolute dominance of discharge gas ions, which was observed in all the prepeak and plateau regime spectra, indicates the argon plasma environment is not significantly altered by the addition of the probing molecules. The Cu^+ signals at 63 and 65 amu originated from the copper cathode in use. Because of the deposition of carbon and tungsten ionic species, the cathode was partially coated during the experiments, resulting in poor sputtering of copper. Hence, the Cu^+ were only observed with low intensities. The $W(CO)_n^+$ (n=0-6) ion peaks were observed in the higher m/z range and can be readily assigned; but the isotope peaks for each species were not well resolved because the system was optimized for sensitivity rather than resolution. The maximum intensity of the isotope peaks was thus taken to calculate P(ε). Also observed were the small fragment ions, such as C^+, CH_x^+ and CO^+, presumably originating from $W(CO)_6$ molecules; however, these ions may suffer interference from contaminant gases like CO_2 and N_2.

In constructing P(ε) curves from mass spectral data, some standard assumptions were made.[16] First, all the molecules having sufficient internal energy underwent ionization and fragmentation to yield the corresponding final product ions. The kinetic effect was assumed to be negligible because of the long residence time of ions in the

GD ion source. Metastable molecular ions were not taken into consideration because they represent a small fraction of total ion population (typically less than 1%). Second, energy partitioning between electrons or neutrals and ionic fragments during ionization and fragmentation in the plasma are similar to that in electron ionization processes. Thus, the thermochemical data determined by the electron ionization method, i.e., the ionization and appearance potentials, were used without any correction. Third, the $W(CO)_n^+$ (n=0-6) species have identical sampling efficiencies and detection sensitivities. Hence, the signal intensity for each species directly reflects its relative ion population.

As listed in Table 3.2, $W(CO)_n^+$ species divide the energy range of 8.5-25.9 eV into 7 intervals with widths of ~2 eV each. Based on the assumption stated above, all molecules with internal energies inside a certain interval yield the corresponding product ions. For example, the molecules with internal energy between 16.0 and 18.6 eV generated $W(CO)_2^+$ ions. The relative population of these molecules was then obtained from the $W(CO)_2^+$ mass spectral signal. The relative population is divided by the width of the energy interval, 2.6 eV, yielding the distribution of the molecules within this energy interval that is assigned to its center at 17.3 eV. Following this procedure, the relative probabilities for all the energy intervals were calculated, yielding 6 data points. Connecting these points approximates the internal energy distribution $P(\varepsilon)$ as can be seen in Figure 3.3b. It is also important to realize that the area covered by the $P(\varepsilon)$ plot reflects the total ion population within the respective energy range.

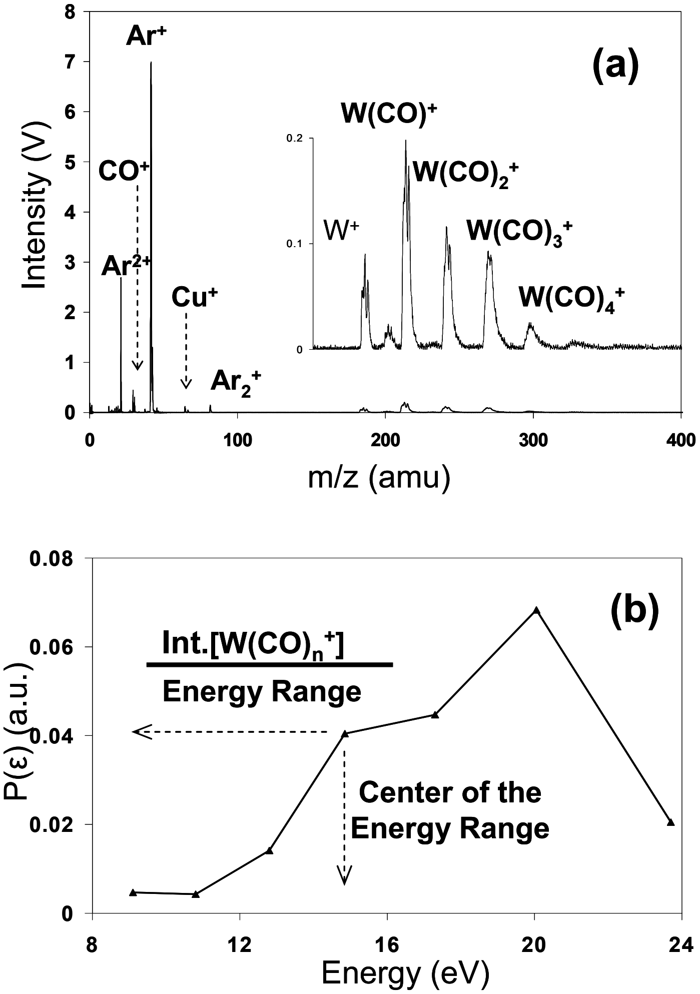

Figure 3.3. (a) $W(CO)_6$ mass spectrum and (b) the resultant P(ε) plot (discharge pressure 0.5 Torr, operating power 100 W and sampling distance 5 mm).

Table 3.2. $W(CO)_6$ ion energetics data.

Ions	Ionization/ Apparence Potential (eV)	Energy Interval (eV)	Average Energy (eV)	Energy Width (eV)
$W(CO)_6^+$	8.5	8.5 – 9.7	9.1	1.2
$W(CO)_5^+$	9.7	9.7 – 11.9	10.8	2.2
$W(CO)_4^+$	11.9	11.9 – 13.7	12.8	1.8
$W(CO)_3^+$	13.7	13.7 – 16.0	14.85	2.3
$W(CO)_2^+$	16.0	16.0 – 18.6	17.3	2.6
$W(CO)^+$	18.6	18.6 – 21.5	20.05	2.9
W^+	21.5	21.5 – 25.9	23.7	3.4
$W(C_2O)^+$	25.9	-	-	-

This simple method allows estimation of molecular internal energies between about 9 eV and 24 eV; the range is limited by the ionization potential of $W(CO)_6$ and the appearance energy of W^+. Energy shifts of about 2 eV can be readily appreciated on the resultant P(ε) plots, although the fine structure of P(ε) is not available. It has been shown that the apparent ionization energy of GD plasmas varies roughly between 27.7 eV and 8.4 eV over a pulse cycle.[1] Hence, the method affords satisfactory monitoring range and sensitivity for the GD plasma energetics studies.

3.3.2. Temporal Characteristics of P(ε) over a Pulse Cycle.

The GD plasma was operated at 100 W rf power, 0.4 Torr argon and sampled at 15 mm from the cathode surface. A series of time-resolved mass spectra of $W(CO)_6$ were acquired over the pulse cycle and converted into P(ε) plots. Based on the observed temporal variations in the mass spectra and the corresponding P(ε) plots, a cycle of the pulsed GD plasma can be divided into three major temporal regimes: the breakdown and transition stage (0-1.0 ms), the steady state stage (1.0-5.0 ms), and the decay stage after power termination (5.0-7.0 ms). The three distinct stages were termed as the prepeak, plateau, and afterpeak regime respectively.[8]

Prepeak regime. The prepeak regime includes a series of fast evolving spectra and P(ε) plots and exhibits a significant energy shift (Figure 3.4). After the application of the rf power, a brief delay is required for the plasma to be initiated. The first stable mass spectrum was acquired at 0.2 ms into the pulse cycle, presumably representing the breakdown of the plasma. Extensive fragmentation was observed, leading to the formation of small fragments such as $W(CO)^{+}{}_{3}$, $W(CO)_2^+$, and $W(CO)^+$, along with a dominant signal of the atomic ion W^+. The molecular ion $W(CO)_6^+$ and larger fragments, $W(CO)_4^+$ and $W(CO)_5^+$, were not present in the spectrum. This observation indicates that, at the breakdown stage, energy deposited into the molecules within the plasma is sufficient to dissociate them to their atomic constituents. The resultant P(ε) shows that the internal energies are populated over the 15-24 eV energy range. The P(ε) is cut off sharply at ~13 eV and has essentially no population at lower energies.

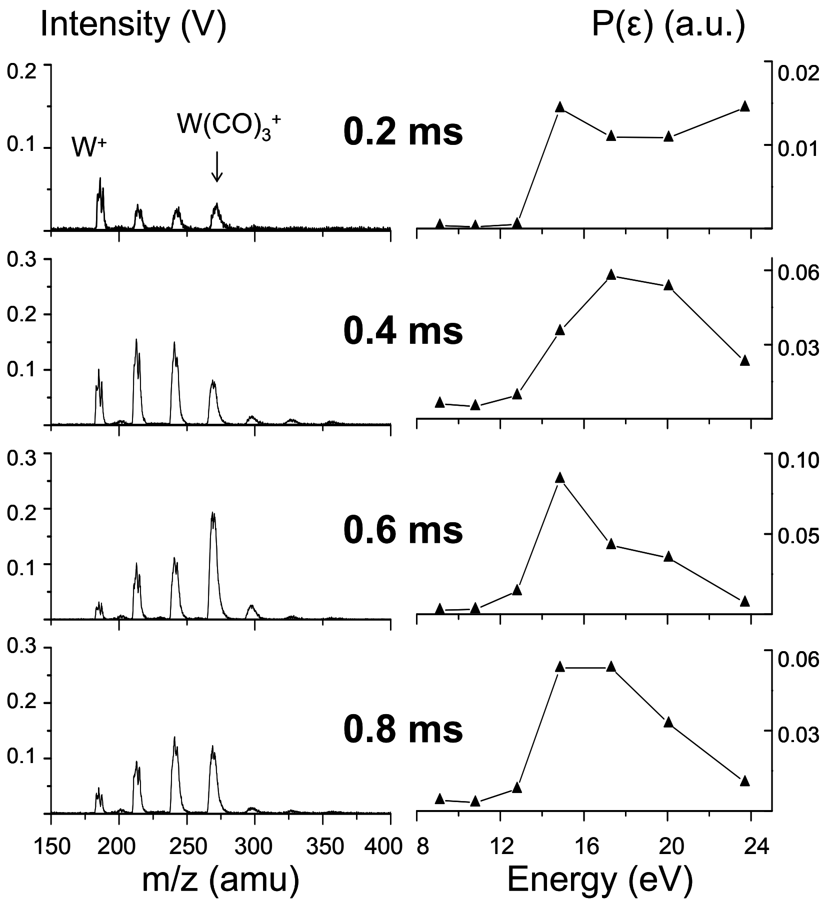

Figure 3.4. Time resolved mass spectra and the corresponding P(ε) plots during the prepeak regime (discharge pressure 0.4 Torr, operating power 100 W, and sampling distance 15 mm).

The prepeak has been characterized by the sudden increases in ion signal intensity for the gas phase species before decaying to plateau values.[8] Since electron ionization is the only possible mechanism in the breakdown stage, the intensity increases were ascribed to the upsurge of energetic electrons and their high ionization efficiency. In this study, the enhanced intensity was also observed for both argon and

$W(CO)_6$ species, as can be seen in plots of ion intensity temporal variation (Figure 3.5). In addition to the enhanced intensities, the prepeak regime is also associated with high internal energy deposition ranging from 15 eV to 24 eV. The observed P(ε) differs significantly from the known P(ε) of $W(CO)_6$ activated by standard 70 eV electron ionization that maximizes around 9 eV and 15 eV.[18] The differences suggest that, although electron ionization was the major ionization mechanism, the upsurge of fast electrons generated at discharge breakdown stage may be of much higher kinetic energies, resulting in more extensive fragmentation and even atomization.

The mass spectra from 0.4 ms to 0.8 ms reflect the transition phase from the discharge breakdown to a steady state. Significant changes were observed during this phase. Larger fragments, $W(CO)_n^+$ (n=4-6) species, became observable in the mass spectra, indicating the P(ε) broadens and extends over the lower energy range. Meanwhile, the base peaks in the mass spectra shifted gradually from W^+ to $W(CO)_3^+$; correspondingly the P(ε) maximum shifted from 24 eV to 15 eV. Note that the mass spectra and P(ε) plot acquired at 0.8 ms closely resemble those acquired in the plateau regime (Figure 3.6), indicating the convergence to the steady state plasma.

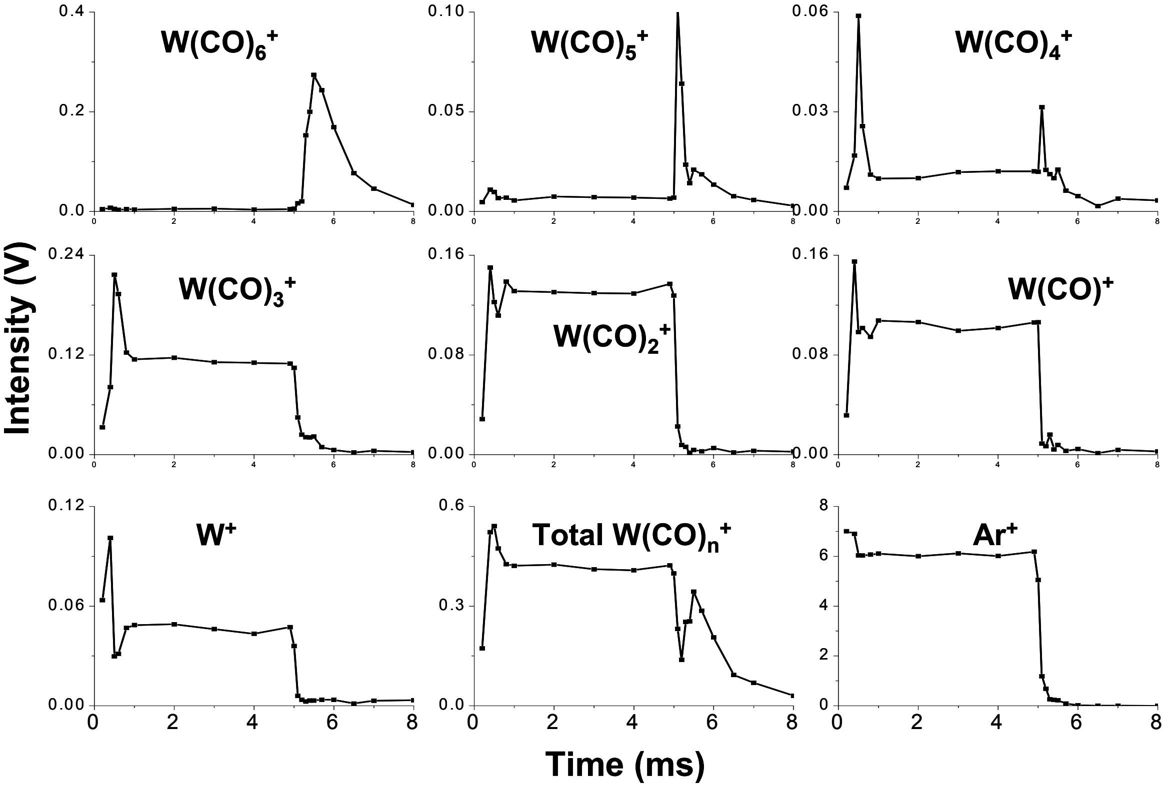

Figure 3.5. Temporal intensity variations over a pulse cycle for the ions of interest (discharge pressure 0.4 Torr, operating power 100 W and sampling distance 15 mm).

The changes in the mass spectra and P(ε) observed in the transition phase can be largely attributed to the changes in ionization mechanisms therein. Shortly after the discharge gas breaks down, the charged particles redistribute as space charge builds up, resulting in the typical GD plasma architecture. The electric field is compressed within the dark space close to the cathode surface while the negative glow region, where ions were sampled, becomes nearly field-free.[7] As a result, both the population and kinetic energy of fast electrons in the negative glow region decrease. Meanwhile, discharge breakdown leads to the formation of argon ions and metastable argon atoms available for charge transfer and Penning ionization processes. As will be discussed in detail later, the energy deposition from charge transfer[19] and Penning ionization [5] processes maximize at the potentials of argon ions (15.76 eV) and metastable argon atoms (~11.6 eV) respectively. The increasing contribution from charge transfer and Penning ionization process, in combination with declining electron ionization, shifts the P(ε) maximum to lower energy as well as broadens the P(ε) range.

Plateau Regime. The plateau mass spectra and P(ε) plots between 1.0 ms and 5.0 ms are essentially identical, indicating a steady state (Figure 3.6). All the $W(CO)_n^+$ (n=1-6) species are present in the mass spectra and the abundant species are $W(CO)_3^+$, $W(CO)_2^+$ and $W(CO)^+$. The P(ε) plots covers the full monitoring range from 8 eV to 24 eV with maxima around 16 eV. The distribution falls off sharply at 13 eV and presents a low probability tail over the 8-12 eV range.

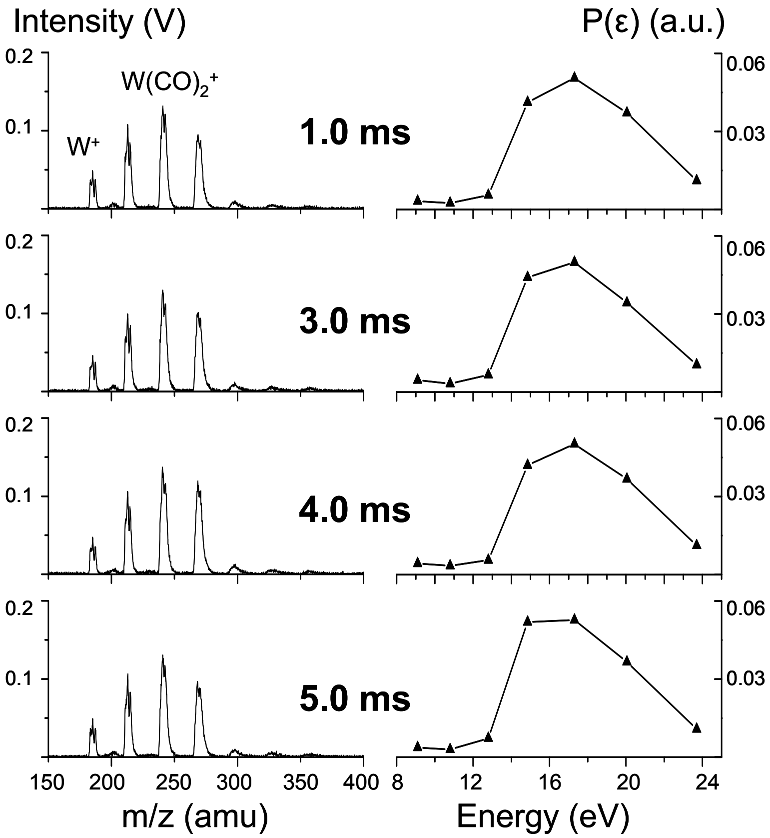

Figure 3.6. Time resolved mass spectra and the corresponding P(ε) plots during the plateau regime (discharge pressure 0.4 Torr, operating power 100 W, sampling distance 15 mm).

The steady state of a pulsed glow discharge resembles its continuous counterpart and the energy transfer processes involved have been thoroughly discussed.[7] Electron ionization, Penning ionization, and charge transfer processes are the major ionization mechanisms within the negative glow region. Electron ionization arises principally from the fast electrons entering the negative glow region from the cathode dark space. Penning ionization is a major ionization mechanism for species with ionization potentials lower than the energy levels of metastable argon atoms. Smith et al. observed that in the steady state plasma, Penning ionization accounts for 40-80% of the ionization of sputtered species;[20] it is thus expected to play an important role in $W(CO)_6$ ionization and excitation as well. Charge transfer processes of Ar^+ with $W(CO)_6$ result in an energy distribution between 13 eV to 20 eV with the maximum around argon's ionization potential at ~15 eV. [19]

Besides the ionization processes, internal energy can be deposited by various excitation processes as well. Among them, collision induced dissociation (CID) and electron excitation are expected to play major roles. The kinetic energy of ions in the negative glow is about 15 eV [21] and hence, could effect low-energy collision induced dissociation. It is well known that multiple low-energy collisions are able to deposit sufficient internal energy to cause extensive fragmentation.[17] Therefore, CID in the plasma may be so effective that the $P(\varepsilon)$ can be shifted significantly toward higher energy, especially under high discharge pressures. Because electrons in the negative glow region have an average energy of 2-4 eV,[7] they can also excite molecules through inelastic collisions, leading to an appreciable $P(\varepsilon)$ shift. Photo-excitation, although possible, is not considered as a major excitation mechanism since its cross section is 2-3 orders of magnitude smaller than those of CID and electron excitation.[22] On the other hand, the excited $W(CO)_6$ species can also be de-excited through stabilizing collisions with ground state atoms in the plasma.[23]

Afterpeak Regime. The first three milliseconds after the termination of applied power pulse exhibit another fast evolving transition phase as indicated by the dramatic changes in the mass spectra and P(ε) plots (Figure 3.7). The signal intensities of small fragment ions, such as W^+, $W(CO)^+$, and $W(CO)_2^+$, decayed sharply while $W(CO)_4^+$ and $W(CO)_5^+$ subsequently became the base peak. Correspondingly, the P(ε) maximum quickly shifted toward the lower energies while the population over the high energy range declined to a negligible level. At 5.3 ms, the $W(CO)_6^+$ became the strongest peak increasing its intensity until it maximized at 5.5 ms and slowly decayed into the background level at 8 ms. The P(ε) maximum shifted to about 9 eV at 5.3 ms and remained steady thereafter.

The termination of applied rf power initiates a series of physicochemical processes, greatly altering the plasma environment and, consequently, the ionization and excitation processes therein. Upon the disappearance of the electric field, electrons in the plasma thermalize within 0.1 millisecond[24] (also Chapter 2 in this document), which not only directly suspends the electron excitation and ionization processes, but also creates prerequisite conditions for ion-electron recombination. As a direct consequence of the recombination, the Ar^+ population, as evidenced by the ion intensity (Figure 3.5), suffered a sharp decrease upon the power termination, eliminating charge transfer from being a major ionization mechanism in the afterpeak regime. Meanwhile, the recombination of argon ions and electrons followed by radiative decay produces a large population of metastable argon atoms, which in turn greatly enhances Penning ionization [12] to the point that it becomes the dominant ionization process in the afterpeak regime.[25]

Penning ionization has been studied thoroughly by Stedman and Setser.[26] Owing to the near-thermal nature of metastable atoms, the maximum energy deposition by Penning processes is limited by the potential energies of the metastable atoms, i.e., 11.55 eV for $^3P_2$ and 11.62 eV for $^3P_0$ Ar. However, the effective energy deposition can be significantly less than these potential limits because the electron ejected during Penning ionization can carry away the energy difference to satisfy the energy conservation requirements. It is therefore reasonable to assign the P(ε) maximum at 9 eV to Penning ionization.

The temporal variation of $W(CO)_n^+$ intensities (Figure 3.5) provides further evidence for Penning ionization as the dominant ionization mechanism during the afterpeak. Energetically, the $W(CO)_n^+$ species can be divided into two groups: the species with ionization or appearance potential lower than, or very close to, the argon metastable potentials, including $W(CO)_6^+$, $W(CO)_5^+$, and $W(CO)_4^+$; and the others which have significantly higher appearance potentials (Table 3.2). As can be seen in Figure 3.5, the first group, $W(CO)_6^+$, $W(CO)_5^+$, and $W(CO)_4^+$, exhibit strong intensity surges after the termination of the pulse while the species in the second group exhibit intensity decreases. This correlation strongly suggests that the increase in the metastable argon atom population during the afterpeak regime is primarily responsible for the ion production. Penning ionization is known as a very efficient energy transfer process with cross-sections approaching the gas kinetic values.[26] The increased ionization efficiency and decreased variety of product ions explain the observed intensity surge during the afterpeak regime.

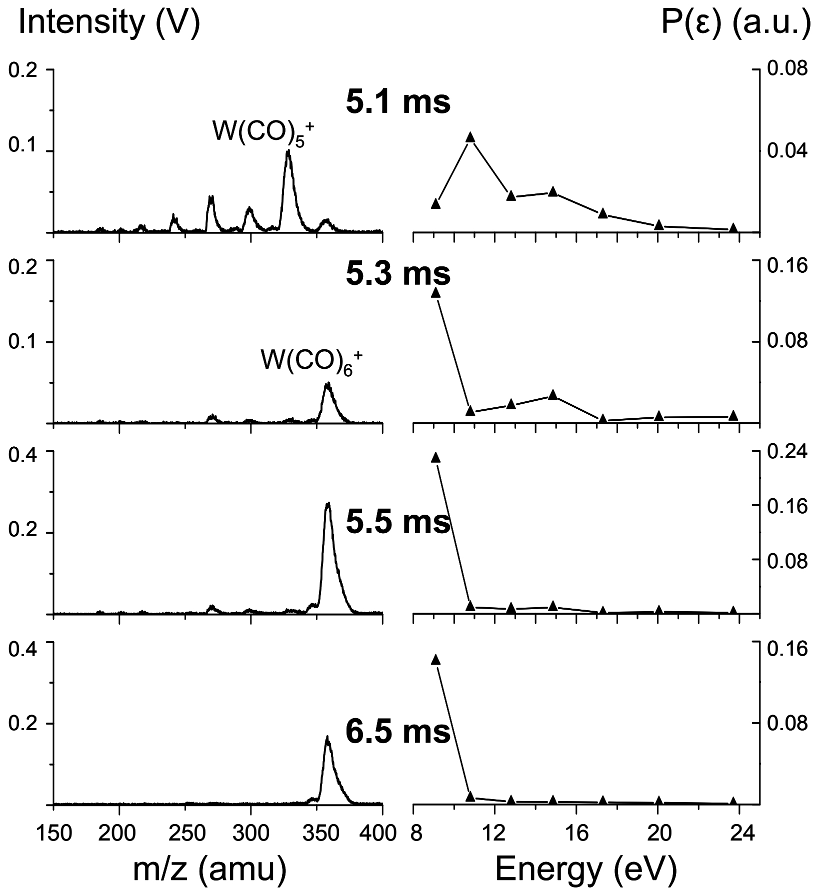

Figure 3.7. Time resolved mass spectra and the corresponding P(ε) plots during the afterpeak regime (discharge pressure 0.4 Torr, operating power 100 W, and sampling distance 15 mm).

Other ionization mechanisms may also take place in the afterpeak regime. Ion-molecule reactions may take place between $W(CO)_6$ molecules and the ions generated during the plateau regime such as CH_x^+. Proton transfer from ArH^+ [27] is also very likely, but can not be confirmed by this study because the quasi-molecular ion $W(CO)_6 \bullet H^+$ could not be identified under the low resolution conditions employed. Note that these mechanisms are of a chemical ionization nature, preferably producing molecular or quasi-molecular ions. Hence, the apparent energy deposition reflected on the P(ε) plot is around the ionization potential of $W(CO)_6$ at about 9 eV as well.

Briefly, The P(ε) of $W(CO)_6$ exhibits temporal variations over a pulse cycle, arising from the alternation of dominant energy transfer processes in the plasma. The P(ε) variations divide a pulse cycle into three distinct temporal regimes: prepeak, plateau, and afterpeak, and their representative instants, i.e. 0.2 ms, 4.0 ms, and 5.6 ms respectively, are established for the following spatial characterization and parametric studies.

3.3.3 Spatial Characteristics of P(ε)

It is known that the glow discharge plasma is spatially heterogeneous: each species has a characteristic spatial distribution and, as a direct consequence, the corresponding excitation and ionization processes exhibit spatial variations. As a result, the P(ε) of $W(CO)_6$ in the plasma is expected to be spatially dependent. The spatial characteristics of P(ε) directly determine the mass spectra obtained at different locations in the plasma.

The spatial characteristics of P(ε) were examined for the prepeak (0.2 ms), plateau (4.0 ms), and afterpeak (5.6 ms) regimes separately under conditions of 0.5 Torr discharge pressure and 120 W operating power. The sampling distance was adjusted by varying the separation between the sampling plate and the cathode. However, when the sampling plate was placed in close proximity to the cathode, the dark space was distorted and the discharge extinguished. The minimum sampling distance is roughly twice the dark space thickness[7], and was found at 3 mm for this set of discharge conditions. The sampling location corresponds to the negative glow region, which is nearly field-free, and the grounded sampling plate is not expected to impose great effect on the plasma. The obtained spectrum mirrors the local ion population closely because the sampled ions are produced in the immediate proximity of the sampling orifice.[28]

Prepeak regime. The mass spectra acquired at 0.2 ms at different distances are analogous and only the one obtained at 3 mm is shown in Figure 3.8a. The atomic ion, W^+, and small fragment ions, $W(CO)_n^+$ (n=1-3), dominate the spectrum while the molecular ion and larger fragments were not observed. The P(ε) plots presented in Figure 3.8b, corresponding to various sampling distances, exhibit nearly identical internal energy distributions: the deposited energies are populated over 15~24 eV and there is essentially no population over lower energies. This observation is consistent with the conclusion previously drawn that electron ionization dominates during the prepeak regime. The strong similarities in P(ε) plots also suggest that the electron energy remains fairly uniform throughout the plasma.

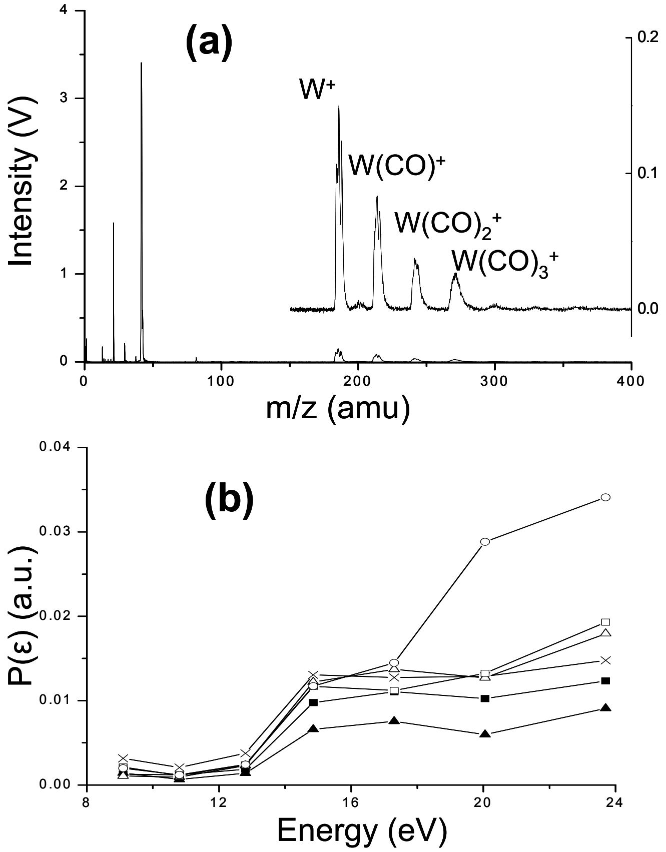

Figure 3.8. (a) Prepeak mass spectrum acquired at 5 mm and (b) prepeak P(ε) plots obtained at 3 mm (○), 5 mm (Δ), 10 mm (□), 15 mm (x), 20 mm (■), and 30 mm (▲) (discharge pressure 0.5 Torr and operating power 120 W).

Plateau regime. The observed P(ε) exhibit strong spatial dependence during the plateau regime. The mass spectra and P(ε) plots at various sampling distances are presented in Figure 3.9. The P(ε) maxima shifted dramatically as distance increases. At 3 mm, P(ε) maximized at 20 eV. As distance increased from 3 mm to 10 mm, the population around 15 eV increased, resulting in a broad P(ε) covering energy range from 12 eV to 20 eV. When sampling distance further increased, the population around 20 eV dropped and that around 15 eV remained relatively stable, leading to an apparent low-energy shift of P(ε) maximum. Eventually, at 30 mm, the P(ε) maximum shifted to ~12 eV.

The P(ε) shift can be largely attributed to the spatial characteristics of the ionization and excitation mechanisms occurring in the plasma during the plateau regime. The major ionization and excitation processes exhibit different spatial dependences. Langmuir probe measurements showed that the argon ion population maximizes at roughly the edge of dark space and negative glow.[29] Charge transfer is expected to overlap with the maximum argon ion population. This hypothesis has been confirmed by an optical investigation performed in this lab, in which charge transfer processes were found to maximize at ~5 mm and decreased sharply with increasing distance. [30] Penning ionization, however, exhibits a different spatial profile because the metastable argon atom density is distributed more evenly throughout the negative glow region.[11] For this reason, Penning ionization is expected to exhibit a more moderate decrease with increasing distance. Electron ionization and excitation is observed to maximize at a distance of 2.5 mm from the cathode surface and decrease with increasing distance.[12]

On the other hand, CID is expected to be independent of sampling distance because of the fixed discharge pressure and the relatively uniform ion kinetic energy in the negative glow region.

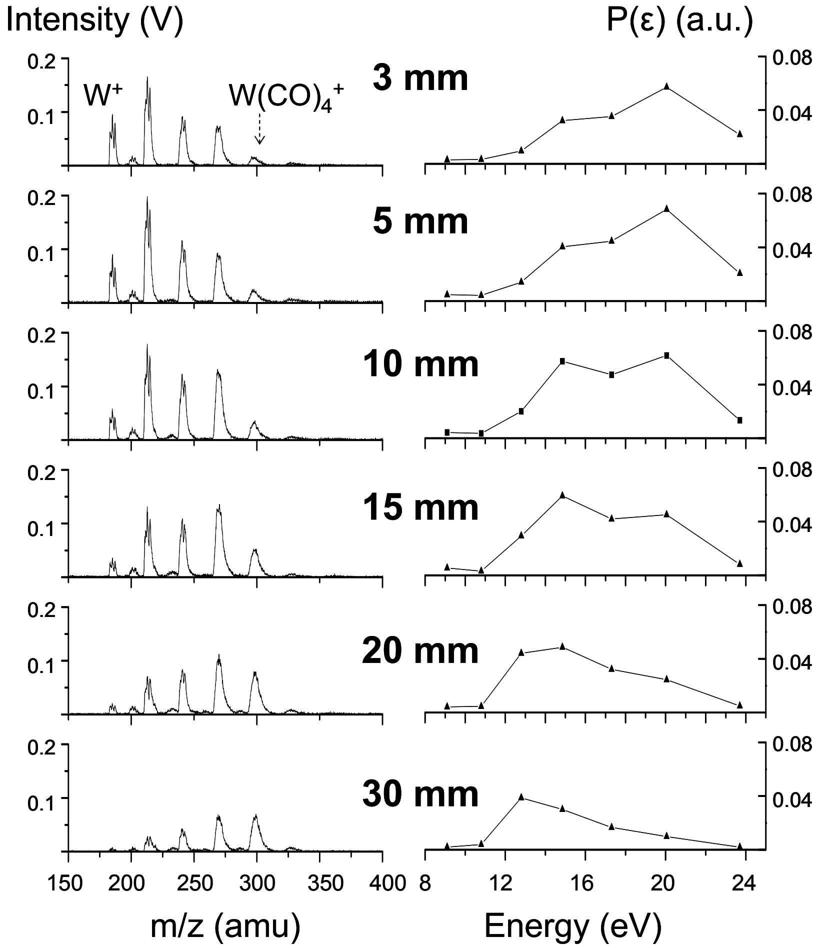

Figure 3.9. Plateau mass spectra acquired at various distances and the corresponding P(ε) plots (discharge pressure 0.5 Torr and operating power 120 W).

The spatial dependence of the ionization and excitation processes result in different convolutions of these energy transfer processes at various distances, leading to changes in the overall P(ε). Close to the vicinity of the cathode surface, charge transfer processes in combination with strong electron excitation processes result in high-energy deposition. At greater distances, the less energetic Penning ionization process becomes more important for ionization because both charge transfer and electron excitation decay sharply with increasing distance. This results in a shift of the P(ε) maximum to lower energies. As distance further increases, Penning ionization eventually prevails over charge transfer processes, resulting in a P(ε) maximum at 12.5 eV and a relatively low probability tail over the higher energy range.

Afterpeak regime. As previously discussed, the afterpeak regime is dominated by Penning ionization throughout the plasma. Therefore, little change in P(ε) is expected for various sampling distances during this regime. The mass spectra acquired throughout the plasma exhibit an intense molecular ion $W(CO)_6^+$ peak while the fragment ions are not evident. The mass spectrum obtained at 15 mm is shown in Figure 3.10a as a representative illustration. The corresponding P(ε) plots (Figure 3.10b) show that the deposited internal energies are distributed around 9 eV throughout the plasma and there is essentially no population at higher energies. One exception was found at 3 mm where considerable $W(CO)_3^+$ signal was observed, leading to a local P(ε) maximum around 15 eV. This exception can be attributed to charge transfer from the residual argon ions. This assumption was supported by the gradual disappearance of the $W(CO)_3^+$ ions as the detection gate was further delayed to allow additional time for the neutralization of these residual argon ions.

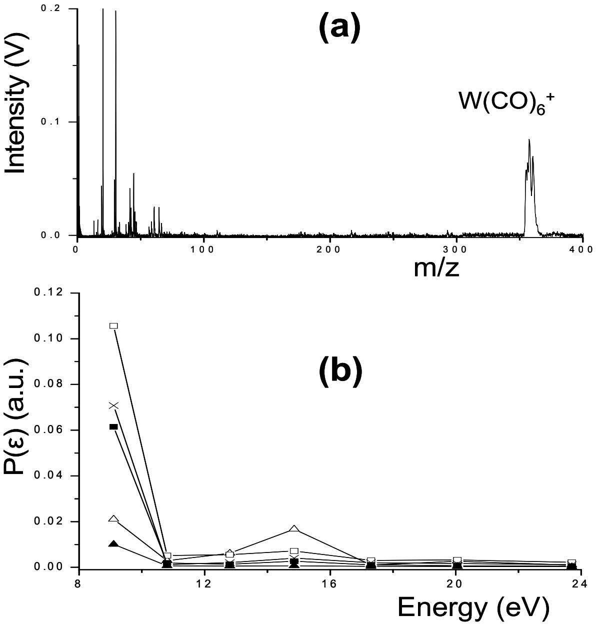

Figure 3.10. (a) Afterpeak mass spectrum acquired at 15 mm and (b) the afterpeak P(ε) plots at 5 mm (Δ), 10 mm (□), 15 mm (x), 20 mm (■), and 30 mm (▲) (discharge pressure 0.5 Torr and operating power 120 W).

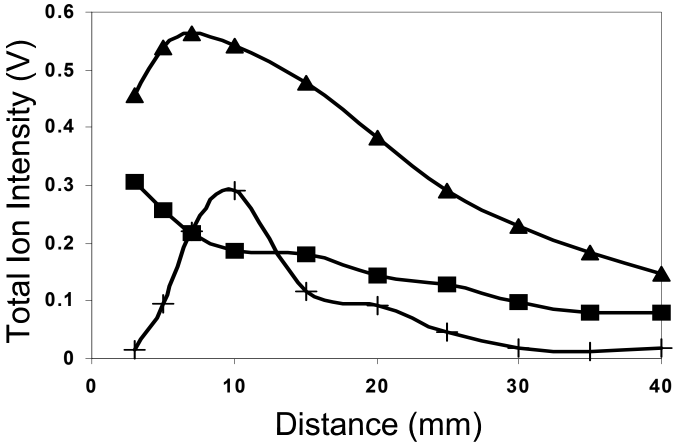

Figure 3.11. Spatial variation of the total $W(CO)_n^+$ ion intensity during the prepeak (■), plateau (▲), and afterpeak regime (+) (discharge pressure 0.5 Torr and operating power 120 W).

It should be pointed out that the spatial dependences of P(ε) described above were also observed under discharge pressures of 0.4-0.6 Torr and operating powers of 60-120 W. Different phenomena were observed for the extreme low (<0.3 Torr) and high (>0.8 Torr) pressures and the detailed results will be given in the following pressure effect discussion.

It is also important to examine the spatial dependence of the ion population because it determines the optimum sampling distance to maximize analytical sensitivity. Judging from the areas covered by the P(ε) curves, the ion population changes significantly with distance. In order for an explicit examination, the total ion signal intensities of $W(CO)_n^+$ (n=0-6) were plotted against sampling distance for the prepeak, plateau, and afterpeak regime (Figure 3.11). For the prepeak, the total ion intensity maximized at the minimum sampling distance (3 mm) and declined monotonously as distance increased, which is consistent with previously observed spatial profile for electron ionization and excitation.[12] This is the result of the existence of a strong electric field in the vicinity of the cathode that produces a large population of energetic electrons. In contrast, the total ion intensity during the plateau regime exhibits a maximum at ~7 mm, which may indicate that the combination of various ionization processes is optimized here. During the afterpeak, the intensity maximum is found farther away from the cathode at ~10 mm. Atomic absorption measurements performed in this lab observed that the maximum metastable argon atom density occurs at ~8 mm during the afterpeak regime.[11] This is also where the most intensive Penning ionization was observed for the sputtered copper atoms.[12] The qualitative agreement among these maxima substantiates Penning ionization as the predominant ionization mechanism for $W(CO)_6$ molecules during the afterpeak regime.

3.3.4 Parametric Effects on P(ε).

Discharge parameters, especially discharge pressure and operating power, strongly influence the respective excitation and ionization processes. These parameters can be adjusted to enhance or suppress a specific excitation or ionization mechanism, which would be subsequently reflected in the resultant internal energy distribution P(ε). Insights into the fundamental plasma processes can then be inferred from the responses of P(ε) to the parametric variations. This methodology is particularly useful in deconvoluting the concurrent mechanisms occurring during the plateau regime. The parametric effect study is important for the real-world applications of the plasma as well. Varying the discharge parameters affords capability to further tune the energy deposition, providing additional flexibility to optimize analytical performance for a given sample.

3.3.4.1 The Effects of Pressure on P(ε)

The discharge pressure determines the mean free path and collision frequency. Therefore, it is expected to have a strong influence on the energy transfer processes and the resultant P(ε). An investigation of the pressure effect was conducted for discharge pressures ranging from 0.2 to 0.8 Torr. In these studies, the operating power was fixed at 100 W and the sampling distance was fixed at 15 mm.

Figure 3.12a shows, during the prepeak regime, the P(ε) plots at various pressures show some similarities: the internal energy distributions appear higher than 15 eV and have essentially zero distribution below 13 eV. As discussed above, these high deposition energies are attributed to the energetic electron processes. In spite of the similarities, a clear shift in P(ε) toward higher energies can be readily observed as operating pressure increases. The apparent high-energy shifts at elevated pressures, which were also observed during the plateau and afterpeak regime, likely arise from increases in CID taking place within the plasma or during the sampling processes at these higher pressures. Elevated pressures increase collision frequency in the plasma to consequently increase the apparent internal energy deposition. The CID effect has also been reported in several previous accounts.[31]

As can be seen in Figure 3.12b, the discharge pressure exerts an strong influence on P(ε) in the plateau regime. Of course the situation is complicated because of the variety of excitation and ionization processes occurring and their uneven response to pressure increases.

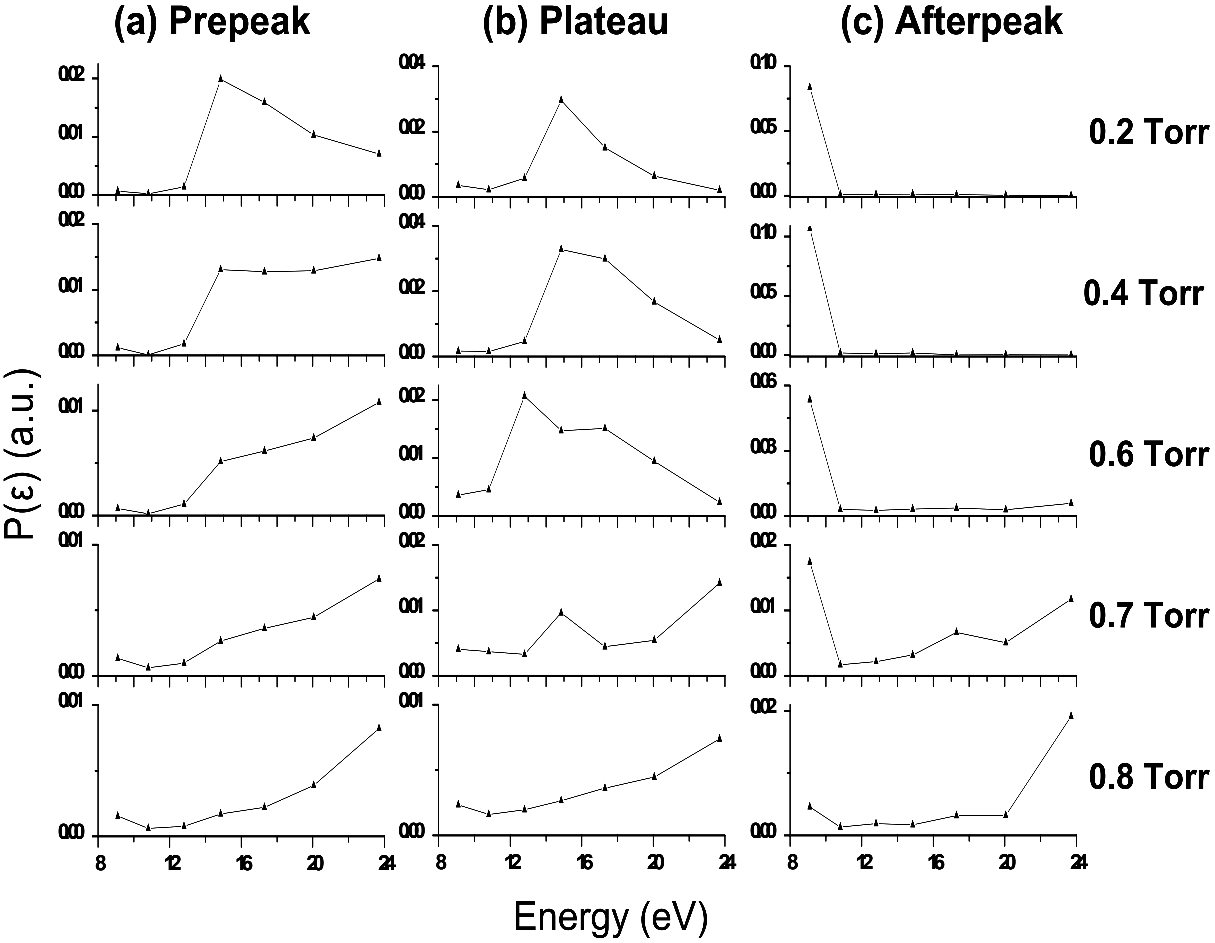

Figure 3.12. P(ε) plots obtained at discharge pressure 0.2-0.8 Torr during the (a) prepeak, (b) plateau, and (c) afterpeak regimes (operating power 100 W and sampling distance 15 mm).

At 0.2 Torr, the internal energy deposition by the plasma exhibits striking similarities with that solely from charge transfer by argon ions, which has been measured by Horning and coworkers.[19] Both P(ε) plots present a narrow energy distribution maximized close to argon's ionization potential at ~15 eV. The strong similarity implies that charge transfer is the dominant ionization mechanism during the plateau regime at low pressures. Energy conservation considerations require an energy resonance for charge transfer to take place: the colliding species must have an excited state that matches the Ar^+ potential.[32] For this reason, charge transfer is not usually considered as an effective ionization mechanism for atomic species.[33] However, for molecular species, the energy resonance requirement may be readily satisfied because of the large number of vibrational and rotational states. The result indicates that charge transfer can be very efficient for the ionization of molecular species in the plasma. Penning ionization, on the other hand, is negligible at pressures lower than 0.3 Torr.[20] This explains the low population of the distribution in the 8-12 eV energy range.

Within the energy range of 18-24 eV, the P(ε) of the plasma is higher as compared to that by charge transfer. This difference can be accounted for by contributions from other possible excitation processes in the plasma, such as electron excitation and CID, which are superimposed on top of the energy deposited by charge transfer. There may also be some charge transfer occuring between excited argon ions and $W(CO)_6$ molecules[19] that can be ultimately attributed to electron excitation of the argon ions prior to collision with $W(CO)_6$.[12] Another possibility, energy conversion from the kinetic energy of the collision, can be eliminated because P(ε) arising from charge transfer exhibit a weak dependence on collision energy [19] within the kinetic energy range of Ar^+ in the negative glow region.

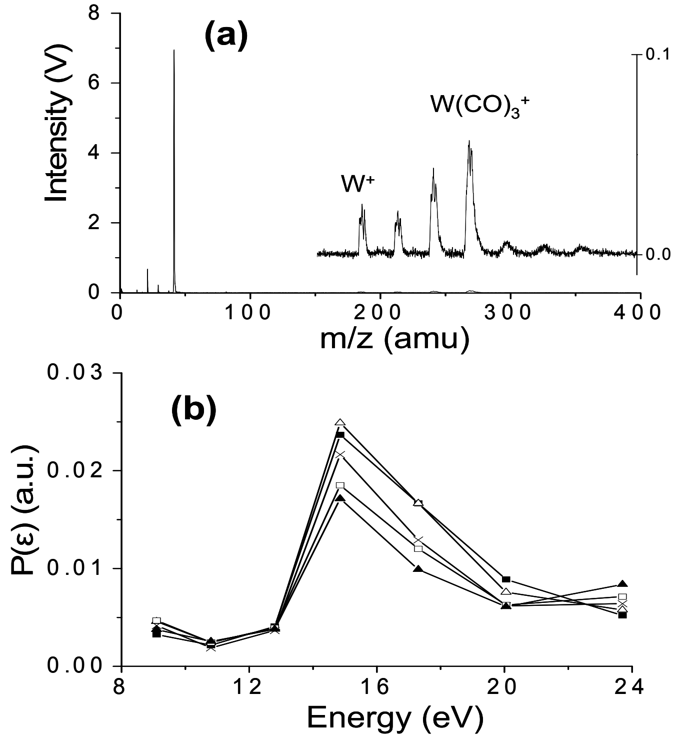

Figure 3.13. (a) Plateau mass spectrum acquired at 15 mm and (b) plateau P(ε) plots obtained at 5 mm (Δ), 10 mm (□), 15 mm (x), 20 mm (■), and 30 mm (▲) (discharge pressure 0.2 Torr and operating power 100 W).

The spatial characteristics of P(ε) at 0.2 Torr provide additional insights into the ionization mechanisms. At higher discharge pressures, the concurrence of various ionization mechanisms during the plateau regime leads to broad P(ε) and the changes in the competition among them cause P(ε) maximum shifts with distance. At 0.2 Torr, however, the P(ε) throughout the plasma remains narrow and nearly uniform: the energy distributions are of the same range and no maximum shift was observed (Figure 3.13). The uniformity strongly supports the dominance by a single ionization mechanism, charge transfer, under these conditions.

The P(E) plots acquired at 0.4 and 0.6 Torr exhibit populations in the lower energy range down to ~11 eV, which can be ascribed to the contribution from Penning ionization. It has been shown that Penning ionization increases with increasing discharge pressure and may account for about 40-80% of total ionization in a continuous glow discharge.[20] Again, the convolution of various ionization and excitation mechanisms results in the broadened energy distributions that can produce mass spectra rich in structural information.

As discharge pressure further increases to 0.7 and 0.8 Torr, the P(ε) shifts to higher energies and extensive fragmentation was observed. When discharge pressure increases, the pressure between the sampling plate and the skimmer increases correspondingly, which may initiate CID effect as ions are sampled through this region, resulting in extensive fragmentation. Although this favors atomic detection, it severely hinders structural elucidation because it reduces the variety of observed fragments.

It has been stated that Penning ionization dominates the afterpeak regime, affording soft ionization and yielding intact molecular ions. This is true for the discharge pressures between 0.2 and 0.6 Torr. However, the softness of the afterpeak regime is greatly offset by CID at elevated pressures. Pressures above 0.6 Torr lead to extensive fragmentation. As shown in Figure 3.12 C, the high-energy shift resulting from such CID can be clearly observed at 0.7 Torr. Although the P(ε) still maximizes at 9 eV, there is a considerable population with internal energies in the 12-24 eV range. As discharge pressure is further increased to 0.8 Torr, the P(ε) maximum is shifted to 24 eV, predominantly yielding W^+ atomic ions through complete CID of the molecular species.

The effect of pressure on ion intensity was also investigated to achieve optimum analytical sensitivity. Knowing that the variation in pressure leads to spatial changes of the resultant plasma, these investigations were undertaken for several positions within the plasma. Figure 3.14 shows the plots of the total ion intensity of $W(CO)_n^+$ (n=0-6) generated during the plateau regime vs. distance at various discharge pressures. Two trends can be observed. First, the total ion intensity decays more sharply with increasing distance at high pressures. Elevated pressures would shorten the mean free path of secondary electrons accelerated off the cathode surface and, correspondingly, decrease the dark space thickness. Consequently, the negative glow region is drawn closer to the cathode and so is the ion population. Similar pressure effects have been observed using Langmuir probe measurements.[29] Second, it was found that the sampled total ion population throughout the plasma, estimated by the area under the intensity-distance plot, decreases dramatically at 0.7 Torr and higher pressures. This decrease likely arises from increases in ion scattering and collisional neutralization at the higher pressures.[23] These two trends were also found during the prepeak and afterpeak regimes as well.

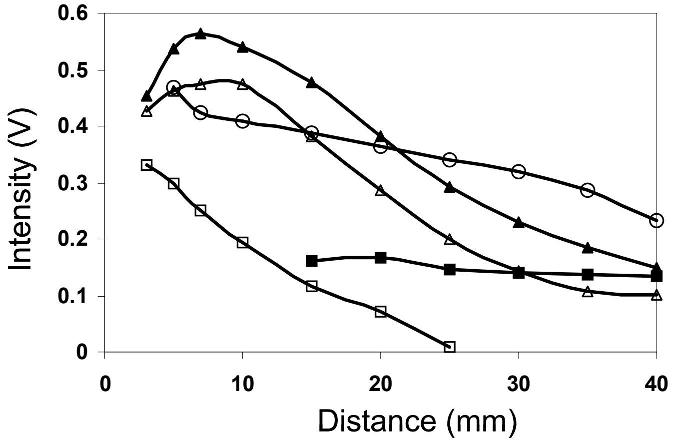

Figure 3.14. Spatial variation of the total $W(CO)_n^+$ ion intensity during the plateau regime at 0.2 Torr (■), 0.4 Torr (○), 0.6 Torr (▲), 0.7 Torr (Δ), and 0.8 Torr (□) (operating power 100 W).

Briefly, the pressure study revealed that the temporal P(ε) variations over the pulse cycle were masked by the effect of CID at elevated pressures, thereby greatly impairing the energy tunability that can be realized with the pulsed GD plasma. In addition, lower sampling efficiencies under high pressures further decreased the analytical performance. Therefore, the optimum discharge pressures were found between 0.2 and 0.6 Torr.

3.3.4.2 The effect of Power on P(ε)

The effect of power on P(ε) was examined by varying operating power from 80 W to 120 W. The sampling distance was fixed at 15 mm. The influence of operating power on P(ε) was found to be similar for discharge pressures ranging from 0.2 to 0.6 Torr and the data acquired at 0.3 Torr are presented as a representative (Figure 3.15).

No apparent changes in P(ε) were observed at various operating powers for all three regimes in a pulse cycle: both the P(ε) maximum and energy distribution range remained relatively unaffected. This observation indicates that the molecular internal energy distribution in the plasma is determined by the dominant ionization and excitation processes rather than the operating power. The charge transfer and Penning ionization processes both represent transfers of potential energy rather than kinetic energy; thus, it is understandable that the molecular internal energy distributions are not heavily dependent on operating power. Electron ionization, the dominant mechanism of the prepeak regime, appears to be weakly dependent on operating power as well. Previous studies have shown that the average electron energy is weakly dependent on operating power in the negative glow region.[29] Therefore, the contribution of energy deposition from electron excitation should remain relatively constant in the plateau regime as the operating power is varied. At a fixed pressure, CID is not expected to vary with operating power. Consequently, the overall P(ε) resulting from these major ionization and excitation mechanisms exhibit little dependence on operating power.

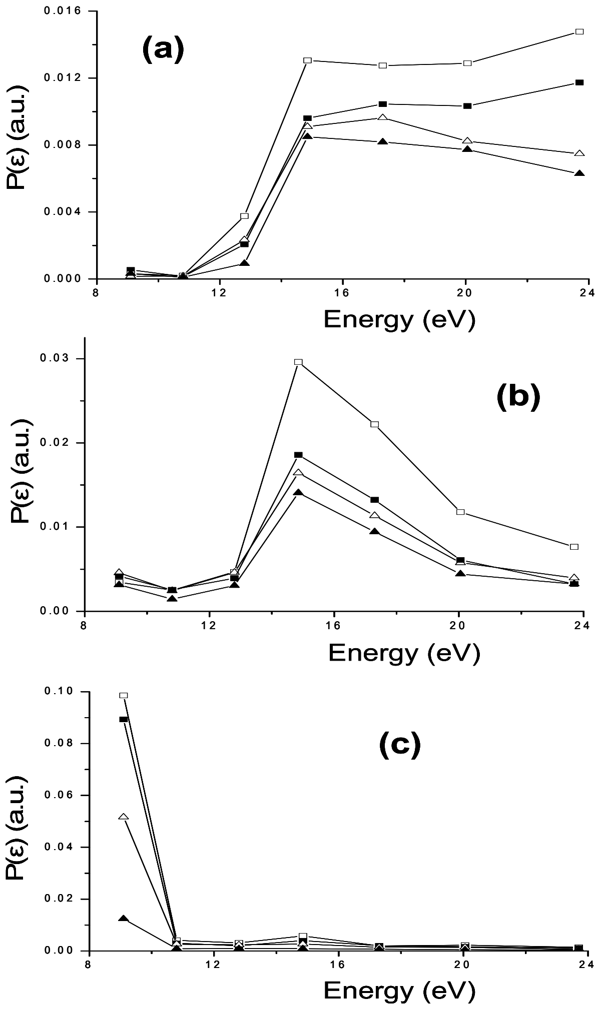

Figure 3.15. P(ε) plots obtained at operating power 60 W (▲), 80 W (Δ), 100 W (■), and 120 W (□) during (a) the prepeak, (b) plateau, and (c) afterpeak regime (discharge pressure 0.3 Torr and sampling distance 15 mm).

Although the operating power has negligible influence on energy distribution P(ε), it exerts great effect on the ion signal intensities. Increasing operating power obviously increased the population of energetic species in the plasma, which, in turn, enhanced ionization efficiency to yield more abundant analyte ions. As can be seen in Figure 3.16, the total ion population, as indicated by the area underneath each curve, increases considerably with increasing operating power; hence, higher analytical sensitivity is expected. In addition, the plots indicate that increases in operating power also lead to plasma expansion.

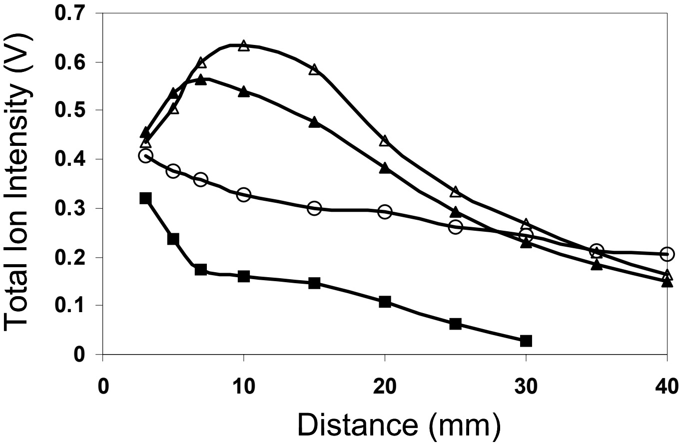

Figure 3.16. Spatial variation of the total $W(CO)_n^+$ ion intensity during the plateau regime at 60 W (■), 80 W (○), 100 W (▲), and 120 W (Δ) (discharge pressure 0.3 Torr).

3.4. Conclusions

The thermometer molecule, $W(CO)_6$, was used to investigate the energy transfer processes in a pulsed glow discharge plasma. The time-resolved internal energy distributions, $P(\varepsilon)$, of $W(CO)_6$ exhibited a strong temporal dependence over the pulse cycle. Upon plasma initiation and electrical breakdown, the internal energies are most heavily populated over a high range of energies, from 15-24 eV. The result of this high-energy population is extensive fragmentation and the production of predominantly atomic ions. After a transition stage, the plasma reaches a steady state and the P(ε) maximum shifts to a lower energy while the distribution range broadens, providing mass spectra rich in structural information. After the termination of the power pulse, the plasma maintains a comparable ion production capacity while the P(ε) further shifts below 9 eV, affording a soft ionization environment that favors the production of intact molecular ions. The temporal variations were correlated to the changes in dominant ionization mechanisms over the pulse cycle of the plasma. The observation suggests that, by pulsing the glow discharge plasma, the apparent plasma energetics can be rapidly tuned over a wide energy range, affording "soft" to "hard" ionization within a single pulse cycle. Coupling the pulsed glow discharge with ToF mass spectrometry allows mass spectra to be acquired at any instant into the pulse cycle to yield the desired information regarding the analyte molecule.

This study also evaluated the spatial variation of P(ε) as well as the influence of glow discharge operating parameters on P(ε). The results provided additional insight into the ionization mechanisms within the plasma. Electron ionization and Penning ionization dominate the prepeak and afterpeak regimes, respectively. The plateau regime is characterized by a convolution of various ionization and excitation mechanisms. Charge transfer processes play a major role, especially at lower discharge pressures and within the close proximity of the cathode. Penning ionization becomes significant under higher discharge pressure and dominates regions further from the cathode.

The optimal discharge pressures were found to be 0.2~0.6 Torr for argon gas. Extensive fragmentation was observed at higher pressures, hindering the ability to obtain molecular and structural information. In addition, the ion intensity was found to decrease at higher pressures. Lower pressures were found to impair plasma stability. The operating power was found to significantly affect signal intensity and, consequently, the analytical sensitivity; but have little effect on the internal energy distribution. The optimum sampling distance was found at ~10 mm from the cathode surface.

It appears that these pulsed glow discharges do exhibit tunability that can be controlled temporally and spatially to afford chemical speciation. The use of multiple detection gates can be employed to achieve elemental, structural, and molecular information. The rapid variation in plasma energy over a 5 ms time window makes the pulsed plasma a good candidate for coupling with chemical separation methods. These advantages indicate that the pulsed glow discharge can be a powerful tunable mass spectrometry source for chemical speciation, particularly when coupled with ToF mass spectrometry.

3.5 References

(1) Majidi, V.; Moser, M.; Lewis, C.; Hang, W.; King, F. L., *J. Anal. At. Spectrom.* 2000**, 15,** 19-25.
(2) Marcus, R. K.; Evans, E. H.; Caruso, J. A., *J. Anal. At. Spectrom.* 2000**, 15,** 1-5.
(3) Houk, R. S.; Thompson, J. J., *Mass Spectrom. Rev.* 1988**, 7,** 425-461.
(4) Levsen, K. *Fundamental Aspects of Organic Mass Spectrometry*; Verlag Chemie: New York, 1978.

(5) Faubert, D.; Giroux, G. J. C.; Bertrand, M. J., *Int. J. Mass Spectrom. Ion Processes* 1993**, 124*,*** 69-77.

(6) O'Connor, G.; Ebdon, L.; Evans, E. H., *J. Anal. At. Spectrom.* 1997**, 12*,*** 1263-1269.

(7) Chapman, B. N. *Glow Discharge Processes*; John Wiley and Sons: New York, 1980.

(8) Klingler, J. A.; Barshick, C. M.; Harrison, W. W., *Anal. Chem.* 1991**, 63*,*** 2571-2576.

(9) Harrison, W. W.; Yang, C.; Oxley, E., *Anal. Chem.* 2001**, 73*,*** 480A-487A.

(10) Steiner, R. E.; Lewis, C. L.; King, F. L., *Anal. Chem.* 1997**, 69*,*** 1715-1721.

(11) Jackson, G. P.; Lewis, C. L.; Doorn, S. K.; Majidi, V.; King, F. L., *Spectrochim. Acta* 2001**, 56B*,*** 2449-2464.

(12) Lewis, C. L.; Jackson, G. P.; Doorn, S. K.; Majidi, V.; King, F. L., *Spectrochim. Acta* 2001**, 56B*,*** 487-501.

(13) Lewis, C. L.; Oxley, E. S.; Pan, C.; King, F. L., *Anal. Chem.* 1999**, 71*,*** 230-234.

(14) Steiner, R. E.; Lewis, C. L.; Majidi, V., *J. Anal. At. Spectrom.* 1999**, 14*,*** 1537-1541.

(15) Lewis, C. L.; Moser, M. A.; Dale, D. E., Jr.; Hang, W.; Hassell, C.; King, F. L.; Majidi, V., *Anal. Chem.* 2003**, 75*,*** 1983-1996.

(16) Wysocki, V. H.; Kenttamaa, H. I.; Cooks, R. G., *Int. J. Mass Spectrom. Ion Processes* 1987**, 75*,*** 181-208.

(17) Kenttamaa, H. I.; Cooks, R. G., *Int. J. Mass Spectrom. Ion Processes* 1985**, 64*,*** 79-83.

(18) Turner, D. W.; Baker, C.; Baker, A. D.; Brundle, C. R. *Molecular Photoelectron Spectroscopy*; Interscience: New York, 1969.

(19) Horning, S. R.; Kotiaho, T.; Cooks, R. G., *Int. J. Mass Spectrom. Ion Processes* 1991**, 110*,*** 1-29.

(20) Smith, R. L.; Serxner, D.; Hess, K. R., *Anal. Chem.* 1989**, 61*,*** 1103-1108.

(21) Jager, R.; Becker, J. S.; Dietze, H.-J.; Bboekaert, J. A. C., *Int. J. Mass Spectrom. Ion Processes* 1997**, 171*,*** 183-189.

(22) Busch, K. L.; Glish, G. L.; McLuckey, S. A. *Mass Spectrometry/Mass Spectrometry: Techniques and Applications of Tandem Mass Spectromerty*; VCH Publishers: New York, 1988.

(23) McLuckey, S. A.; Glish, G. L.; Asano, K. G.; Grant, B. C., *Anal. Chem.* 1988**, 60*,*** 2220-2227.

(24) Biondi, M. A., *Phys. Rev.* 1952**, 88*,*** 660.

(25) King, F. L.; Pan, C., *Anal. Chem.* 1993**, 65*,*** 735-739.

(26) Stedman, D. H.; Setser, D. W., *Prog. Reaction Kinetics* 1971**, 6*,*** 193-238.

(27) Smith, R. D.; Futrell, J. H., *Int. J. Mass Spectrom. Ion Phys.* 1976**, 20*,*** 71-76.

(28) Hang, W.; Harrison, W. W., *Anal. Chem.* 1997**, 69*,*** 4957-4962.

(29) Ye, Y.; Marcus, R. K., *Spectrochim. Acta* 1996**, 51B*,*** 509-531.

(30) Lewis, C. L.; Li, L.; Millay, J. T.; Downey, S.; Warrick, J.; King, F. L., *J. Anal. At. Spectrom.* 2003**, 18*,*** 1-7.

(31) King, F. L.; McCormack, A. L.; Harrison, W. W., *J. Anal. At. Spectrom.* 1988**, 3*,*** 883-886.

(32) Steers, E. B. M.; Fielding, R. J., *J. Anal. At. Spectrom.* 1987**, 2*,*** 239-244.

(33) Coburn, J. W.; Kay, E., *Appl. Phys. Lett.* 1971**, 18*,*** 435-438.

Chapter 4: Chemical Speciation of Organic and Organometallic Compounds Using Pulsed Glow Discharge Time-of-Flight Mass Spectrometry

4.1. Introduction

For decades, glow discharge mass spectrometry (GDMS) has been experiencing great success as a direct elemental analysis technique for solid samples.[1] The technique exhibits advantages such as applicability to a wide variety of suitable samples, minimal matrix effect, relatively high sensitivity, and excellent stability and reproducibility.[2] While its traditional applications in direct analysis of solid samples are facing challenges and competition from the recently developed alternative techniques, such as laser ablation inductively coupled plasma mass spectrometry (ICP-MS), GDMS has expanded its utility as a potential technique for chemical speciation to provide molecular weight and structural information along with elemental composition.[3] Various approaches have been employed to achieve this goal, including using different discharge gases,[4] switching polarity of the electrodes,[5] and pulsing the glow discharge[6].

The pulsed GD plasma is one of the most promising approaches. Pulsing the GD plasma leads to temporal separation among the various excitation and ionization mechanisms, resulting in discrete temporal regimes with distinct plasma energetics.[7]

Upon the onset of the power, the applied energy is directly coupled into free electrons and leads to discharge gas breakdown, which results in efficient electron ionization in the prepeak regime. The plateau regime is approached as the pulsed plasma reaches a quasi-steady state that closely resembles its continuous counterpart containing the major ionization mechanisms, i.e., electron ionization, charge transfer, and Penning ionization.[8] Then the plasma energy starts decaying at the termination of the discharge power because electron ionization and charge transfer cease. The ion-electron recombination leads to a temporal increase in the population of the metastable atoms of the discharge gas,[9] affording a soft ionization environment dominated by Penning ionization.[10]

The shifting of dominant ionization and excitation mechanisms gives rise to temporal variations in plasma energetics within a pulse cycle. Recently, Li et al. [11] (also Chapter 3 in this document) studied the temporal and spatial plasma enegetics of a pulsed GD plasma using the thermometer molecule $W(CO)_6$. It was found that the apparent plasma energy, or the internal energy distribution of $W(CO)_6$, $P(\varepsilon)$, rapidly varied over a wide energy range within a pulse cycle. The prepeak regime is characterized by a high internal energy well above 20 eV. At the plateau regime, the $P(\varepsilon)$ maximum shifts to a lower energy with a wide distribution ranging from 12 eV to 24 eV. After the termination of the power, the apparent plasma energy further shifts down to ~9 eV. The study also revealed spatial variations in plasma energetics inherent in the heterogeneity of GD plasmas. During the plateau regime, the observed $P(\varepsilon)$ maximum decreased from ~20 eV to ~12 eV as the sampling distance increased from 5 mm to 30 mm.

The observed temporal and spatial shifts of the apparent plasma energy provide significant analytical utility in mass spectrometry. The apparent plasma energy is closely associated with the amount of internal energy deposited into the molecular species in the plasma. It is well known that molecular internal energy plays a decisive role in the ionization and subsequent fragmentation, and, hence, the appearance of the resultant mass spectrum. Therefore, the varying plasma energies of the pulsed GD plasma can lead to the production of molecular mass spectra with varying degrees of fragmentation. The rich information included in these diverse spectra can certainly facilitate the identification and structural elucidation of the given analyte.

This report demonstrates the analytical utilities of the pulsed GD plasma as a tunable ion source for the organic compounds, benzene and hexane, and the organometallic compound, ferrocene. The fragmentation pathways and the associated energetics data of these compounds are well known; therefore, the obtained mass spectra can also be used to evaluate plasma enegetics. The vapor of each compound was introduced into a pulsed GD plasma and the resultant ions were monitored by a time-of-flight (ToF) mass spectrometer. The time-resolved mass spectra were acquired using a time-gated detection technique; these spectra exhibit various degrees of fragmentation, ranging from ones abundant in atomic ions to those dominated by molecular ions. During the plateau regime, the mass spectrum appearance was found to be spatially dependent, effecting sampling distance as a variable to optimize the desired ion abundance. The observed temporal and spatial variations were further correlated to shifts of the apparent plasma energy.

4.2 Experimental Section

Glow Discharge ToF Mass Spectrometer. The Pulsed GD ToF mass spectrometer has been described in detail in Chapter 3 and is only briefly re-introduced here. A high vacuum bellows (MDC Vacuum Products Co., Hayward, CA) served as the GD chamber. A copper disk cathode, mounted on a direct insertion probe (DIP), was introduced into the discharge chamber to generate plasmas; the transportable DIP allows adjustment of the sampling distance. The GD plasma was powered by a 13.56 MHz radio frequency (rf) power supply equipped with an automatic matching network (RF Plasma Product Inc., Marlton, NJ, USA). The rf power pulse was set at 5 ms pulse with 25% duty cycle. The resultant ions in the pulsed GD plasma were monitored by a ToF mass spectrometer (R. M. Jordan Company, Grass Valley, CA).

Sample Introduction to the Glow Discharge Plasma. Benzene (99%), hexane (anhydrous), and dicyclopentadienyl iron (a.k.a. ferrocene, 98%) were obtained from Aldrich Chemical Company (Milwaukee, WI). The sample vials were immersed in water baths to ensure the constant vapor pressure. An ice-water bath was used for benzene and hexane while a 50 ^{o}C water bath was used to for dicyclopentadienyl iron. The chemical vapors were then introduced into the GD chamber through a 0.2 mm I.D. stainless-steel capillary. The sample introduction rates were regulated by a metering valve; the partial pressures of the chemical vapors were maintained at ~10 mTorr. The introduction capillary and GD chamber were heated to 50 ^{0}C using a heat tape to prevent the chemical vapors from condensing.

Data Acquisition and Processing. The orthogonal ToF mass spectrometer permits ion extraction from the GD source by pulsing the repeller. A digital delay generator (EG&G Princeton Applied Research, Princeton, NJ), synchronized with the rf power pulse, subsequently triggers the repeller pulse and the initiation of the signal detection system. Ions formed at a specific time within the power pulse sequence can be extracted and analyzed, resulting in a time-gated spectrum. The time-gate position can be easily selected by adjusting the digital delay generator. The mass spectra of prepeak, plateau, and afterpeak regime were acquired at 0.2 ms, 4.0 ms, and 5.6 ms after pulse initiation, respectively. The plasma was sampled at different locations by varying the relative distances between the discharge cathode and the ToF sampling plate. The mass spectrometric signal was amplified and fed to a 1-GHz oscilloscope (LeCroy 9370M, Chestnut Ridge, NY), digitized and averaged for 150 sweeps. Through a GPIB interface, the averaged mass spectral data were imported into a Microsoft Excel 97 spreadsheet program (Microsoft, Redmond, WA) for construction of mass spectra.

4.3. Results and Discussion

4.3.1. Selection of Glow Discharge Parameters

Discharge parameters, especially discharge pressure and operating power, significantly influence the plasma energetics and, consequently, the ionization and fragmentation of the analyte molecules therein. In order to achieve the optimal analytical performance, discharge parameters have to be judiciously selected.

The results from Chapter 3 suggest that the optimal discharge pressures be 0.2~0.6 Torr for molecular analysis.[11] Higher pressures cause severe collision-induced dissociation, leading to extensive fragmentation and hindering the ability to obtain molecular and structural information. In addition, the measured ion intensity was found to decrease at high pressures, presumably because of the severe ion scattering during the sampling process. On the other hand, extremely low pressures impair plasma stability. In this study, the discharge pressure was set at 0.5 Torr.

The operating power significantly affects signal intensity and, consequently, the analytical sensitivity; but has little effect on the internal energy distribution. Hence, higher operating powers are preferred to achieve better analytical sensitivity. A 100W rf operating power was used throughout the study, which ensured satisfactory signals as well as excellent plasma stability.

The sample introduction rate needs to be carefully chosen and controlled as well. It is evident that extremely low sample introduction rates would not provide intense analyte ion signals. However, the introduction of excess amount of sample would drastically alter the argon plasma environment and even impair the plasma stability. In this study, the sample introduction rates were regulated such that the analyte partial pressure in the ion source was maintained at ~10 mTorr, which provided both plasma stability and analyte signal intensity. Under these conditions, the resultant mass spectra were dominated by the intense argon ion peaks, indicating the argon plasma was relatively unaffected.

The GD power pulse is of 5 ms “pulse-on” duration with 15 ms “pulse-off” period, giving 25% duty cycle. The long “pulse-off” period ensured that the ion species resulting from a pulse cycle will not be carried over to the following pulse. The representative sampling increments for the prepeak, plateau, and afterpeak regime have been established at 0.2 ms, 4.0 ms, and 5.6 ms into the pulse cycle, respectively. At each instant, the plasma was sampled at distances from 5 mm to 30 mm.

The GDMS operating parameters used in this study are summarized in Table 4.1.

Table 4.1. Operating parameters used for the pulsed GD ToF-MS experiments.

Glow Discharge	
Argon pressure	0.5 Torr
Analyte partial pressure	~10 mTorr
RF power	100 W (peak)
RF Pulse duration	5 ms
duty cycle	25%
Sampling Instant	
Prepeak	0.3 ms into the pulse
Plateau	4.0 ms
Afterpeak	5.6 ms
Sampling distance	5-30 mm

4.3.2 Analysis of Benzene

The extensively conjugated structure makes benzene a rugged molecule. The breakdown diagram [12] shows that the molecular ion $C_6H_6^+$ appears at the ionization potential 9.2 eV and persists up to 16 eV. The dissociation channel with the lowest activation energy lies at ~14 eV,[13, 14] which is ~5 eV higher than the ionization potential of benzene. The stability of benzene is reflected in the NIST electron ionization (at 70 eV) reference spectrum (Figure 4.1).[15] The molecular ion peak dominates the spectrum as the base peak. Few fragment ions are present with low intensities; the most intense fragment ion, $C_6H_5^+$, is only of ~30% relative intensity.

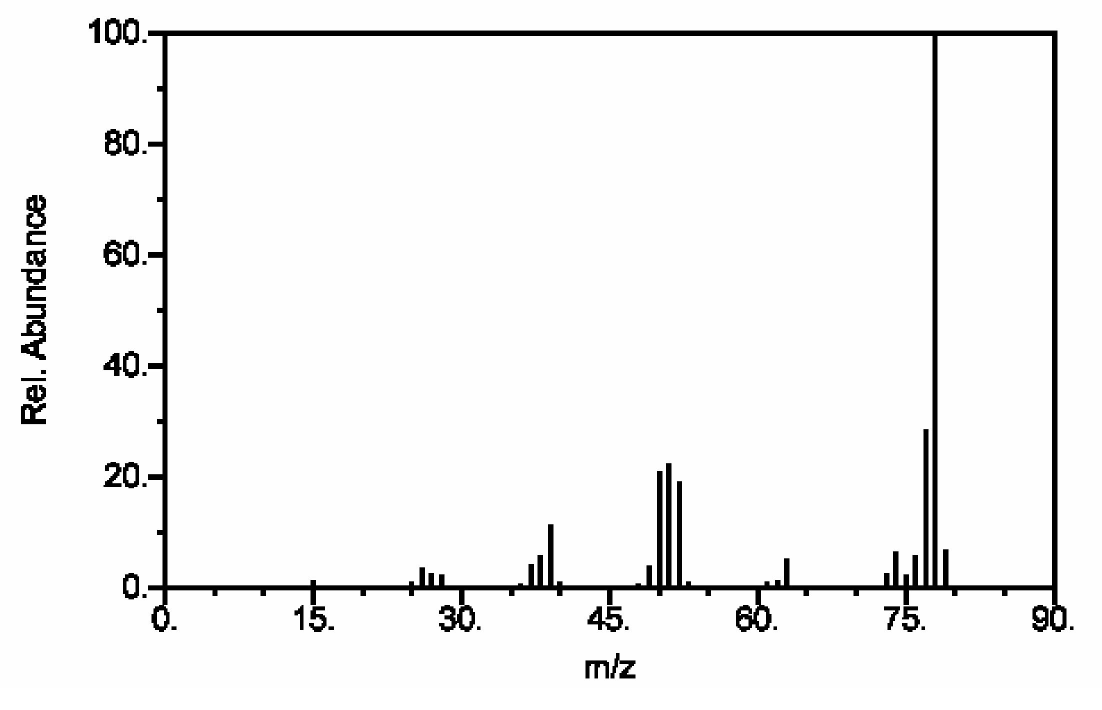

Figure 4.1. NIST electron impact (70 eV) reference spectrum of benzene.

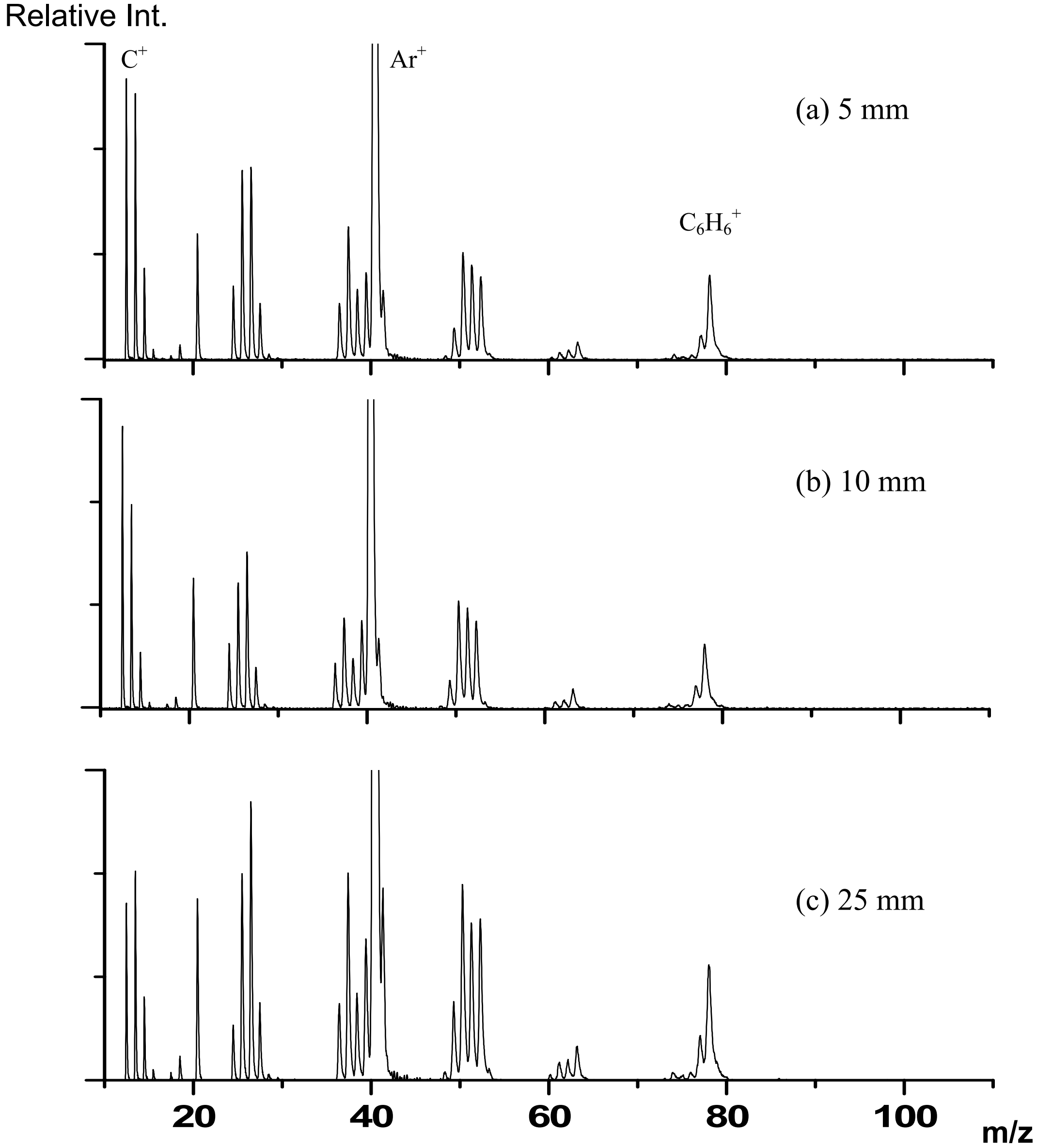

Figure 4.2. Mass spectra of benzene obtained within the prepeak regime at (a) 5 mm, (b) 10 mm, and (c) 25 mm.

The benzene mass spectra acquired at prepeak regime of the pulsed GD plasma are shown in Figure 4.2. The plasma background ions were observed at 40 (Ar^+), 18 (H_2O^+), 20 (Ar^{2+}), and 28 amu (N_2^+), which can be attributed to the discharge gas and contaminants. These background peaks were usually observed with predominant intensities and are cut off in the spectra to emphasize the analyte signals. The sputtered species Cu^+, although usually present as background ion, is not expected in the prepeak spectra because of the delay of sputtering, diffusion and ionization processes.[7]

The prepeak spectra of benzene exhibit extensive fragmentation, contrasting sharply with the NIST electron impact spectrum. The dominant species are small fragment ions containing one and two carbon atoms while the molecular ion $C_6H_6^+$ is observed with much lower intensity. The strikingly intense atomic ion C^+ clearly reveals the organic nature of the analyte molecule. Considering the structural ruggedness of benzene molecule, these spectra vividly demonstrate the ability of the pulsed GD plasma to produce extensive fragmentation and even yield constituent atomic ions.

From the standpoint of molecular energetics, the dominance of small fragment ions, especially one and two-carbon species, combined with the low intensity of the molecular ion $C_6H_6^+$, indicates that most of the primary molecular ions generated in the prepeak regime had sufficient internal energy such that further dissociation occurred. Judging from the appearance potential data (Table 4.2) of the major fragment ions, the molecular internal energy must have exceeded ~19 eV to yield abundant $C_2H_2^+$ ion, and extended to at least 28 eV as evidenced by the presence of CH_3^+. These observations agree with the previously measured plasma energetics data at this regime.[16] In the previous study, the apparent plasma energy was also found to be spatially uniform within the prepeak regime; consequently, the mass spectra acquired at various distances exhibit strong similarities.

Table 4.2. Ionization potentials (I.P.) of benzene, hexane, and ferrocene; and the appearance potentials (A.P.) of their major fragment ions.

Benzene		**Hexane**		**Ferrocene**	
Ions	**I.P./A.P. (eV)**	**Ions**	**I.P./A.P. (eV)**	**Ions**	**I.P./A.P. (eV)**
$C_6H_6^+$	9.24	$C_6H_{14}^+$	10.13	$Fe(C_5H_5)_2^+$	6.71
$C_6H_5^+$	13.7	$C_5H_{11}^+$	11.045	$Fe(C_5H_5)^+$	13.2
$C_6H_4^+$	14.04	$C_5H_{10}^+$	11.005	$Fe(C_3H_3)^+$	18.06
$C_5H_3^+$	15.7	$C_4H_8^+$	11.00	Fe^+	14.00
$C_4H_3^+$	17.6	$C_3H_7^+$	11.33		
$C_3H_3^+$	15.34	$C_3H_6^+$	11.00		
$C_2H_2^+$	18.6				
CH_3^+	28.2				

Data were adapted from Ref 15.

The spectra of benzene acquired in the plateau regime are presented in Figure 4.3. In general, the plateau spectra exhibit less fragmentation as compared to the prepeak spectra. The intensity of atomic ion C^+ is dramatically suppressed while the large fragment ions, such as $C_4H_3^+$, and the molecular ion peak are considerably enhanced. The plateau mass spectra exhibit strong spatial dependence, which is most evidently indicated by the change in relative intensity of molecular ion $C_6H_6^+$. The molecular ion intensity dramatically increases with increasing sampling distance and eventually became the base peak at 25 mm. Note that, disregarding the plasma background ions, the spectra exhibit reasonable agreement with NIST reference spectrum.

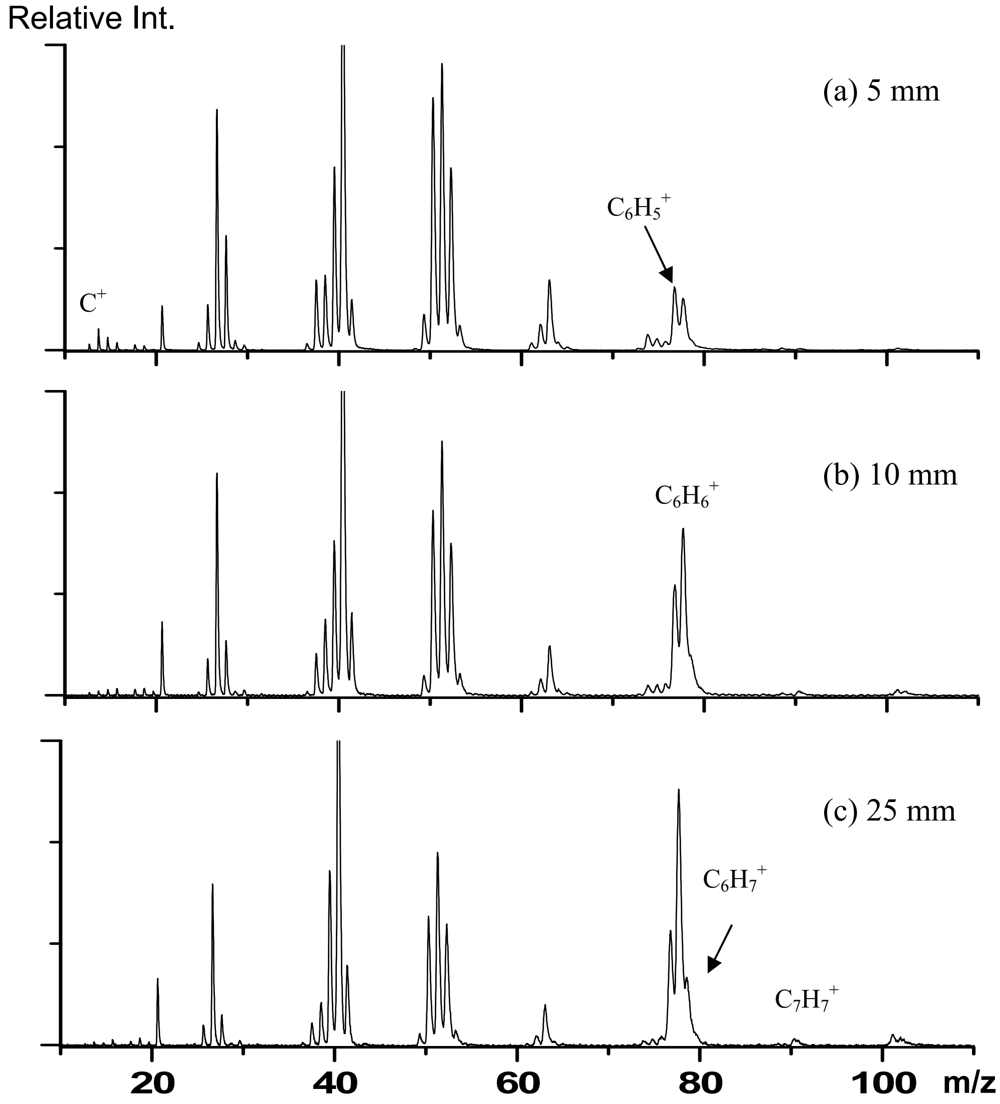

Figure 4.3. Mass spectra of benzene obtained within the plateau regime at (a) 5 mm, (b) 10 mm, and (c) 25 mm.

Two types of ions observed in the spectra are of special interest: the quasi-molecular ion $C_6H_7^+$ observed at 79 amu and the adduct ions observed between 91 and 107 amu, presumably $C_7H_7^+$ and $C_6H_6 \cdot C_2H_5^+$ respectively. These ions arise from ion-molecule reactions, as often observed in the chemical ionization.[16, 17] The reagent ions are most likely from the fragment ions of benzene molecule itself, for example, CH_5^+ and $C_2H_5^+$;[16] proton transfer from ArH^+ was also previously observed.[18] The presence of these species indicates the significance of ion-molecule reaction in the plasma, along with the well established plasma ionization mechanisms, i.e., electron ionization, Penning ionization, and argon ion charge transfer.

The temporal and spatial variation in the mass spectrum appearance is closely correlated to the shift of the plasma energetics. As the plasma evolves into the plateau regime, the internal energy distribution, $P(\varepsilon)$, decreases at higher energies (>20 eV) and increases within 12-15 eV range, resulting in fewer small fragments and more molecular ions. Similarly, $P(\varepsilon)$ maxima down shift from ~20 eV to ~12 eV as the sampling distance increases from 5 mm to 30 mm is translated into the striking increase in the relative intensity of the molecular ion.

The afterpeak spectra of benzene (Figure 4.4) clearly demonstrate the “soft” nature of the plasma in the afterpeak regime. The benzene molecular ion absolutely dominates the spectra while fragment ions, including $C_4H_4^+$, $C_5H_3^+$ and $C_6H_5^+$, only accounts for less than 10% relative abundance. The spectral simplicity greatly facilitates the molecular ion identification and molecular weight determination. The predominance of the molecular ion is attributed to the lower apparent plasma energy in the afterpeak regime resulting from Penning ionization. It is also noteworthy that the quasi-molecular, $C_6H_7^+$, and adduct ions are still present, implying that ion-molecule reactions remain an effective ionization mechanism during the afterpeak regime along with Penning ionization. Corresponding to the known spatial uniformity of the apparent plasma energy in the afterpeak regime[11] (Chapter 3), the spectra acquired at various distances bear strong similarities.

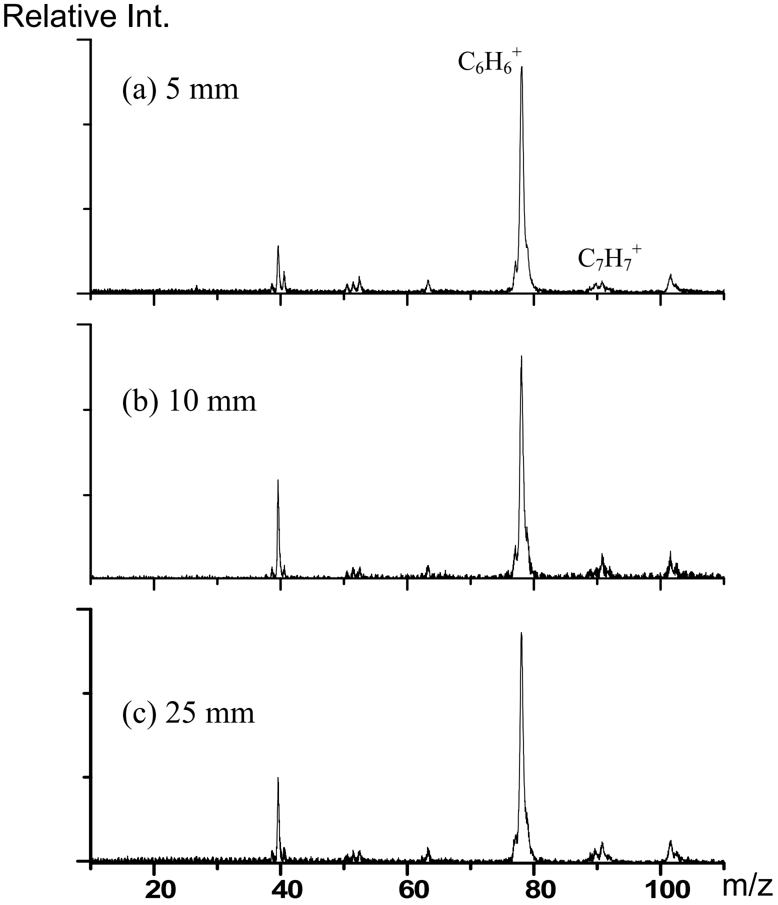

Figure 4.4. Mass spectra of benzene obtained within the afterpeak regime at (a) 5 mm, (b) 10 mm, and (c) 25 mm.

4.3.3. Analysis of Hexane

In contrast with benzene, the hexane molecule is extremely fragile. The major fragments, $C_3H_7^+$, $C_4H_9^+$, and $C_5H_{11}^+$ have appearance potentials around 11 eV, which is just ~1 eV higher than the ionization potential of hexane at 10.2 eV (Table 4.2). Hence, the molecular ion is exceptionally labile to further dissociation. The breakdown diagram[19] showed that the molecular ion yield decreases sharply to essentially zero at 11 eV. The molecular ion lability subsequently hinders the availability of the molecular information using mass spectrometric analysis.

The fragile nature of hexane molecule can also be readily recognized in the NIST reference mass spectrum (Figure 4.5). The base peak is fragment ion $C_4H_9^+$ and smaller fragment ions containing two and three carbon atoms are also abundant. Even one-carbon fragment ions CH_3^+ can be observed. However, the molecular ion $C_6H_{12}^+$ and large fragments $C_5H_n^+$ are present in the spectrum with much lower intensity, revealing little molecular information.

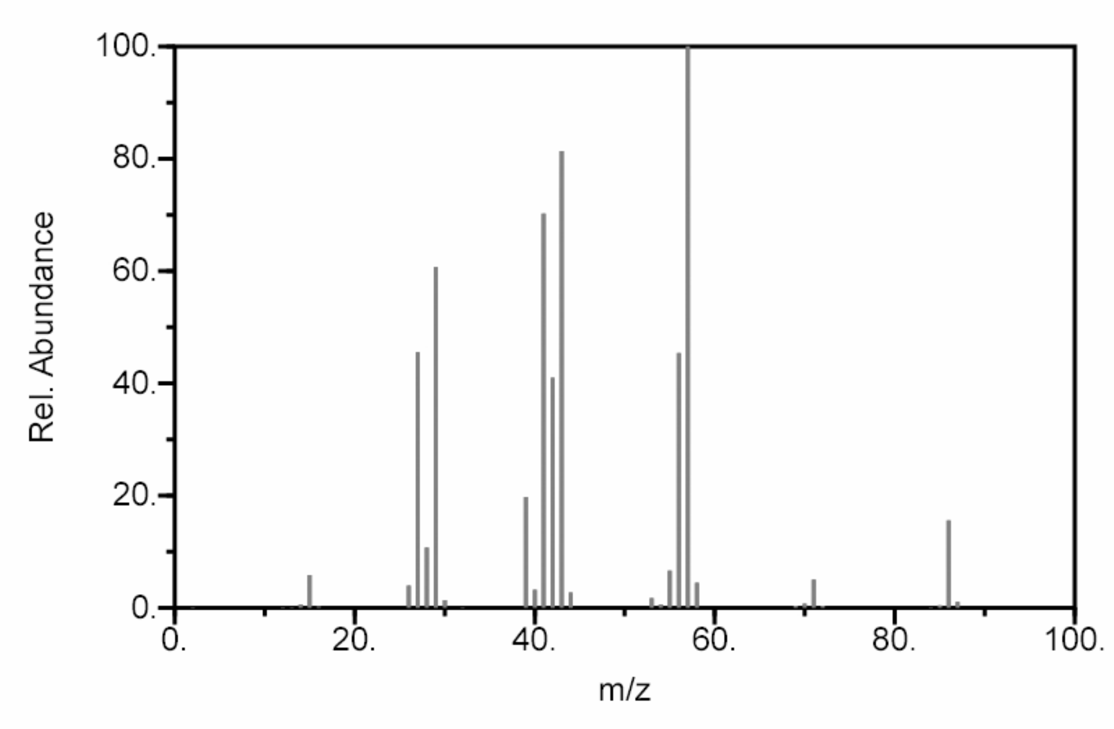

Figure 4.5. NIST electron impact (70 eV) reference spectrum of hexane.

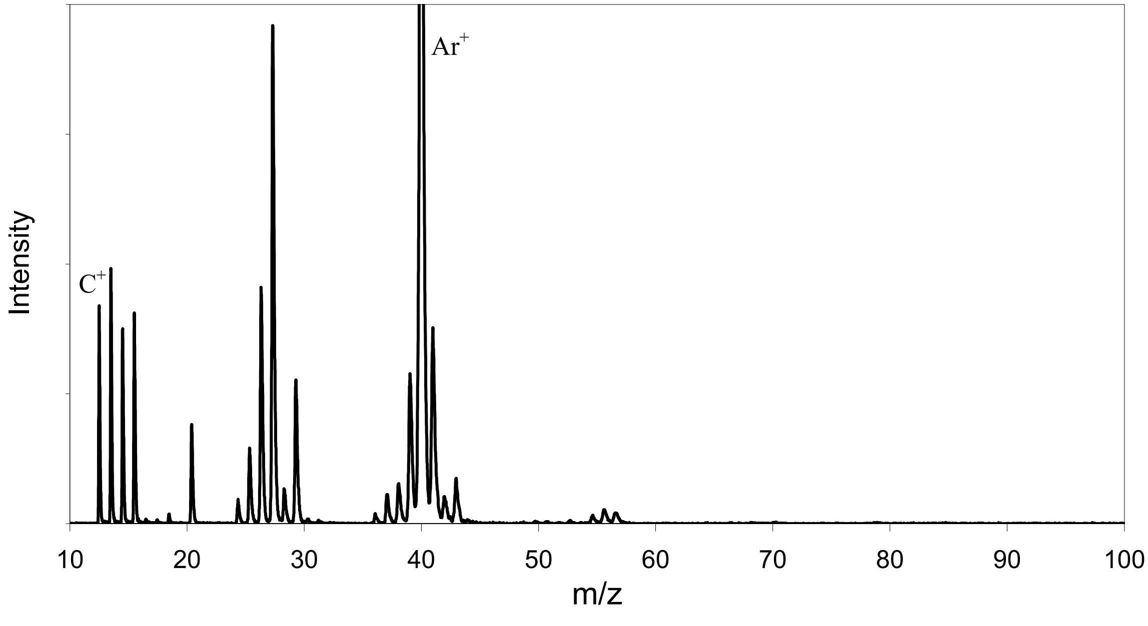

Figure 4.6. Representative mass spectrum of hexane obtained within the prepeak regime.

The prepeak regime spectra of hexane acquired at various distances are similar and only the one obtained at 10 mm is shown in Figure 4.6 as a representative spectrum. The prepeak mass spectrum consisted principally of small hydrocarbon ions containing less than three carbon atoms and abundant carbon atomic ion. No molecular ion was observed. Obviously, it exhibits greater extent of fragmentation as compared to the NIST reference spectrum.

As expected from the down-shift of P(ε), the plateau regime mass spectra of hexane (Figure 4.7) show less fragmentation, which is mirrored by the dramatic decrease in the yield of the atomic ion C^+. Large fragment ions, such as $C_5H_{11}^+$, are present in the spectra, providing additional structural information. The molecular ion $C_6H_{14}^+$ is still hardly observable. Keep in mind that the P(ε) at the plateau regime is mainly distributed over 12-24 eV [11] (Chapter 3), which, although lower than that of the prepeak, is still too high to generate intact hexane molecular ions.

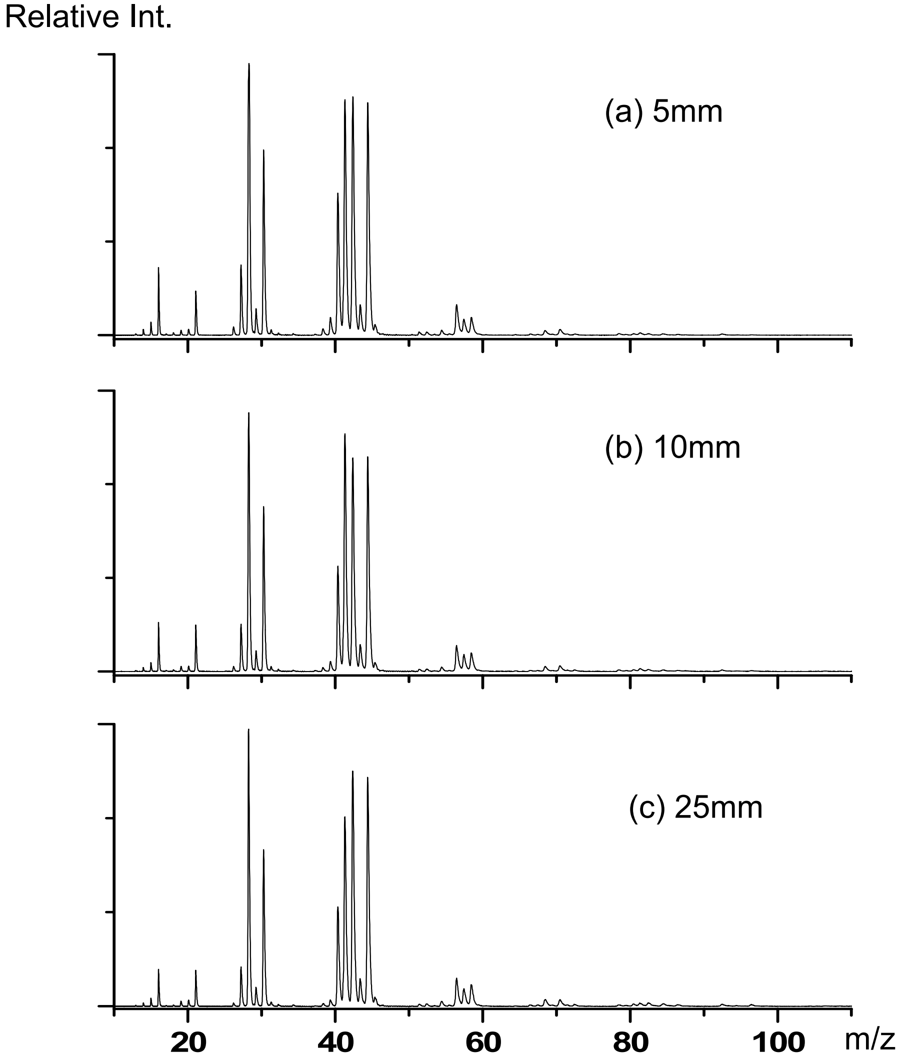

Figure 4.7. Mass spectra of hexane obtained within the plateau regime at (a) 5 mm, (b) 10 mm, and (c) 25 mm.

Unlike the case for benzene, no evident spatial variation is observed in the plateau spectra: the spectra acquired between 5 mm and 30 mm exhibit strong similarities. This observation is somehow surprising since the known spatial variation in P(ε) is expected to cause significant differences in the resultant mass spectra. Close examination attributes the "unexpected" observation to the unique fragmentation pathways and the associated activation energies of the hexane molecule. Note that the appearance potentials of the major hexane fragment ions happen to coincide within a narrow range around 11 eV (Table 4.2); hence, all these fragmentation pathways are accessible as long as the internal energy of hexane molecule is greater than 11 eV. That is, in terms of final fragment product ion, higher internal energy depositions are offset to the same level at ~11 eV. Consequently, the spatial P(ε) variation , as known to be between 12 eV and 20 eV, did not exert significant influences on the appearance of the resultant mass spectra.

The molecular ion, $C_6H_{14}^+$, although not present in the prepeak and plateau spectra, can be easily identified as the base peak in the afterpeak spectrum (Figure 4.8). In the afterpeak regime, the spectra acquired at various distances are similar (not shown). The spectrum clearly demonstrates that the plasma energy can be tuned to a suitable low-energy range during the afterpeak regime to produce abundant molecular ions even for the fragile molecules. The molecular information is therefore readily available. However, because of the extremely low dissociation energy of hexane molecular ions, considerable fragment ions are still present in the spectra. Among them, large fragments, such as five-carbon fragments and H loss fragments, are particularly abundant, providing additional structural information complementary to that obtained from the plateau regime spectra. Also observed are the quasi-molecular ion $C_6H_{15}^+$ peak at 87 amu and various adduct ions at the higher mass range up to 160 amu, which are believed to arise from ion-molecule reactions as has been discussed previously.

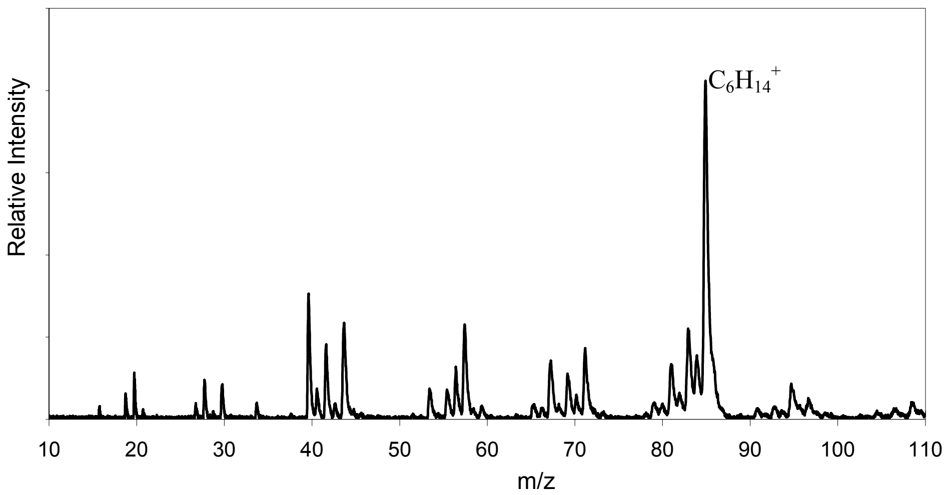

Figure 4.8. Representative mass spectrum of hexane obtained within the afterpeak regime (sampling distance: 10mm).

The preceding discussion regarding benzene and hexane revealed a strong correlation between the apparent plasma energy and the resultant mass spectrum. The temporal and spatial shifts of the apparent plasma energy of the pulsed GD plasma appear to explain the changes observed in the mass spectra. The extent to which the plasma energy shift alters the observed mass spectrum is determined by the fragmentation pathways and their associated activation energies. For most organic compounds, the apparent plasma energy shift between ca. 9 eV and 20 eV can lead to significant differences in their ionization and subsequent fragmentation. The prepeak plasma with apparent energy as high as 28 eV is able to cause extensive fragmentation and favors production of abundant atomic ions. In the plateau regime, the wide energy range promotes various fragmentation pathways, yielding a great variety of fragment ions and hence rich structural information. During the afterpeak regime, the plasma energy is further lowered to ~ 9 eV which is comparable to the ionization potentials of organic compounds and thus strongly prefers the production of intact molecular ions. In addition, the appearance of the plateau spectrum can be further adjusted by varying the sampling distance. The time-resolved mass spectrum at each regime can be obtained using time-gated ToF mass spectrometry (ToF-MS),[20] providing the elemental composition, structural elucidation, or molecular weight information of the given analyte in a single pulse cycle.

4.3.4. Analysis of Ferrocene

For organometallic compounds, as represented here by ferrocene, the identity and quantity of the metal constituent(s) contained is of analytical interest. In order to obtain the elemental information using mass spectrometry, sufficient internal energy must be deposited to drive the primary ions undergo complete fragmentation and yield abundant atomic ions. For the ferrocene molecule, the appearance potential of Fe^+ is ~14 eV (Table 4.2), corresponding to the fragmentation pathway A. However, this pathway is in competition with the formation of $Fe(C_5H_5)^+$ and has a very low branching factor [21-23] and hence yields little Fe^+. An internal energy of ~18 eV is required to yield abundant Fe^+ through pathway B.

$$Fe(C_5H_5)_2^+ \rightarrow Fe^+ + (C_5H_5)_2 \qquad \text{(A)}$$

$$Fe(C_5H_5)_2^+ \rightarrow Fe(C_5H_5)^+ \rightarrow Fe^+ + 2\ (C_5H_5) \qquad \text{(B)}$$

In order for high energy deposition, a “hard” ion source, as represented by ICP, is usually employed. Because the pulsed GD plasma is also capable of depositing tremendous internal energies (>20eV) into the analyte molecule within its prepeak regime, it is plausible to utilize prepeak regime mass spectra for elemental determination. As can be seen in the prepeak spectrum (Figure 4.9), the absolute dominance of the atomic ion, Fe^+, among the ferrocene species is readily realized. The $Fe(C_3H_3)^+$ ion with 18 eV appearance potential is also observed, along with $Fe(C_5H_5)^+$ ion peaks. The much less intense $Fe(C_5H_5)_2^+$ indicates that most of the primary molecular ion population has undergone further dissociation .

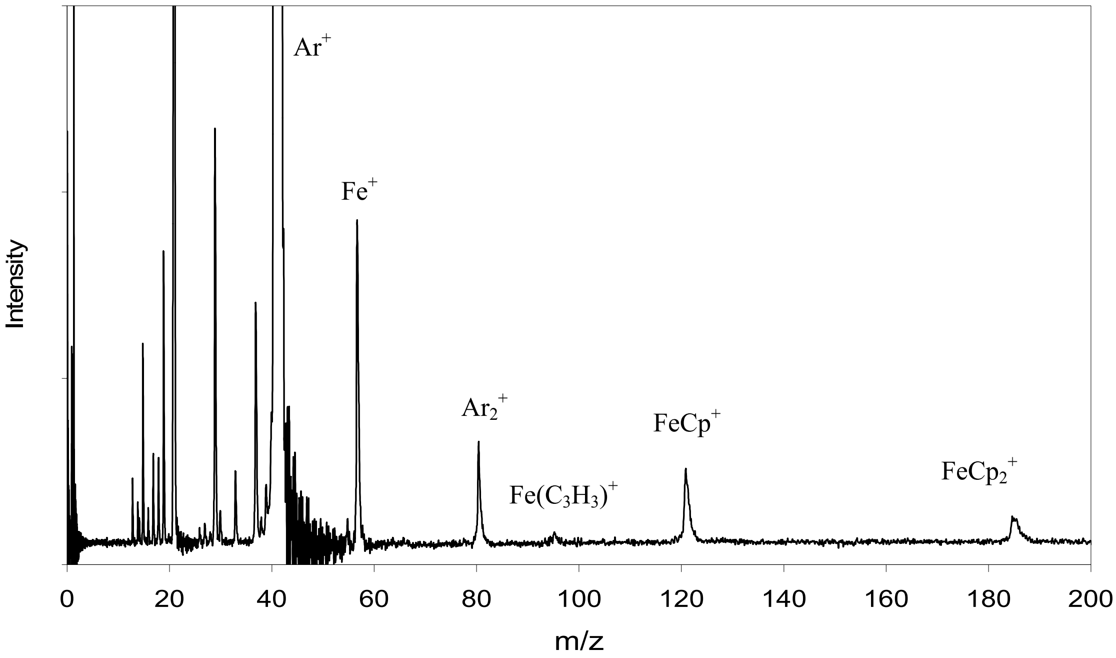

Figure 4.9. Representative mass spectrum of ferrocene obtained within the prepeak regime.

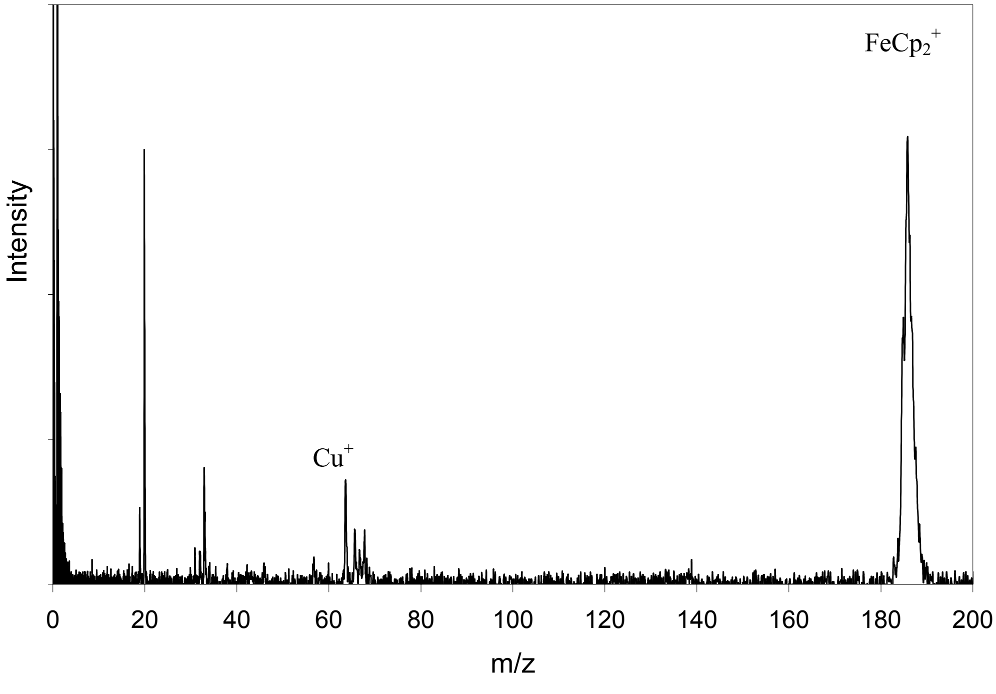

Figure 4.10. Representative mass spectra of ferrocene obtained within the afterpeak regime

Note that “hard” ion sources, such as the ICP, completely sacrifice the molecular and structural information of the analyte in exchange for sensitive elemental analysis. The pulsed GD plasma, although not able to provide equivalent performance for elemental detection, affords additional molecular and structural information within the plateau and afterpeak regimes as the plasma energy decays.

Molecular weight information was easily achieved from the afterpeak spectrum (Figure 4.10) thanks to the predominance of the ferrocene molecular ion peak. Because the apparent plasma energy in the afterpeak regime is lower than the required fragmentation energies, no significant fragment ion is observed in the spectrum. The peaks observed at 63 and 65 amu originate from the sputtered copper atoms, which can also be ionized in the afterpeak regime owing to their low ionization potential.

Structural information can be obtained from the plateau regime mass spectra as shown in Figure 4.11 (only the mass range from 50 to 200 amu is shown for clarity). As a result of wide $P(\varepsilon)$ range, a great variety of analyte ion species is observed in these spectra, including the atomic ion, Fe^+, fragment ions, $Fe(C_5H_5)^+$ and $Fe(C_3H_3)^+$, and the molecular ion, $Fe(C_5H_5)_2^+$; thereby, rich structural information can be obtained. In addition, the plateau spectra reasonably match the NIST reference spectrum (Figure 4.12), affording a potential advantage for analyte identification through a spectral library search. Note the spatial dependence of the plateau mass spectra: the Fe^+ intensity decrease dramatically while the molecular ion $Fe(C_5H_5)_2^+$ intensity increases with increasing sampling distance. Thus, sampling distance can be utilized to “tune” the mass spectrum appearance and to optimize the desired ion abundance.

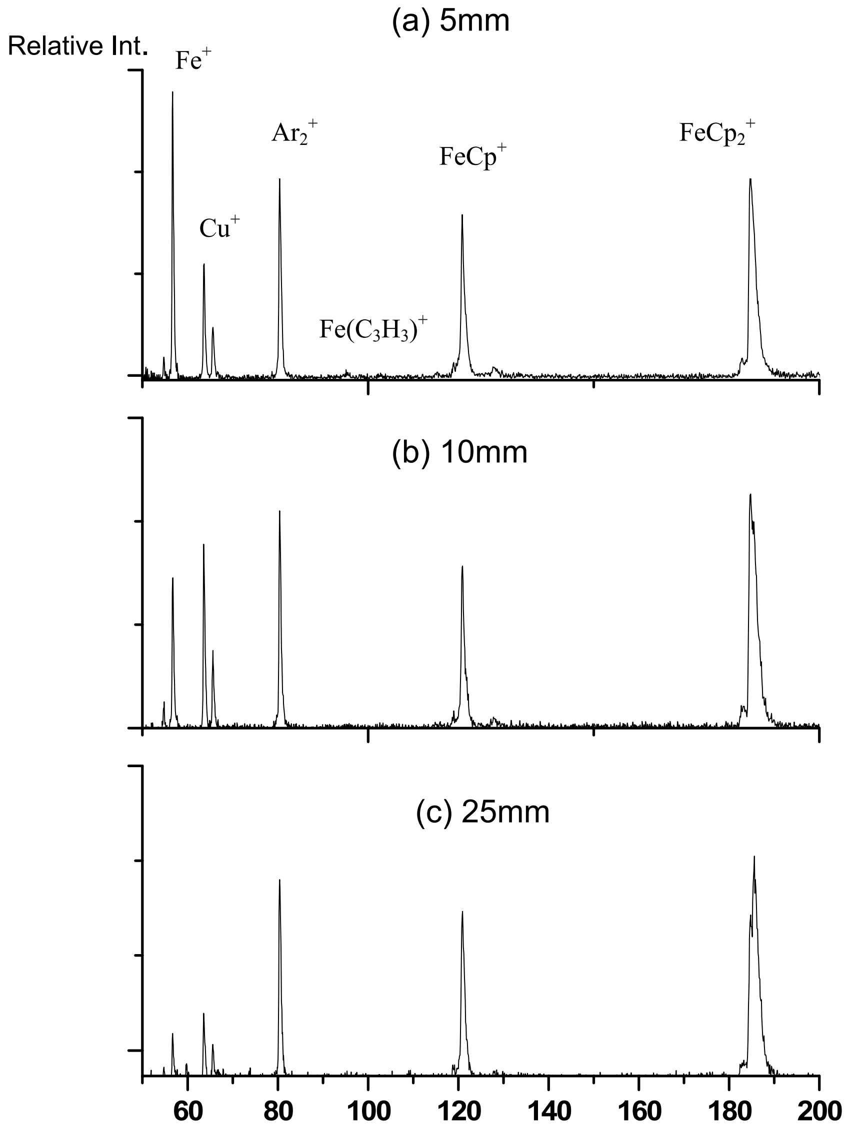

Figure 4.11. Mass spectra of ferrocene obtained within the plateau regime at (a) 5 mm, (b) 10 mm, and (c) 25 mm.

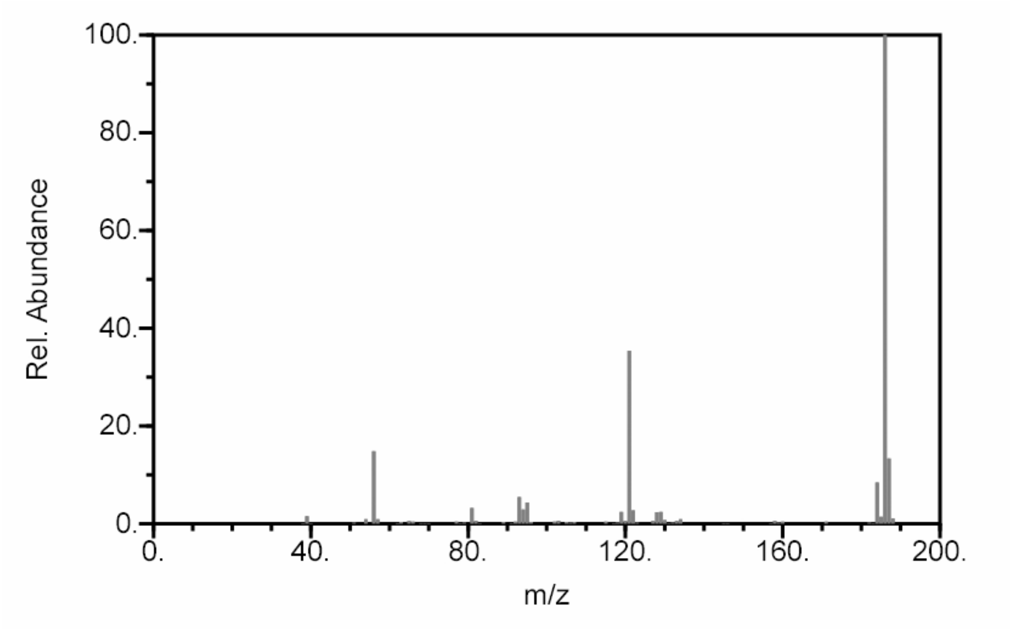

Figure 4.12. NIST electron impact (70 eV) reference spectrum of ferrocene.

4.4. Conclusions

The analytical applications of a pulsed GD plasma as a tunable ion source have been demonstrated using benzene, hexane, and ferrocene. The mass spectra of these organic or organometallic compounds at each temporal regime of the pulse were found to be distinct. The prepeak regime of the pulsed plasma is of a "hard" ionization nature. Even rugged molecules, such as benzene, can be extensively dissociated to yield atomic ions, revealing the elemental composition of the analyte molecule. On the other hand, the afterpeak regime provides a soft ionization environment that can generate intact molecular ions for very fragile molecules like hexane; the molecular information is thus readily available. Rich structural information of the analyte can be obtained from the plateau regime spectra as a great variety of fragment ions are generated therein.

Furthermore, the spatial dependence of the plateau regime spectra affect sampling position offering an additional parameter to optimize the desired ion abundance. As illustrated by benzene and ferrocene, the plateau spectra resemble their EI reference spectra, indicating a potential means for unknown identification through a spectral library search. The observed temporal and spatial variations in mass spectra were found to be well correlated with the known shifts of the apparent plasma energy.

It is worth noting that discharge power supplies can be pulsed readily at high frequency; therefore, all the information can be achieved in rapid succession within a transient period (usually a few microseconds). Owing to speed and ease in operation, the pulsed GDMS can be readily coupled with a chemical separation procedure, such as gas chromatography, serving as an on-line and real-time detector. The pulsed GDMS can provide elemental, structural, and molecular information for each separated component, which can be judiciously pieced together to facilitate analyte identification. These advantages make pulsed GDMS a potentially powerful tool for chemical speciation. Future work will focus on the development of the interface and increase its stability and sensitivity.

4.5. References

(1) King, F. L.; Teng, J.; Steiner, R. E., *J. Mass Spectrom.* 1995**, 30*,*** 1061-1075.

(2) Harrison, W. W.; Hess, K. R.; Marcus, R. K.; King, F. L., *Anal. Chem.* 1986**, 58*,*** 341A-350A.

(3) Marcus, R. K.; Evans, E. H.; Caruso, J. A., *J. Anal. At. Spectrom.* 2000**, 15*,*** 1-5.

(4) Guzowski, J. P.; Hieftje, G. M., *J. Anal. At. Spectrom.* 1999**, 14*,*** 1121-1127.

(5) Guzowski, J. P.; Hieftje, G. M., *J. Anal. At. Spectrom.* 2000**, 15*,*** 27-36.

(6) Majidi, V.; Moser, M.; Lewis, C.; Hang, W.; King, F. L., *J. Anal. At. Spectrom.* 2000**, 15*,*** 19-25.

(7) Klingler, J. A.; Barshick, C. M.; Harrison, W. W., *Anal. Chem.* 1991**, 63*,*** 2571-2576.

(8) Chambers, D. M.; McLuckey, S. A.; Glish, G. L., *Anal. Chem.* 1993**, 65*,*** 778-783.

(9) Jackson, G. P.; Lewis, C. L.; Doorn, S. K.; Majidi, V.; King, F. L., *Spectrochim. Acta* 2001**, 56B*,*** 2449-2464.

(10) Pan, C.; King, F. L., *J Am Soc Mass Spectrom* 1993**, 4*,*** 727-732.

(11) Li, L.; Millay, J. T.; Turner, J. P.; King, F. L., *J. Am. Soc. Mass Spectrom.* 2004**, 15*,*** 87-102.

(12) Eland, J. H. D.; Frey, R.; Schulte, H.; Brehm, B., *Int. J. Mass Spectrom. Ion Phys.* 1976**, 21*,*** 209-211.

(13) Rosenstock, H. M.; McCulloh, K. E., *Int. J. Mass Spectrom. Ion Phys.* 1977**, 25*,*** 327-341.

(14) Rosenstock, H. M.; Larkins, J. T.; Walker, J. A., *Int. J. Mass Spectrom. Ion Phys.* 1973**, 11*,*** 309-328.

(15) NIST *NIST Chemistry Webbook (http://webbook.nist.gov/chemistry)*, March, 2003 Release ed.; National Institute of Standards and Technology: Gaithersburg, MD, 2003.

(16) Munson, M. S. B.; Field, S. H., *J. Am. Chem. Soc.* 1967**, 89*,*** 1047-1052.

(17) Tsuji, M.; Oda, E.; Nishimura, Y., *Chemistry Letters* 1997***,*** 781-782.

(18) Smith, R. D.; Futrell, J. H., *Int. J. Mass Spectrom. Ion Phys.* 1976**, 20*,*** 71-76.

(19) Steiner, B.; Giese, C. F.; Inghram, M. G., *J. Chem. Phys.* 1961**, 34*,*** 189-220.

(20) Steiner, R. E.; Lewis, C. L.; King, F. L., *Anal. Chem.* 1997**, 69*,*** 1715-1721.

(21) Flesch, G. D.; Junk, G. A.; Svec, H. J., *J. Chem. Soc. Dalton Trans.* 1972**, 11*,*** 1102-1105.

(22) Bar, R.; Heinis, T.; Ch., N.; Jungen, M., *Chem. Phys. Lett.* 1982**, 91*,*** 440-442.

(23) Begun, G. M.; Compton, R. N., *J. Chem. Phys.* 1973**, 58*,*** 2271-2280.

Chapter 5. Excitation and Ionization Processes in Nitrogen-Containing Pulsed Glow Discharge Plasmas

5.1. Introduction

The excitation and ionization mechanisms of atomic species in a glow discharge are well understood;[1] however, the behaviors of molecular species have not been thoroughly studied. To make the pulsed GDMS a viable and reliable technique for molecular chemical speciation, it is essential to understand the behavior of molecular species in the pulsed glow discharge plasma, in particular, their interactions with various active plasma species. Of special interest are the energy transfer pathways involving molecular species.

This study employed spectroscopic techniques to investigate the energy transfer processes between nitrogen molecules and various plasma species. Nitrogen was chosen as the probe molecule because the spectroscopic properties of the diatomic molecule N_2 are well known.[2] Nitrogen was introduced into glow discharge plasmas at various concentrations ranging from 0.5% to 3%. The excited N_2 and N_2^+ species, as well as the effects of nitrogen on various plasma species, were monitored using spectroscopic techniques. The results reveal that molecular species undergo extensive interactions with various plasma species, including discharge ions and metastable atoms, electrons, and sputtered species, which make the plasma an efficient ion source for molecular ionization. The improved understanding of molecule-containing glow discharge plasmas proves valuable in our recent efforts to use the device as an ion source for chemical speciation of molecular species. The results also hold potential for the development of new means of ameliorating the interfering effects of working gas impurities on elemental analysis in glow discharge mass spectrometry and optical spectroscopies.

5.2. Experimental Section

The glow discharge device and optical spectrometry apparatus employed here have been described in detail in Chapter 2 and elsewhere.[3, 4] Some modifications have been made to suit this study.

The argon and helium discharge support gas (ultra pure, Airgas, Randor, PA) and nitrogen gas were used in this study. The introduction flow rates and corresponding partial pressures were controlled using metering valves. A thermocouple pressure gauge (Varian 801, Lexington, MA) is used to monitor the pressures. Throughout the experiments, the discharge pressure was fixed at 0.8 Torr for argon and 2 Torr for helium (uncorrected). The concentrations of admixed nitrogen were calculated from its partial pressures.

A copper disk cathode (NIST SRM 495, Gaithersburg, MD), 5 mm in diameter and 2 mm in thickness, was mounted on a direct insertion probe (DIP) and introduced into the discharge chamber. The discharge power is kept on for 5ms and turned off for 15 ms, giving 50 Hz pulsing rate with 25% duty cycle. For the argon plasma, the pulse voltage was set at 800V and the resultant peak current was measured to be 3.2 mA. For helium plasma, the pulse peak voltage was set at 1200 V, giving rise to 2.2 mA peak current.

5.3. Results and Discussion

5.3.1. Interactions between Metastable Atoms and Nitrogen

It has been known that nitrogen molecules can be efficiently excited to $C^3\pi_u$ state by metastable argon atoms through the Penning process:[5]

$Ar^m + N_2(X1\Sigma_g^+,v) \rightarrow Ar^0 + N_2\ (C^3\pi_u)$ (Equation 1)

Having a short lifetime of ~50 ns, $N_2\ C^3\pi_u$ rapidly decays to $B^3\pi_a$ state; therefore, the excitation process can be monitored by measuring the corresponding second positive emission system (Figure 5.1).

The v'-v'' = -2 emission bands of the nitrogen $C^3\pi_u$ to $B^3\pi_a$ transition are shown in Figure 5.2. The pure argon discharge spectrum serves as the background spectrum; only emissions from argon and copper are observed and no N_2 emission is present. The pure nitrogen plasma spectrum clearly shows the emission bands with band heads at 371.1, 375.5, and 380.5 nm. The spectrum of the nitrogen-containing argon plasma exhibits emissions from argon, copper, and nitrogen. As compared with the pure nitrogen plasma, differences can be observed in the nitrogen emission bands: the spectrum of argon-nitrogen mixture exhibits intense emissions originating from highly excited rotational states. It has been established that metastable argon atoms can populate the excited rotational states as high as k’=49,[6, 7] which are not accessible by electron excitation. Therefore, the characteristic intense emissions from the highly excited rotational states indicate that Penning excitation of nitrogen molecules by metastable argon atoms indeed takes place in the argon-nitrogen plasma.

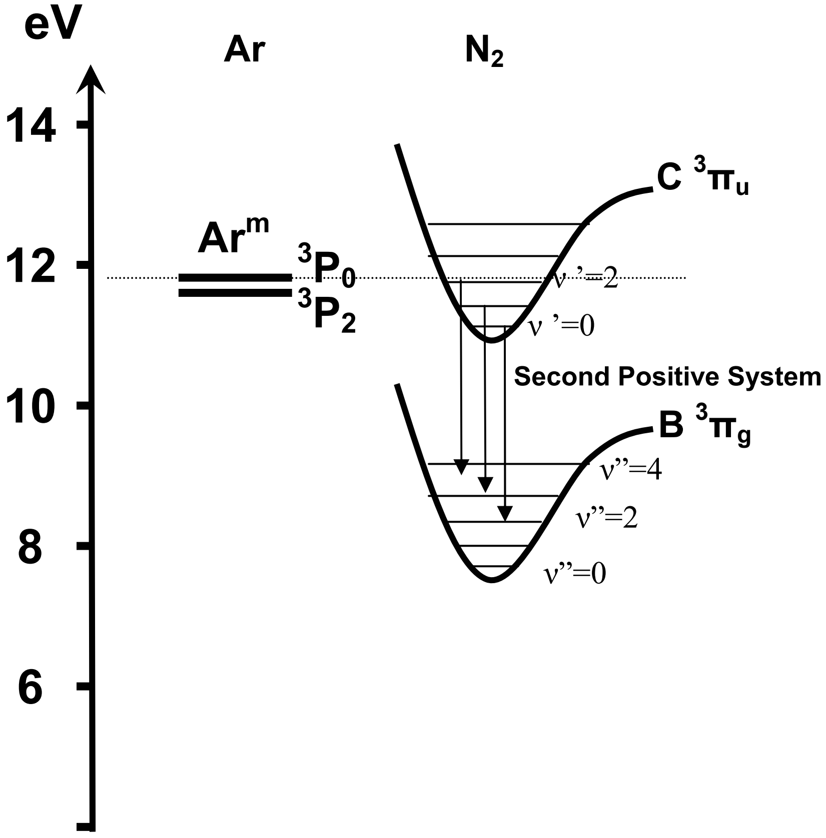

Figure 5.1: Partial energy level diagrams of argon and nitrogen showing the energy transfer process and subsequent radiative decays.

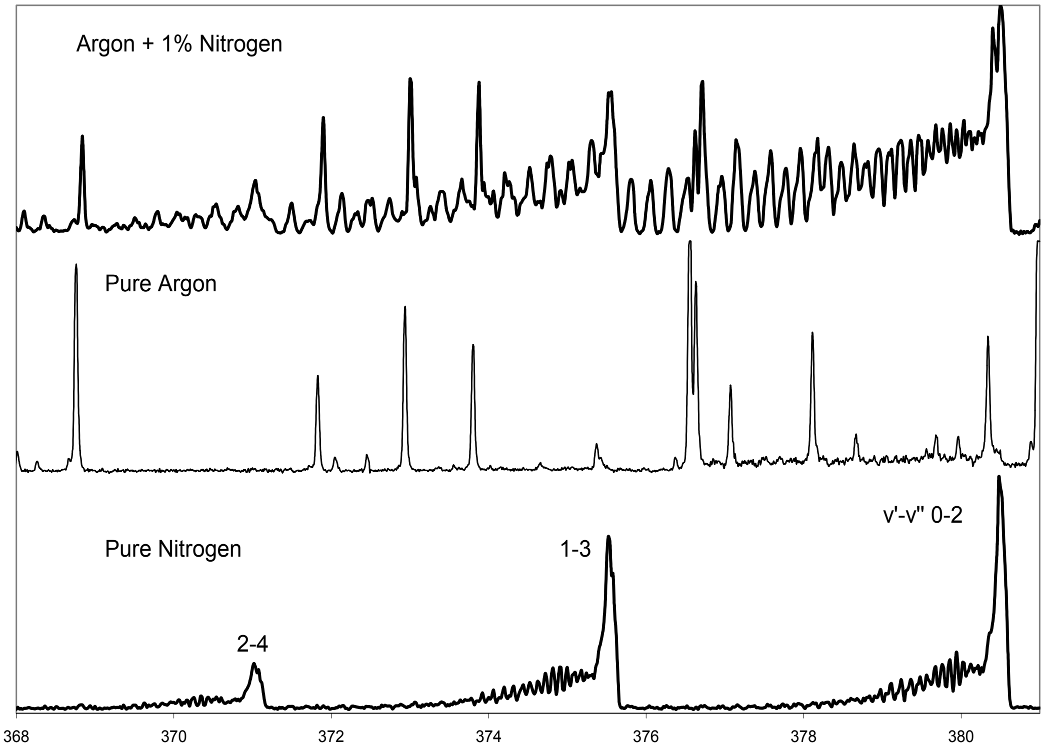

Figure 5.2: Emission spectra of glow discharge plasmas between 368 and 381 nm.

It has been shown that distribution of metastable atoms in a pulsed glow discharge is temporally and spatially inhomogeneous. If the Penning excitation is the dominant mechanism to populate $C^3\pi_u$ state, the excited N_2 population in the plasma should closely match the distribution of metastable argon atom population. In order to make the comparisons, the temporal and spatial population distributions of excited N_2 $C^3\pi_u$ were measured by monitoring 380.5 nm band head emission intensity. The metastable argon atom population was measured using atomic absorption at 811.5 nm, corresponding to the transition from the metastable state 4s $^3P_2$ (11.55 eV) to 4p $^3D_3$ (13.08 eV) state.

As can be seen in Figure 5.3, the temporal profiles of metastable argon atoms and excited nitrogen $C^3\pi_u$ exhibit strong correlation. After the power termination, recombination of argon ions and thermalized electrons yields a large population of metastable argon atoms (Chapter 2);[4] hence, the absorption signals exhibit an intensity increase. In turn, the upsurge of metastable argon atoms should enhance excitation of nitrogen through Penning excitation, yielding a large population of excited nitrogen. Indeed, the population of $C^3\pi_u$ nitrogen molecules was found to increase after power termination, as indicated by the enhancement of its emission observed at the 380.5 nm band head. The maximum of excited nitrogen emission matches that of the metastable argon atom; further indicating that the Penning process is largely responsible for nitrogen excitation to the $C^3\pi_u$ state.

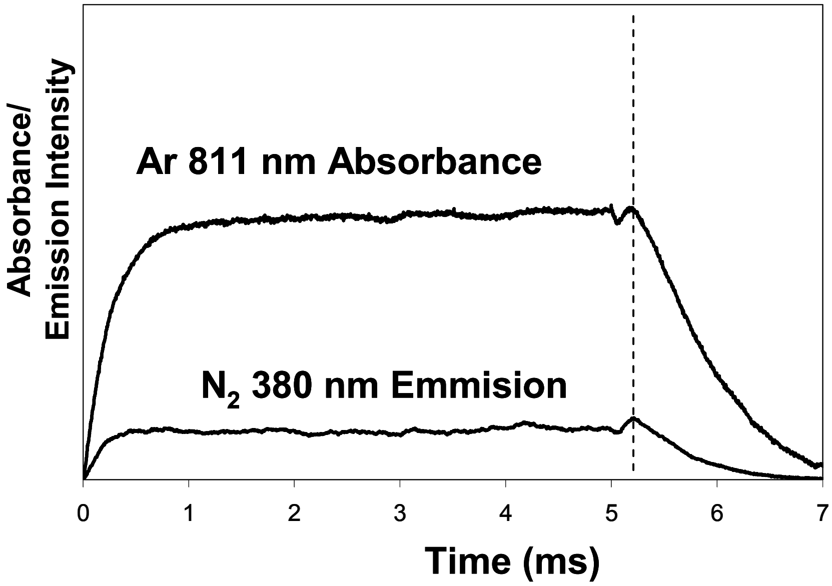

Figure 5.3: Temporal absorbance profile of metastable argon atom at 811.5 nm and the emission profile of nitrogen molecule at 380.5 nm in a pulsed glow discharge plasma.

The spatial distributions were also compared. It has been shown that metastable argon atoms are distributed differently during the plateau and afterpeak regime.[4] During the plateau regime, fast atom processes take place within the cathode dark space, producing abundant metastable argon atoms immediately above the cathode surface. In the afterpeak regime, ion-electron recombination becomes dominant and the metastable argon atom population maximizes at ~5 mm above the cathode. In this study, a similar population maximum shift was observed, as illustrated in Figure 5.4a. Meanwhile, the population maxima of excited $C^3\pi_u$ nitrogen molecules shift from the proximity of the cathode to ~6 mm above the cathode (Figure 5.4b), which closely follows the changes in metastable argon atom distribution (Figure 5.4a). The close spatial and temporal matches strongly indicate that excited nitrogen $C^3\pi_u$ state is predominantly populated by metastable argon atoms via Penning excitation.

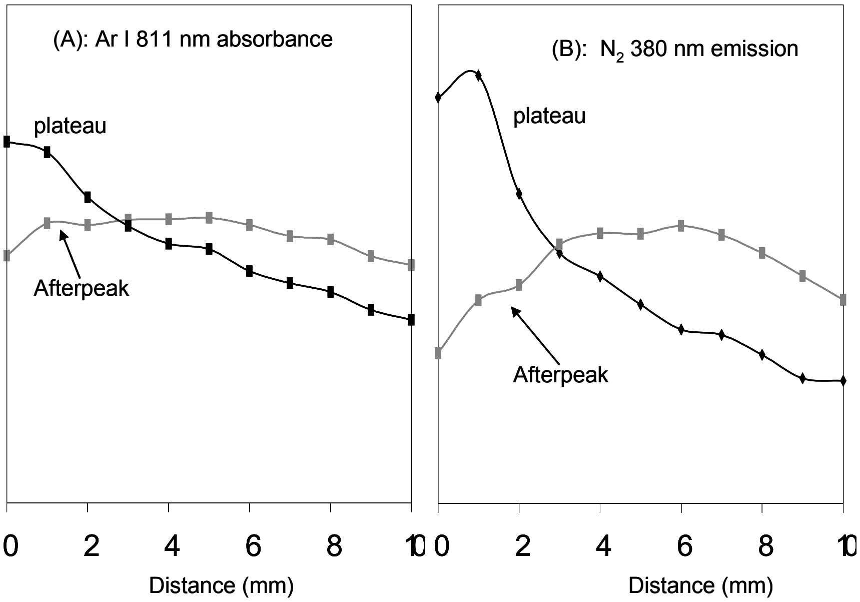

Figure 5.4: Spatial profiles of (a) absorbance of metastable argon atom at 811.5 nm and (b) nitrogen emission at 380.5 nm in a pulsed glow discharge.

5.3.2. Significance of Penning Processes

In glow discharge plasmas, metastable atoms play a significant role in ionization and excitation of sputtered species. Smith et al. [8] showed that metastable atoms account for 40-80% of total ionization of sputtered copper atoms in an argon plasma. For molecular species, the contribution of Penning processes has not been thoroughly studied. Because the reactions between the rare gas metastable atoms and molecular species are known to be efficient,[9] Penning processes are expected to play a significant role in exciting or ionizing such molecular species.

In order to characterize the significance of Penning processes, comparisons were made among the nitrogen emissions arising from a pure nitrogen plasma, a nitrogen-containing argon plasma, and a nitrogen-containing helium plasma. The pure nitrogen plasma spectrum (Figure 5.5a) clearly shows the nitrogen emission bands. Among them, the band heads at 357.7 and 353.7 nm belong to neutral nitrogen $C^3\pi_u$ - $B^3\pi_g$ transition (v'-v'' 0-1 and 1-2, respectively); the band head at 358.2 nm corresponds to nitrogen ion N_2^+ $B^2\Sigma_u^+$ - $X^2\Sigma_g^+$ transition (v'-v'' 1-0). Presumably, both neutral nitrogen and nitrogen ion emission are due to excitation by electron processes. However, in the nitrogen-argon mixture plasma, the nitrogen $C^3\pi_u$ state is selectively populated by metastable argon atoms via Penning excitation while the nitrogen ion N_2^+ $B^2\Sigma_u^+$ state is populated by energetic electrons. In contrast, in a nitrogen-helium plasma, the N_2^+ $B^2\Sigma_u^+$ state is selectively populated by metastable helium atom via Penning ionization (Figure 5.6) [10, 11] while neutral nitrogen N_2 $C^3\pi_u$ state is populated through electron excitation.

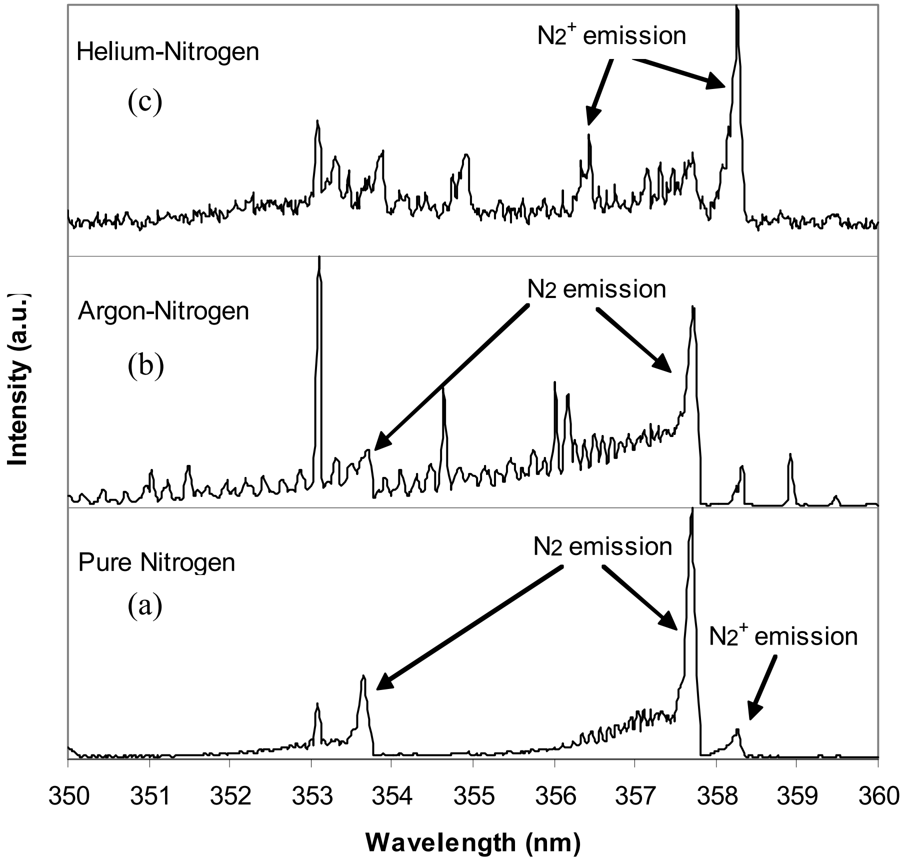

Figure 5.5: Time-averaged emission spectra (350 – 360 nm) of (a) a pure nitrogen plasma, (b) an argon plasma containing 1% nitrogen, and (c) a helium plasma containing 1% nitrogen.

The spectrum of the nitrogen-argon plasma (Figure 5.5b) shows that the neutral nitrogen $C^3\pi_u$ emissions dominate the spectrum. However, in the nitrogen-helium plasma (Figure 5.5c), the neutral $C^3\pi_u$ nitrogen emissions are barely observed whereas the nitrogen ion $B^2\Sigma_u^+$ state emissions become dominant. The variation in relative intensity can be readily attributed to the Penning processes that selectively populate the respective states in these plasmas. The sharp contrast qualitatively indicates that

Penning processes indeed play a significant role in exciting or ionizing molecular species.

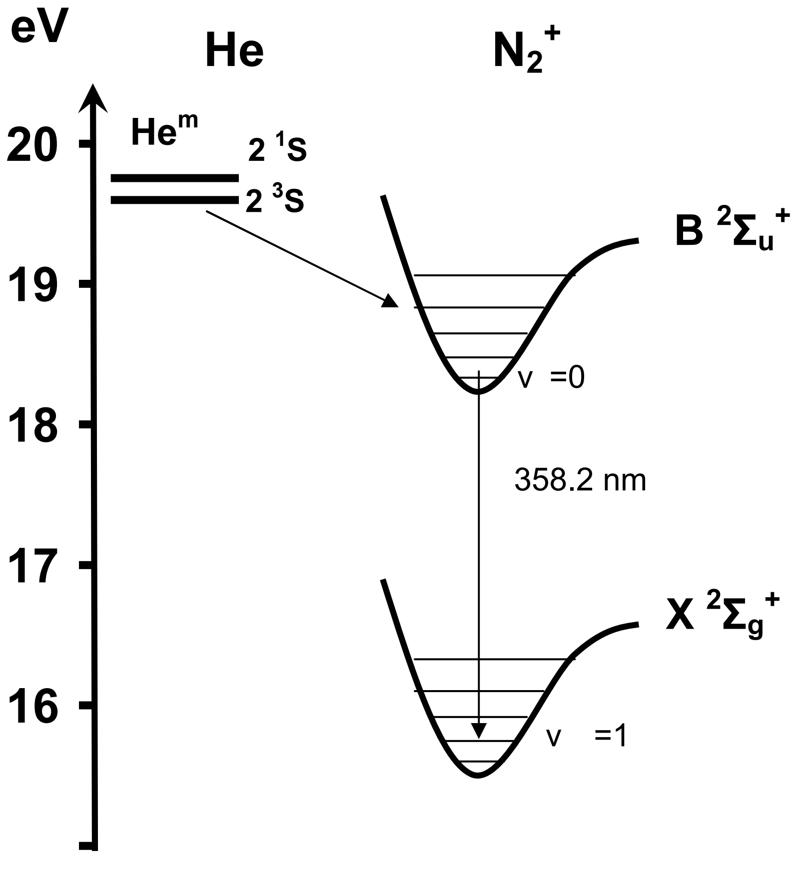

Figure 5.6: Partial energy diagrams of helium and nitrogen showing the Penning ionization process and the subsequent radiative decay

5.3.3. Quenching of Metastable Atoms by Nitrogen

In a typical glow discharge plasma, the metastable atom population accounts for less than 0.1% of the discharge gas atoms.[12] If the molecular species is introduced into the plasma at 1%, the molecular species significantly outnumber the metsatable population. Efficiently reacting with metastable atoms, the molecular species can quench the metastable atom population in the plasma.

In order to examine the expected quenching effect, nitrogen was introduced into argon plasmas at 0.5%, 1%, and 3%. The metastable argon atom populations were measured by monitoring the absorption at 811.5 nm. As shown in Figure 5.7a, the metastable argon atom population decreases with increasing nitrogen concentration. Meanwhile, the emission intensity of excited N_2 $C^3\pi_u$ significantly increases with increasing nitrogen concentration, as suggested by the intensities of nitrogen $C^3\pi_u$ emission band head at 380.5 nm (Figure 5.7b). Furthermore, close matches can be realized between the nitrogen emission profile and the respective metastable argon atom profiles at each concentration. The observations indicate that nitrogen efficiently reacts with metastable argon atoms, thereby quenching their population. Also note that the decrease is more significant during the afterpeak regime. For example, at 3% nitrogen, the metastable argon atom concentration decreases by ~25% during the plateau but by ~70% during the afterpeak regime. Because ionization during the afterpeak regime exclusively depends on Penning ionization,[13] the severe quenching effect would significantly attenuate and even completely disable the plasma ionization capability in the afterpeak regime.

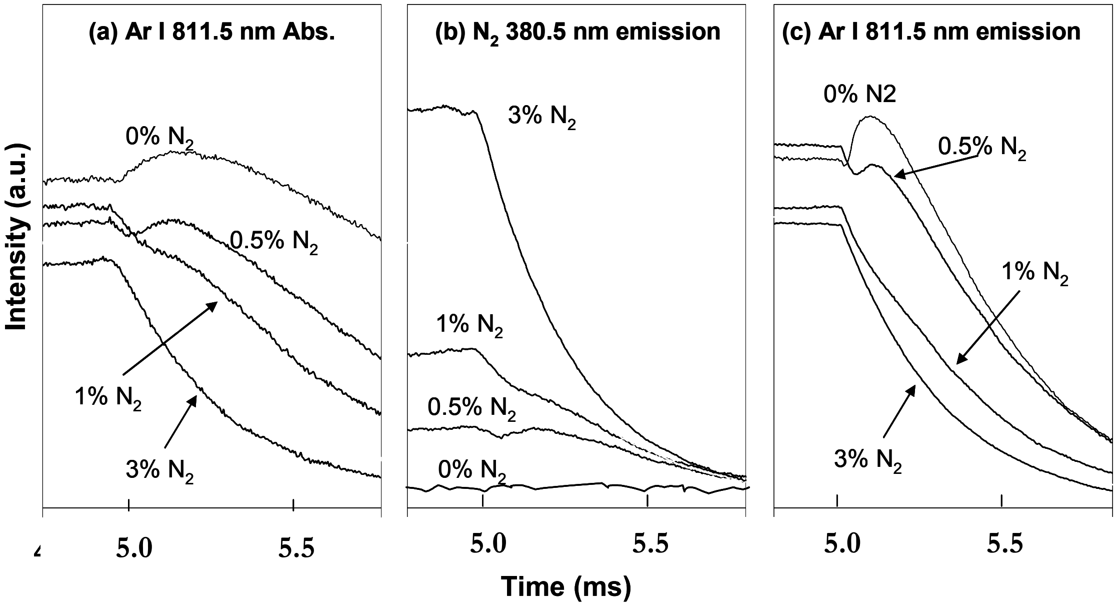

Figure 5.7: Temporal profiles of (a) absorbance of metastable argon atom at 811.5 nm; (b) nitrogen molecule emission at 380.5 nm; and (c) argon atom emission at 811.5 nm.

Further examination revealed that, in the afterpeak regime, nitrogen molecules not only react with metastable argon atoms after their formation, but also prevent the formation of metastable argon atoms, thereby causing more significant quenching effects. This can be seen from the argon 811.5 nm emission profile. With no nitrogen added, the emission intensity increases after power termination (Figure 5.7c), indicating that a large number of metastable atoms are formed through argon ion-electron recombination-decay mechanism.[4] However, as nitrogen was added, the intensity increase was significantly attenuated and completely disappeared at high nitrogen concentrations. This suggests that the argon ion-electron recombination process is hindered and fewer metastable argon atoms would be produced. Presumably, the effect of nitrogen on metastable argon formation is due to two factors. First, the addition of nitrogen decreases argon ion population through charge transfer during the plateau regime; hence fewer argon ions are available for recombination after the power termination. Second, the addition of nitrogen molecules significantly delays electron thermalization in the plasma after power termination. Without nitrogen, electrons quickly thermalize after power termination and subsequently recombine with argon ions. However, in the presence of nitrogen, the vibrational energy stored in nitrogen molecules can be efficiently transferred to electrons via superelastic collisions.[14-16] The electron thermalization is then delayed with respect to power termination, which subsequently hinders ion-electron recombination and metastable atom formation.[17] In our lab, measurements of electron average energy using Langmuir probes are under way to confirm the hypothesis.

The quenching of metastable atoms by nitrogen bears significant implications for the real-world application of the pulsed glow discharge. When a pulsed glow discharge is used for chemical speciation, it heavily depends on the soft Penning ionization during the afterpeak regime to provide molecular information. Because a small amount of molecular species can have dramatic effects on metastable atom formation and population, the plasma has limited sample capacity for molecular ionization. The sample introduction has to be well controlled to ensure efficient plasma ionization. In addition, special attention be paid to vacuum practice and discharge gas purity to prevent unnecessary presence of molecular species of no analytical interest.

5.3.4. Interactions between Nitrogen and Copper

As explained earlier, Penning excitation by metastable argon atoms produces a large number of excited nitrogen ($C^3\pi_u$) molecules in the plasma. The C $^3\pi_u$ nitrogen can radiatively decay to the $B^3\pi_g^+$ state; the $B^3\pi_g^+$ state further vibrationally relaxes to the $A^3\Sigma u^+$ state because of the relatively long life time of nitrogen $B^3\pi_g^+$ state (~1 μs). Being the lowest excited triplet state of nitrogen, the A $^3\Sigma u^+$ state is forbidden to radiatively decay to the ground state; therefore, the $A^3\Sigma u^+$ nitrogen molecules have an extremely long lifetime of ~12s. Because the lifetime is much longer than the mean collision intervals, collisional energy exchange is expected to be the dominant decay mechanism for the $A^3\Sigma u^+$ state nitrogen.

An effective approach for an excited nitrogen $A^3\Sigma u^+$ molecule to release energy is excitation of a copper atom upon collision.[18, 19]

$$\underset{\text{(triplet)}}{N_2(A^3\Sigma u^+, v')} + \underset{\text{(doublet)}}{\text{Cu(ground)}} \rightarrow \underset{\text{(singlet)}}{N_2(X^1\Sigma g^+, v)} + \underset{\text{(quartet / doublet)}}{\text{Cu (excited)}} + \Delta E \quad \text{(Equation 2)}$$

The reaction is expected to be highly selective because it requires resonant energy transfer processes, i.e., the energy level of excited copper atom closely matches the energy loss of nitrogen from ($A^3\Sigma u^+$, v') to ($X^1\Sigma g^+$,v) state. The preferential energy transfer processes suggest that some specific copper states be selectively populated. Therefore, measuring excited copper atom populations can provide direct evidence for the energy exchange process shown in Equation 2.

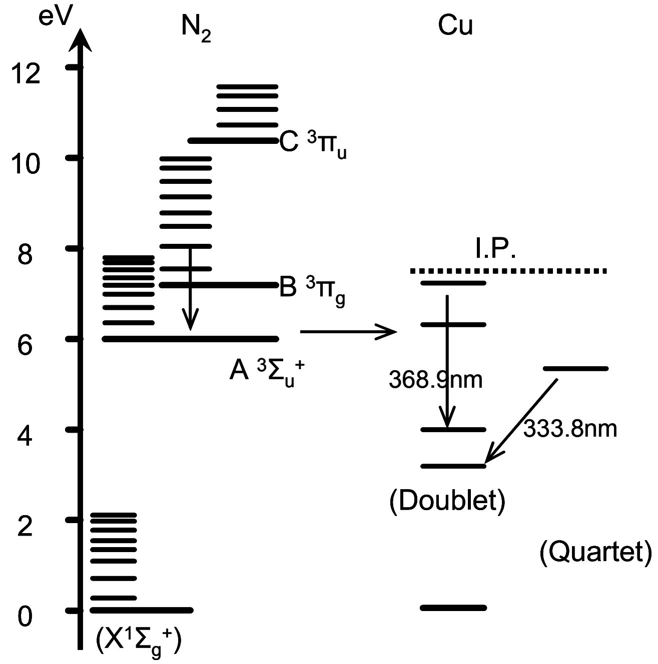

Figure 5.8: Partial energy diagrams of nitrogen and copper showing the energy transfer processes and the subsequent radiative decays.

The population of excited copper atoms can be monitored by measuring the emission intensity associated with the respective excited state. Two emissions are shown as examples and will be discussed in detail. The emission at 368.9 nm corresponds to the transition originating from 4p $^2P^0$ state at 7.18 eV (Figure 5.8); its plateau intensity was severely reduced by the presence of 1% nitrogen (Figure 5.9a). Note N_2 ($A^3\Sigma u^+$, v=0) state lies ~1 eV lower than the 4p $^2P^0$ state, i.e. an energy deficit for ΔE in Equation 1; therefore, the energy transfer process is unlikely. As a result, the high-lying energy states can not be populated by $A^3\Sigma u^+$ excited nitrogen molecules and, hence, the intensities decrease. In sharp contrast, the plateau intensity of 333.8 nm emission (Figure 5.9b) is significantly enhanced when nitrogen is added. This emission originates from 4s ^2D state lying at 5.1 eV above the ground state (Figure 5.8). Note this state level closely matches the energy of $A^3\Sigma u^+$ nitrogen; hence, selective excitation by the $A^3\Sigma u^+$ nitrogen is most likely the reason for the intensity enhancement. It is also noteworthy that the afterpeaks of both emissions are considerably quenched by nitrogen, which can be ascribed to the severe quenching of metastable argon atoms by nitrogen molecules as explained in the previous section.

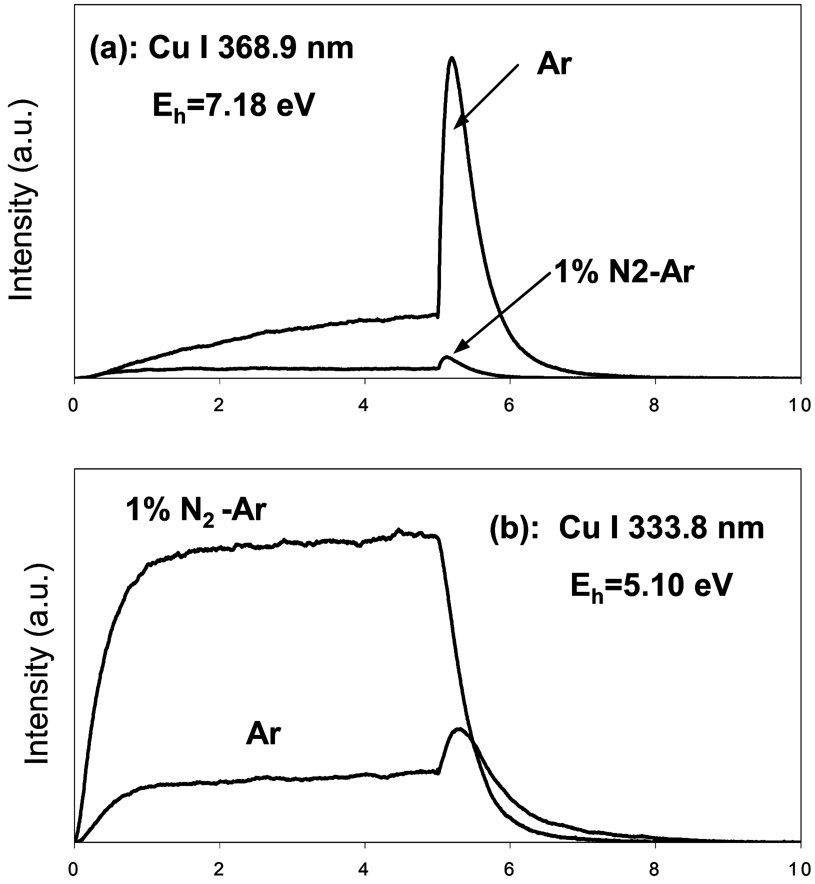

Figure 5.9: Temporal emission profiles of copper atom at (a) 368.9 nm and (b) 333.8 nm.

More copper transitions were further examined; these transitions originate from energy levels across the range between 3.79-7.35 eV. The intensities of these emissions during the plateau regime were measured for the pure argon plasma and 1% nitrogen-argon mixture plasma and the ratios were calculated. Because of the lower sputter yield of nitrogen ions, the sputtered ground state copper atom population is slightly lower in the nitrogen-containing plasma.[20] In this study, atomic absorption measurements showed the copper atom population decreases by 10% when 1% nitrogen is added. Therefore, a factor is integrated in the ratio calculation (Equation 3) to correct the difference in ground copper atom population.

$$\text{Ratio} = \frac{\text{Abs.}_{\text{of Cu in Ar plasma}}}{\text{Abs.}_{\text{of Cu in N2 - Ar plasma}}} \times \frac{\text{Emission Int.}_{\text{of Cu in N2 - Ar plasma}}}{\text{Emission Int.}_{\text{of Cu in Ar plasma}}} \qquad \text{(Equation 3)}$$

The calculated intensity ratios are listed in Table 5.1. When the ratios are plotted against the energies of the upper excited states (Figure 5.10), the selective excitation of Cu by $A^3\Sigma u^+$ nitrogen can be readily realized. The emission intensities of transitions originating from 4.8-5.8 eV are enhanced by $A^3\Sigma u^+$ nitrogen, strongly suggesting these energy states are selectively populated. The different enhancement factor may be associated with the transition probability from $N2(A^3\Sigma u^+, v')$ to $N2(X^1\Sigma g^+,v)$.

Table 5.1. Copper atom emissions and the respective intensity ratios.

Wavelength (nm)	E_L (eV)	E_H (eV)	Transition	Intensity Ratio
202.4	0	6.12	4s ^{2}S-5p ^{2}P^0	0.49
216.5	0	5.72	4s ^{2}S-4p’ ^{2}D^0	1.88
217.9	0	5.69	4s ^{2}S-4p’ ^{2}P^0	1.66
218.2	0	5.68	4s ^{2}S-4p’ ^{2}P^0	1.92
222.6	0	5.57	4s ^{2}S-4p’ ^{4}D^0	1.53
249.2	0	4.97	4s ^{2}S-4p ^{4}P^0	2.59
261.8	1.39	6.12	4s ^{2}D-5p ^{2}P^0	0.78
276.6	1.64	6.12	4s ^{2}D-5d ^{2}P^0	0.60
282.4	1.39	5.78	4s ^{2}D-4p’ ^{2}D^0	0.32
296.1	1.39	5.57	4s ^{2}D-4p’ ^{2}F^0	2.35
299.7	1.64	5.78	4s ^{2}D-4p’ ^{2}D^0	0.91
301.1	1.39	5.51	4s ^{2}D-4p’ ^{4}D^0	2.32
309.4	1.39	5.35	4s ^{2}D-4p’ ^{4}D^0	3.53
319.4	1.64	5.52	4s ^{2}D-4p’ ^{4}D^0	3.11
320.8	1.64	5.51	4s ^{2}D-4p’ ^{4}D^0	3.65
324.7	0	3.82	4s ^{2}S-4p ^{2}P^0	0.68
327.4	0	3.79	4s ^{2}S-4p ^{2}P^0	0.45
328.0	1.64	5.42	4s ^{2}D-4p’ ^{2}F^0	3.65
329.3	1.39	5.15	4s ^{2}D-4p’ ^{4}F^0	3.24
333.8	1.39	5.1	4s ^{2}D-4p’ ^{4}F^0	5.24
344.0	1.64	5.24	4s ^{2}D-4p’ ^{4}F^0	3.84
351.2	3.82	7.35	4s ^{2}S-5p ^{2}P^0	0.51
353.0	1.64	5.15	4p ^{2}P^0-7d ^{2}D	3.76
359.4	1.39	4.84	4s ^{2}D-4p’ ^{4}P^0	5.65
365.4	3.78	7.18	4p ^{2}P^0-6d ^{2}D	0.12
368.9	2.82	7.18	4p ^{2}P^0-6d ^{2}D	0.06
386.2	3.82	7.03	4p ^{2}P^0-7s ^{2}S	0.45
406.3	3.82	6.87	4p ^{2}P-5d ^{2}D	0.09
448.0	3.79	6.55	4p ^{2}P^0-6s ^{2}S	0.33
510.6	1.39	3.82	4s ^{2}D-4p ^{2}P^0	0.71
515.3	3.79	6.19	4p ^{2}P^0-4d ^{2}D	0.72
521.8	3.82	6.19	4p ^{2}P^0-4d ^{2}D	0.21
570.0	1.64	3.82	4s ^{2}D-4p ^{2}P^0	0.78
578.2	1.64	3.79	4s ^{2}D-4p ^{2}P^0	0.36
793.3	3.79	5.35	4p ^{2}P^0-5s ^{2}S	1.18
809.3	3.82	5.35	4p ^{2}P^0-5s ^{2}S	1.19

No enhancement was observed for the energy states out of this range because energy transfer (Equation 2) is not likely with large energy differences ΔE. Significant intensity attenuations are observed for the emissions that originate from highly excited energy levels (E_H> 6 eV). Because these highly-excited states are predominantly populated by copper ion-electron recombination-decay,[13] their populations are closely related with copper ion population in the plasma. The added nitrogen quenches the metastable argon atom population and subsequently Penning ionization of copper; hence, a lower copper ion population would be expected. Therefore, the highly excited copper states would be less populated when nitrogen is added.

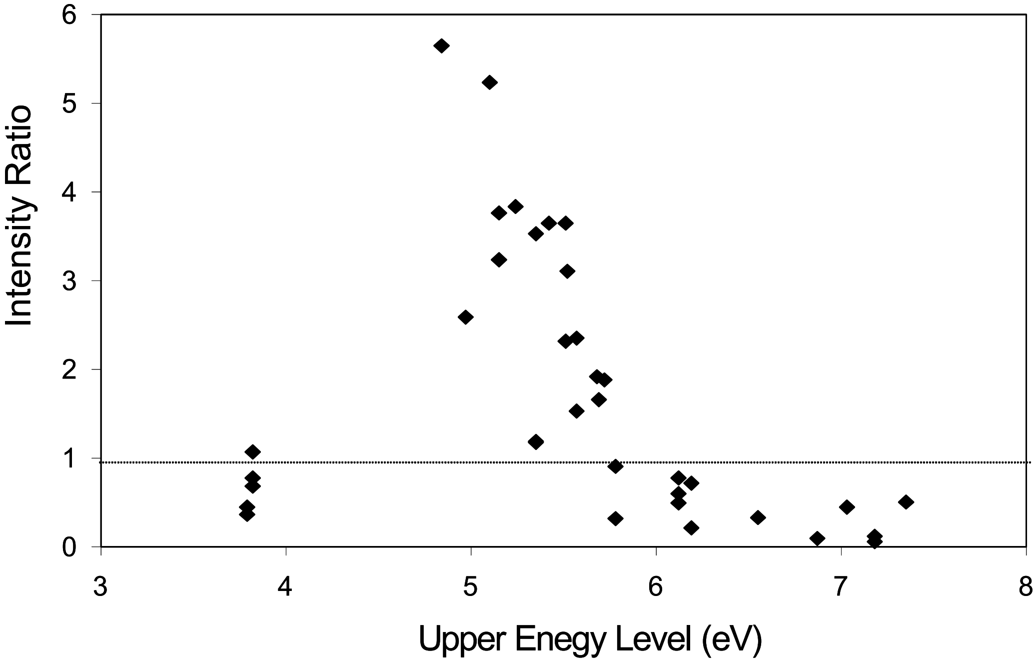

Figure 5.10: Plot of intensity ratios vs. the respective upper energy levels.

5.3.5. Interactions between Nitrogen and Argon Ion

Using mass spectrometry, Jackson et al. [21] observed that the argon ion population was reduced by factors of 5-13 when 1% nitrogen was introduced into an argon glow discharge. The decrease was ascribed to the efficient charge transfer from argon ions to nitrogen molecules.

$Ar^+ + N_2$ (ground) $\rightarrow$ Ar (ground) + N_2^+ $\Delta E=0.2$ eV (Equation 4)

In a glow discharge, the excited argon ions are produced through electron excitation. Because electron temperature is not expected to change significantly upon the addition of 1% nitrogen, the decrease in argon ion population will result in decreases in excited argon ion states. Therefore, argon ion emission would be significantly reduced. However, in this study, the argon ion emissions were found to be virtually unaltered by the addition of nitrogen. The argon ion 427.7 nm emission, corresponding to transition from $3p^4 3d$ state, is shown in Figure 5.11 as an example. It suggests that the introduced nitrogen has no significant influence on the argon ion population.

In a plasma, nitrogen ions can be vibrationally excited by electrons. Several studies have shown that the vibrationally excited nitrogen ions are capable of ionizing argon through charge transfer.[22, 23]

N_2^+ (v=1,2,..) + Ar (ground) $\rightarrow$ N_2 (ground) + Ar^+ (Equation 5)

Because potential energies of the excited nitrogen ions exceed the ionization potential of argon (Figure 5.12), the reaction is energetically favored and proceeds very fast. Even though argon ions are lost through charge transfer to nitrogen, they can be quickly regenerated through Equation 5. Therefore, the argon ion population may not be significantly reduced by the addition of nitrogen. Mass spectrometric measurements of argon ion and electron energy measurements are necessary to better understand the interactions between nitrogen and argon ion.

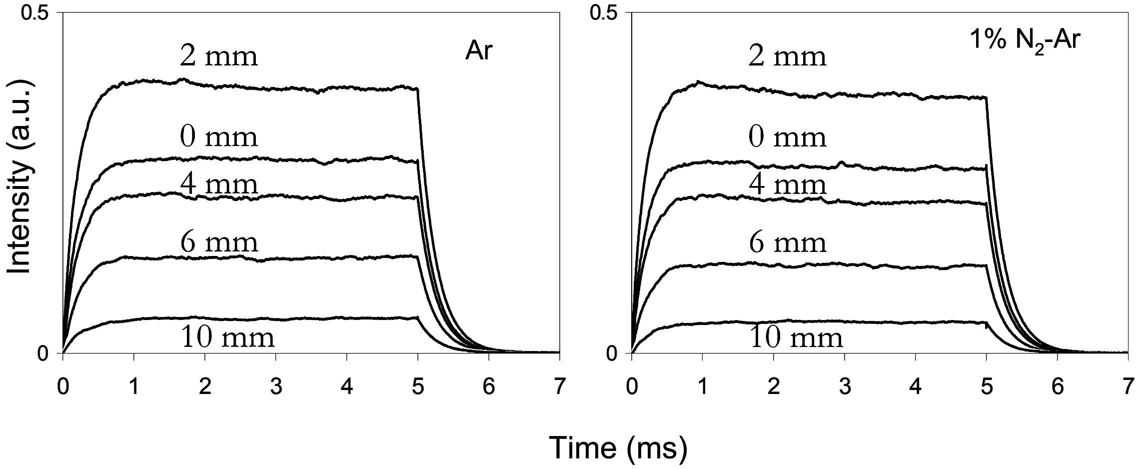

Figure 5.11: Temporal emission profiles of argon ion at 427.7 nm in (a) a pure argon glow discharge and (b) a 1% N2-Ar glow discharge.

Charge transfer between argon and nitrogen are further complicated by the presence of a low-lying argon ion metastable state $^2P_{1/2}$ at 15.94 eV (Figure 5.12). As the transition from $^2P_{1/2}$ to $^2P_{3/2}$ is forbidden, the $^2P_{1/2}$ state can not be directly observed spectroscopically. However, this state can be monitored indirectly through copper ion emission 224.7 nm which originates from charge transfer from $^2P_{1/2}$ argon ion to copper atom (Eauqtion 6).

$Ar^+ (^2P_{1/2}) + Cu^0 \rightarrow Ar^0 + Cu^{+*} (4p\ ^3P_2)$ (Equation 6)

The 4p $^3P_2$ copper ion radiatively decays, giving off 224.7nm emission. As copper atom population is known to be relatively stable, the emission change largely reflects the population changes of $^2P_{1/2}$ argon ion.

Figure 5.13 shows the profile of the copper ion 224.7 nm emission. When nitrogen is absent (Figure 5.13a), the emission quickly reaches a plateau value at ~1 ms, indicating Ar^+ ($^2P_{1/2}$) population quickly reaches a steady state. However, when nitrogen was introduced, the emission (Figure 5.13b) increases slowly till the power termination; no evident plateau is observed. At power termination, the emission intensity is approximately equal to that without nitrogen, suggesting that the Ar^+ ($^2P_{1/2}$) population was not significantly influenced. The addition of nitrogen clearly influences the kinetics of Ar^+ $^2P_{1/2}$ state being populated, as indicated by the difference in the temporal profiles. Although the exact pathway cannot be resolved at this point of time, it is presumed that the charge transfer process between argon and nitrogen affect the Ar^+ $^2P_{1/2}$ state population. It is also likely that N_2^+ (v=1,2) directly ionizes copper through charge transfer and produces excited copper ion 4p $^3P_2$ because of the close energy matches.

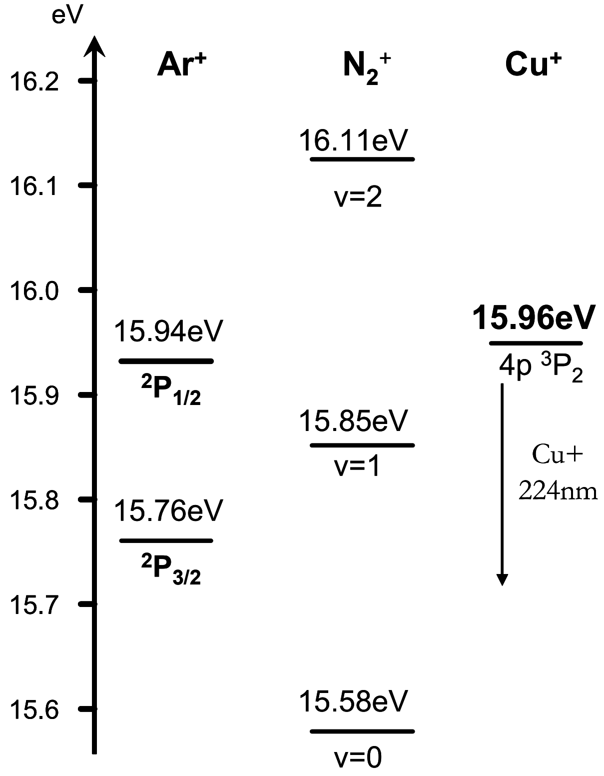

Figure 5.12: Partial energy diagrams of Ar^+, N_2^+, and Cu^+.

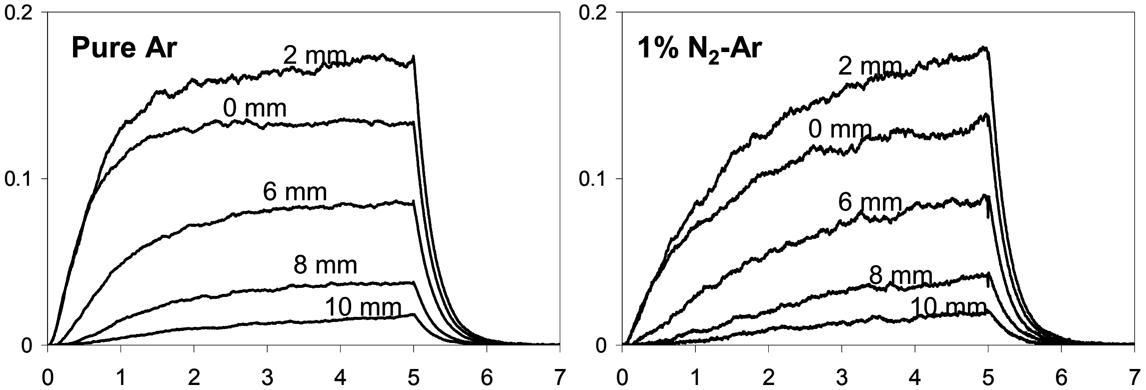

Figure 5.13: Temporal emission profiles of copper ion at 224.7 nm in (a) a pure argon discharge; and (b) a 1% N2-Ar discharge.

The interactions of nitrogen molecules with various plasma species are summarized in Figure 5.14. Of special interest are the Penning excitation by metastable argon atoms, charge transfer by argon ions, and electronic and vibrational excitation by electrons. In turn, the excited nitrogen can also transfer energy to the sputtered copper atoms, leading to selective excitation.

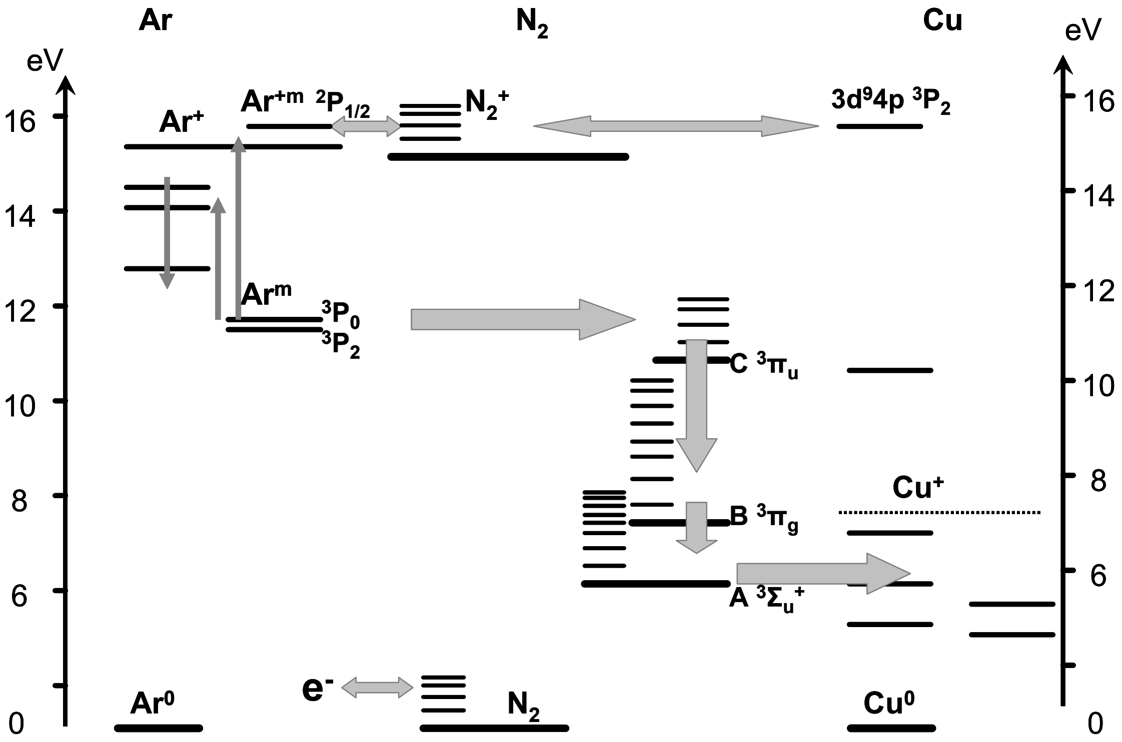

Figure 5.14: Partial energy level diagrams of argon, nitrogen, and copper showing the energy transfer processes.

5.4. Conclusions

Molecular species introduced into a glow discharge can efficiently interact with plasma species through various energy transfer processes. A glow discharge plasma provides a rich excitation/ionization environment for molecular species. In addition, the ionization of molecular species varies as the dominant ionization mechanisms alternate over a pulse cycle. Introduced molecules can also significantly alter the plasma environment and may have adverse effects on molecular ionization. High concentrations of molecular species can dramatically lower, and even completely quench, plasma ionization efficiency; therefore, the plasma has limited ionization capacity for molecular species. Sample introduction control is critical for the analytical performance of glow discharge ion source.

It has also been shown that even a small amount of a molecular impurity in the discharge gas may cause considerable interference with elemental analysis in glow discharge mass spectrometry and optical spectroscopic techniques. It is difficult to correct the interfering effects because they are specifically dependent on the identities of the impurity and analyte element. Hence, high purity gases and good vacuum practice are essential for good precision and accuracy.

Furthermore, this study showed that spectroscopic techniques can provide rich insights into the plasma chemistry of molecular ionization and excitation. Further study will employ this technique for various molecule-containing plasma, such as O_2 and

$Fe(CO)_5$ in argon or helium plasmas. The results can be further combined with other information, such as ion population data obtained from mass spectrometry and electron characteristics obtained from Langmuir probe measurements, to achieve a better understanding of molecule-containing plasmas.

5.5. References

(1) Chapman, B. N. *Glow Discharge Processes*; John Wiley and Sons: New York, 1980.

(2) Lofthus, A.; Krupenie, P. H., *J. Phys. Chem. Ref. Data,* 1997**, 6*,*** 133-301.

(3) King, F. L.; Pan, C., *Anal. Chem.* 1993**, 65*,*** 735-739.

(4) Jackson, G. P.; Lewis, C. L.; Doorn, S. K.; Majidi, V.; King, F. L., *Spectrochim. Acta* 2001**, 56B*,*** 2449-2464.

(5) Wagatsuma, K.; Hirokawa, K., *Anal. Chem.* 1989**, 61*,*** 326-329.

(6) Fishburne, E. S., *J. Chem. Phys.* 1967**, 47*,*** 58-63.

(7) Stedman, D. H.; Setser, D. W., *Chem. Phys. Letters* 1968**, 2*,*** 542-544.

(8) Smith, R. L.; Serxner, D.; Hess, K. R., *Anal. Chem.* 1989**, 61*,*** 1103-1108.

(9) Stedman, D. H.; Setser, D. W., *Prog. Reaction Kinetics* 1971**, 6*,*** 193-238.

(10) Richardson, W. C.; Setser, D. W., *J. Chem. Phys.* 1973**, 58*,*** 1809-1825.

(11) Schmeltekope, A. L.; Ferguson, E. E.; Fehsenfeld, F. C., *J. Chem. Phys.* 1968**, 48*,*** 2966-2973.

(12) Ferreira, N. P.; Strauss, J. A.; Human, H. G. C., *Spectrochim. Acta* 1983**, 38B*,*** 899-911.

(13) Lewis, C. L.; Jackson, G. P.; Doorn, S. K.; Majidi, V.; King, F. L., *Spectrochim. Acta* 2001**, 56B*,*** 487-501.

(14) Hurle, I. R., *J. Chem. Phys.* 1966**, 41**.

(15) Shulz, G. J., *Phys. Rev.* 1962**, 125*,*** 229-232.

(16) Dilecce, G.; De Benedictis, S., *Plasma Sources Sci. Technol.* 1993**, 2*,*** 119-122.

(17) Jackson, G. P.; King, F. L., *Spectrochim. Acta* 2003.

(18) Rosenwaks, S., *Chem. Phys. Letters* 1979**, 64*,*** 352-356.

(19) Nadler, I.; Rosenwaks, S., *Chem. Phys. Letters* 1980**, 69*,*** 266-269.

(20) Wagatsuma, K., *Spectrochim. Acta* 2001**, 56B*,*** 465-486.

(21) Jackson, G. P.; King, F. L., *Spectrochim. Acta* 2003**, 58B*,*** 185-209.

(22) Smith, D.; Adams, N. G., *Physical Review A* 1981**, 23*,*** 2327-2330.

(23) Lindinger, W.; Howorka, F.; Lukac, P.; Kuhn, S.; Villinger, H.; Alge, E.; Ramler, H., *Phys. Rev. A* 1981**, 23,** 2319-2325.

CHAPTER 6: Determination of Bromine in Flame Retardant Plastics Using Pulsed Glow Discharge Time-of-Flight Mass Spectrometry

6.1. Introduction

Since the 1950s the production of plastics has grown into a major industry with profound influence on technology and modern lifestyles. Plastics are now one of the most widely used materials in the world. Motivated by the needs of the plastics industry, analytical techniques applied to polymers have been evolving in the last several decades. These techniques predominantly focus on the characterization of basic polymer resins, for example, chemical conformation and structural elucidation, molecular weight determination, and surface characterization. For these purposes, techniques including infrared and Raman spectroscopies[1], X-ray photoelectron spectroscopy[2], gas chromatography[3], and secondary ion mass spectrometry (SIMS)[4] have been successfully employed.

In the modern plastics industry, the selection and use of additives are important to the successful development and application of products. Additives are used extensively to modify the physical properties and cosmetic appearance, or to facilitate the processing of plastics. These additives vary widely in function, from colorants to antimicrobials, and over a large range of concentrations, from a few ppm to a few percent. Many contain elements that play significant roles in their functions, such as bromine or chlorine in flame retardants, zinc in antimicrobials, and titanium in white pigments. Consequently, qualitative and quantitative elemental analyses are of increasing importance.

Many elemental analysis techniques have been adopted for application to plastic samples.[5] Solution-based methods involve sample preparation, usually by ashing, wet oxidation, and/or organic solvent dissolution, followed by atomic absorption/emission spectroscopy (AAS/AES) or mass spectrometry. Because standard solutions can be readily prepared for calibration curve construction or standard addition, quantification, with high degrees of accuracy and precision, is straightforward. These methods also provide excellent detection limits. Unfortunately, sample preparation for these solution-based methods is time-consuming and subject to contamination or loss of volatile elements. Moreover, for plastic samples with limited solubility, these methods are either inconvenient or impractical. For these reasons, the development of direct analysis methods is justified and draws growing attention.

Although the unmatched speed of X-ray fluorescence (XRF) and neutron activation analysis (NAA) has led to their routine use for production control, they are able only to provide semiquantitative results and suffer from poor sensitivities and detection limits. Solid sampling techniques, especially laser ablation, has been successfully coupled to ICP-MS[6], AES[7] and other sensitive analysis methods. Low limits of detection can be achieved, but quantitative measurements still depend on the availability of standard plastic materials.

Glow discharge mass spectrometry (GDMS) has been well established as a direct elemental analysis method for solid samples.[8,9] Its advantages include low detection limits, minimum matrix effects, stable ion signals, and simple sample preparation.[10] The development of a radio frequency glow discharge (rf-GD) source allowed direct analysis of non-conductive solids including ceramics, glasses, and semiconductors.[11,12] This source, coupled with mass spectrometric detection, also proves useful in the structural characterization of polymers.[11,13-15]

Using direct current GDMS with the secondary cathode technique, Schelles and Grieken determined elemental species in plastics.[16] With this technique iron contained in a PTFE sample at 100-500ppm was readily observed. Although the authors postulated GDMS could provide trace element analysis for polymer samples, quantification was not accomplished because certified polymer standards were not available.

There are many challenges to the use of GDMS for plastics analysis. Among these, thermal degradation of samples is a major concern. Electric power dissipation and ion bombardment generate tremendous heat. Because of the thermal lability of plastics, overheating can result in unwanted thermal desorption, plasma instability, and even sample melting. One approach to overcoming this concern is the use of a sample cooling system to alleviate sample overheating.[17] Unfortunately such systems not only introduce additional complications to GD cell design, they are also not very efficient for plastic samples because of their low thermal conductivity – i.e., local overheating at the sample surface may still be problematic.[16] Another issue is some plastic samples, especially hydrocarbon polymers, provide relatively weak ion signals.[11] This not only hinders molecular structure elucidation, but also severely limits sensitivity. It is important these challenges be met for GDMS to be accepted as a general analysis technique for plastic samples. Pulse powered GDMS may afford solutions to these challenges.

Pulsing the glow discharge power permits operation at a higher instantaneous power compared to continuous power operation at the same average power.[18] The higher instantaneous power over the pulse period significantly enhances the sputter yield and ionization efficiency. Time-gated detection methods measure intense signals only during the short pulse period, yielding better analytical results.[19] On the other hand, the lower average power limits heat generation. Sample heating generated during “on” pulses tends to dissipate during “pulse-off” periods. Hence, sample temperature can be kept low throughout the experiment. Furthermore, temporal variation of mass spectra over a pulse cycle allows for discrimination of analytical signals from background interferences.[20]

This study concerns the application of pulsed rf-GDMS for the identification and quantification of bromine in plastic samples. Bromine was selected as the target element because bromine-substituted organic compounds are widely used as flame-retardants in plastics. In addition, bromine compounds are often sensitive to thermal decomposition so the bromine signal can be used to test the ability of the pulsed glow discharge to alleviate sample overheating. Direct analysis of bulk plastics was undertaken because we believed it would provide both elemental composition and molecular information. Comparison of sputter rates of various polymers provided insight into the sputter atomization of polymer molecules, thereby improving our understanding of fundamental rf glow discharge processes. Ultimately, the low sputtering rate of the selected polymers required the use of sample cathodes consisting of powdered plastics compacted into a silver host matrix to facilitate quantitative bromine analysis.

6.2. Experimental Section

Mass Spectrometer. The time-of-flight mass spectrometer (ToF) and data acquisition system have been described in detail previously[21] and are only briefly re-introduced here. A flexible coupling (MDC Vacuum Products Co., Hayward, CA) attached to the ToF flange serves as the glow discharge chamber. Samples, mounted on a direct insertion probe (DIP)[22], can be introduced into the glow discharge chamber through a ball-valve interlock assembly without breaking vacuum. The glow discharge was powered by a 13.56 MHz radio frequency generator (Model RF 10-S, RF Plasma Product Inc., Marlton, NJ) coupled through an automatic matching network (Model AM-10, RF Plasma Product Inc.). The internal pulsing mode of the rf power supply permits control of applied power, pulse width, and duty cycle. Throughout the experiments, the rf pulse width was set at 5 ms while the pulse duty cycle and power, as well as discharge gas pressure were varied. Ultra pure argon and helium (Airgas, Randor, PA) were used as discharge support gases.

General operating conditions for the ToF mass spectrometer are presented in Table 6.1. The conditions were optimized to yield maximum signal for bromine ions. The orthogonal flight tube design of the ToF permits ion extraction from the glow discharge source by pulsing the ToF repeller. A digital delay generator (Model 4144, EG&G Princeton Applied Research, Princeton, NJ), synchronized with the plasma rf power pulse, subsequently triggers the application of an 1 μs ion extraction pulse to the ToF repeller. This timing scheme allows for setting a detection gate to monitor the ions formed at a specific time within the power pulse sequence. The temporal position of the detection gate can be easily adjusted on the digital delay generator.

Table 6.1. Operating parameters used for the GD ToF-MS experiments.

Time-of-flight mass spectrometer	
Flight path length	1 m
Skimmer potential	-700 V
Repeller pulse duration	2 μs
potential	+200 V
Extractor grid potential	0 V
Accelerator grid potential	-2100 V
Flight tube liner potential	-2100 V
Deflection plate (X1) Potential	-2200 V
Deflection plate (Y1) Potential	-2100 V
Detector potential	-1800 V
Vacuum Conditions	
1st Stage	0.4-2 Torr
2nd Stage	10^{-5} Torr
3rd Stage	10^{-6} Torr

The gated mass spectrometric signal is amplified and fed to a 1-GHz oscilloscope (LeCroy 9370M, Chestnut Ridge, NY), digitized and averaged for 100 sweeps. Through a GPIB interface, averaged mass spectral data were imported into a Microsoft Excel 97 spreadsheet program (Microsoft, Redmond, WA) for construction of mass spectra.

Sample Preparation. All samples were provided by GE Plastics (GEP, Washington, WV). Samples numbered 1-4 were a series of acrylonitrile-butadiene-styrene (ABS) based plastics containing different concentrations of 4-4$^{'}$ – (1-methylethylidene) bis [2, 6 – dibromophenol], commonly referred to as tetrabromobisphenol A or TBBPA. A bromine-free ABS plastic sample was used as a blank. Poly-tetrafluoroethylene (PTFE), acrylic-styrene-acrylonitrile (ASA), and polycarbonate (PC) polymers were used to gauge sputter rate. All of the samples were molded bars with dimensions of 165×15×5 mm.

Two different procedures were followed to prepare plastic samples for GDMS analysis. For bulk plastic samples, cylinders of 4 mm diameter and 8 mm height were cut directly from the sample bar. A 3 mm diameter cavity was drilled from the bottom of the cylinder and its depth was carefully controlled such that the thickness of the top layer extended 0.3 mm (unless noted otherwise) beyond the cathode holder, described below. This was done so as to minimize sample thickness and provide efficient rf power density at the surface. The samples were washed using distilled water and methanol, and dried overnight in an oven at 80 ^{0}C. During sample assembly, the specimen was first slid onto the cathode holder, a 15 mm long copper rod, with the end sides tightly fitted against the copper rod to ensure good electric contact. The other end of the copper rod was inserted into a beryllium-copper connector and secured by a screw set to the end of the DIP. A schematic of the assembly is shown in Figure 6.1.

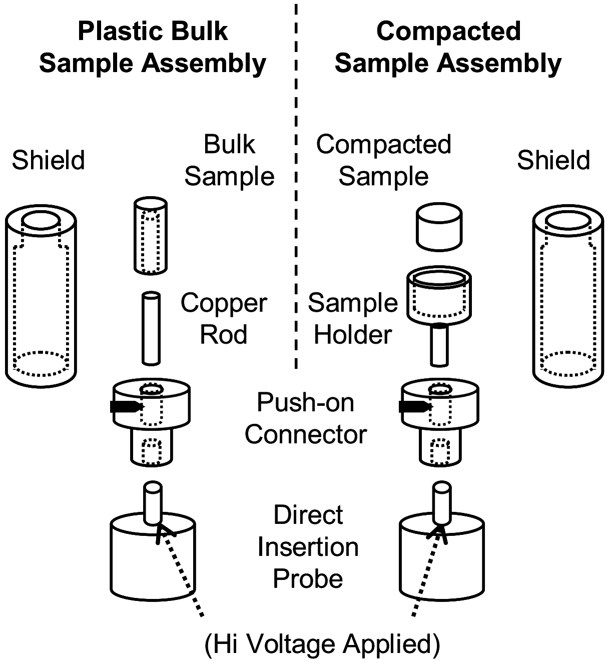

Figure 6.1. Schematic presentation of the sample holders for bulk plastic and compacted plastic samples.

For the compacted samples, the plastic sample bars were first milled to powders using a cryogenically cooled mill (SPEX 6700 Freezer/Mill, SPEX CertiPrep, Metuchen, NJ). The large particles therein were excluded using a U.S. standard #60 sieve. The sieved powders were collected, dried, and then mixed with silver powder (crystalline, -60+80 mesh, premion ®, Alfa Aesar, Ward Hill, MA) at 18:1 silver to polymer mass ratio.

The mixtures were homogenized for 2 minutes using a laboratory mixer (Wig-L-Bug, SPEX, Edison, NJ). After drying overnight in an oven at 80 ^{0}C, each mixture was compacted, at 5000 psi for 1 minute, into sample cathode disks of 5mm diameter and 3 mm thickness. The resultant sample disk was loaded in a push-on connector by way of a machined stainless steel sample holder (Figure 6.1). When preparing compacted standards, the bromine-free ABS plastic powder was mixed with a known amount of TBBPA (99%, Aldrich, Milwaukee, WI, USA) or KBr (anhydrous, 99.95%, Aldrich, Milwaukee, WI, USA). The bromine concentration was calculated (as elemental Br) for each standard.

For both bulk and compacted samples, each sample assembly was mounted on the DIP through the push-on connector and shielded by an aluminum sleeve such that only the top surface was exposed to the plasma. Then, the DIP was inserted into the glow discharge chamber to pump down for 15 minutes before the glow discharge plasma was initiated.

6.3. Results and Discussion

6.3.1. Direct Sampling of Bulk Polymer Samples

Direct bulk sample analysis is obviously preferred for its simplicity and speed. To assess the GD's capability for direct analysis of ABS, Sample Number 1 (9.23% bromine) was examined extensively. The glow discharge was operated using 0.8 Torr argon, 90 W rf power, and 25% duty cycle. A pale-blue glow discharge plasma can be seen at the sample surface and it is noted its intensity decreases dramatically as distance from the cathode increases. The nearness of the plasma to the cathode surface produces difficulties for sampling because arcing and plasma instability arise when the cathode is moved close to the grounded ion exit orifice. The sampling distance was adjusted to maximize Br^+ analyte signals while maintaining plasma stability. The optimum sampling distance was found to be 4-5 mm from the cathode surface at 0.8 Torr.

Pulsed operation of the rf power supply yields a plasma with excitation and ionization processes exhibiting a strong temporal dependence. Consequently, temporal variation of bromine ion signal was observed over the pulse cycle. The bromine signal is first observed at 0.5 ms into the power pulse, 0.3ms after the breakdown of the working gas. The delay is caused by a cascade of processes responsible for generating sputtered species (i.e., atomization via sputtering, diffusion into the negative glow, and ionization therein). After 1 ms, bromine signal reaches a steady state and remains practically unchanged until the termination of the power pulse at 5 ms. Once the power is terminated, bromine signals starts decaying into the noise in less than 0.2 ms. The behavior can be rationalized by the disappearance of electron ionization and charge transfer ionization mechanisms. Although the Penning ionization mechanism should be enhanced after the pulse termination[23], it has no effect on bromine ion signal because the ionization potential of bromine (11.81 eV) is higher than the energy levels (11.55 and 11.62 eV) of metastable argon atoms responsible for Penning ionization. The temporal profile of bromine requires the detection gate be set within the steady state regime during the pulse, i.e., between 1 and 5 ms. It should be noted that the argon dimmer ion exhibits a similar temporal profile.

A mass spectrum acquired from Sample Number 1, 4.0 ms after pulse application and 4 mm away from the cathode surface, is shown in Figure 6.2. Signals arising from the discharge support gas, argon, are observed at m/z values of 40 (Ar^+), 80 (Ar_2^+), and 41 (ArH^+), along with an H_2O^+ peak arising from the imperfect vacuum and moisture trapped in the sample. Also observed, at much lower intensities, are signals arising from sputtered plastic species in m/z ranges 12-17 and 26-31, corresponding to CH_x^+ or NH_x^+ and $C_2H_x^+$ or CNH_x^+ (where x=0,1,2,etc.) respectively. Bromine ion signals are observed at m/z values of 79 and 81.

The surface of Sample Number 1 was examined by scanning electron microscopy (SEM) both before and after sputtering. Prior to sputtering, microscopy reveals that sample surface is essentially smooth with the exception of very shallow concentric grooves caused by machining. In contrast, a micrograph of the sample surface after sputtering (Figure 6.3 A) exhibits the cone and needle-like projections that are characteristic of the sputtering process.[14] Although these observations give merit to the idea that classical glow discharge processes are responsible for the creation of analyte ions, the signal-to-noise ratio is unsatisfactory for quantitative analysis. Various measures were undertaken to increase bromine signal intensities to afford quantitative analysis.

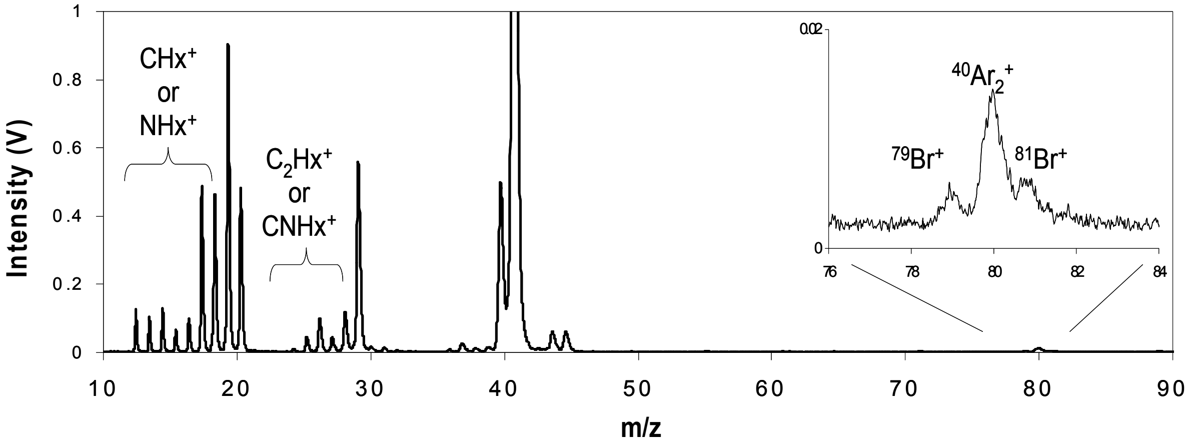

Figure 6.2. Mass spectrum of Sample Number 1 obtained from the bulk (operating power 90 W, 25% duty cycle, and argon pressure 0.8 Torr).

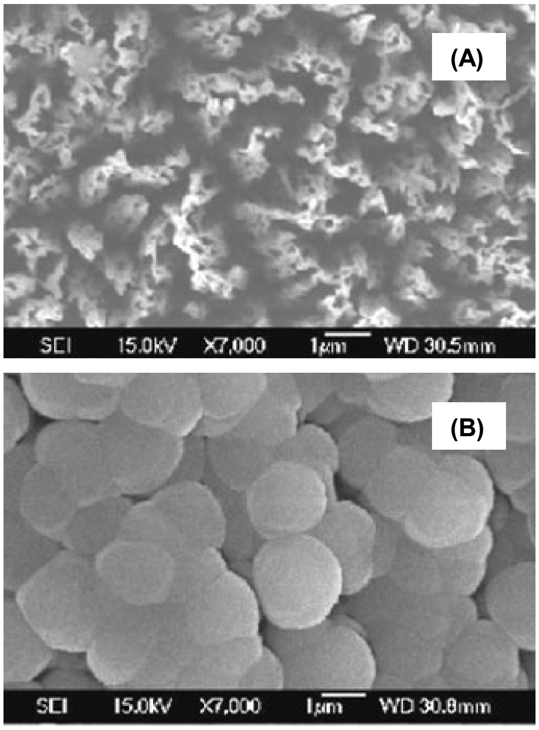

Figure 6.3. Scanning electron micrographs (1300x magnification) of Sample Number 1. (A): sputtered for 8 hours under 90 W, 25% duty cycle, and 0.8 Torr argon; (B): overheated after applying 140 W power, 25% duty cycle for about 10 min at 0.8 Torr.

Variation in the sample thickness was the first variable considered. Increased sample thicknesses result in greater rf power loss and lower dc-bias in nonconductive samples.[24] The result of these effects is a reduction in sputter rates and analyte signal intensities.[14,25] To optimize sample thickness and thereby enhance bromine signal intensity, a set of samples with thicknesses of 0.3, 0.6, 0.9, 1.2, and 1.5 mm were examined. None of these samples exhibited a significant difference in the bromine signal intensity, presumably because the absolute changes in thickness were so small.

The effect of pressure was evaluated by varying the argon gas at 100 W operating power; the results are illustrated in Figure 6.4. Previous studies showed elevated pressures favor the observation of atomic species because of the increased collision induced dissociation (CID).[14,26-28] This CID effect was also observed in the present study, as indicated by the increasing ratio of C^+ to CH_3^+. Increased dissociation of bromine containing species may explain the increase in bromine signal intensity observed in going from 0.6 Torr to 1.4 Torr, although the effect of changing atomization rate (both sputter and thermal) as a function of pressure must also be considered. The decrease in bromine signal intensity at 1.6 Torr can be attributed to a decrease in sampling efficiency that arises from ion scattering and collisional neutralization common at higher pressures.[29,30]

Finally, the influence of power on bromine signal intensity was evaluated at 0.8 Torr argon. A plot of signal intensity as a function of power, Figure 6.5, shows that $^{79}Br^+$ increases monotonously with increasing operating power. This is not surprising because an increase in operating power enhances both the sputter rate and ionization efficiency, resulting in more intense ion signals.[31,32] However, at 140 W, the bromine peaks show a strikingly disproportionate increase as compared to other peaks resulting from the plastic sample, which is mirrored in the Br^+/C^+ profile illustrated in Figure 6.5 as well. It should also be mentioned that the bromine signal fluctuated dramatically and would not reach a steady-state value. The sample was slightly deformed and was later examined using SEM.

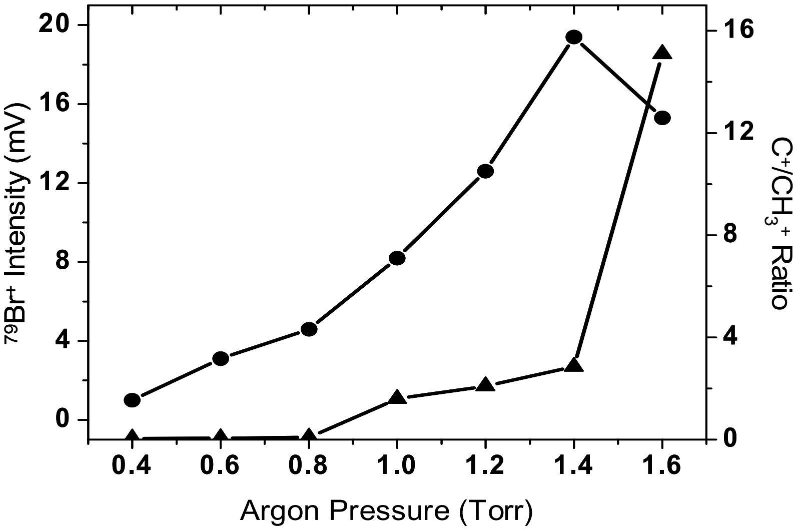

Figure 6.4. Effect of discharge pressure on intensities of $^{79}Br^+$ signal (●) and the ration of C^+/CH_3^+ signals (▲) at 100 W operating power.

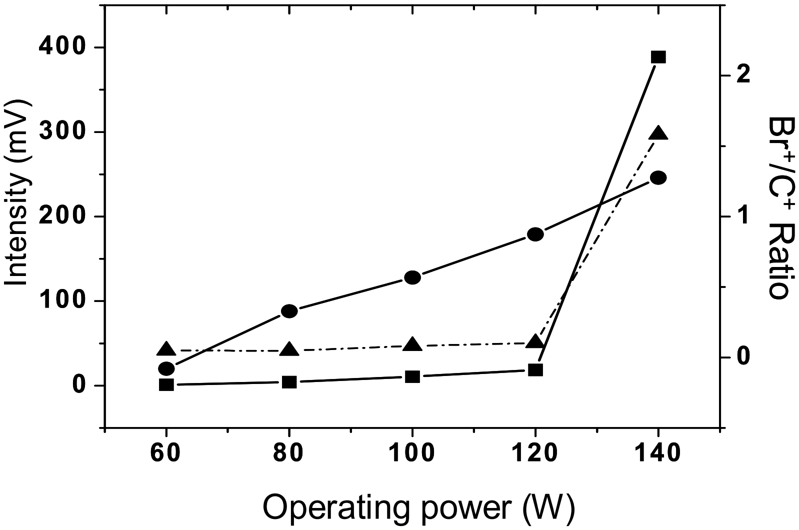

Figure 6.5. Effect of operating power on intensities of $^{79}Br^+$ signal (■) and $^{12}C^+$ signal (●), and the ratio of Br^+/C^+ signals (▲) at 0.8 Torr discharge pressure.

The SEM micrograph (Figure 6.3 B) reveals the surface topography of this sample is quite different from the sputtered sample surface (Figure 6.3 A). The classic cones and spires that are produced during the sputtering event are replaced with smooth microbead-like structures – the apparent result of melting and re-solidification of the polymer. It is obvious sample overheating can initiate thermal desorption, which we believe explains the sharp increase in $^{79}Br^+$ intensity.

Operating powers higher than 140 W caused almost instantaneous sample melting and would not produce meaningful mass spectra. Although elevated operating power is appealing because of the intense signals it provides, it will almost certainly cause sample overheating as well, thus initiating an uncontrolled thermal atomization process. This is of concern because thermal desorption inevitably leads to fluctuations in signal intensity, especially for volatile elements such as bromine, rendering quantitative analysis impractical. For this reason it was determined the atomization mechanism deserved further investigation.

6.3.2. Evaluation of Atomization Mechanisms

To better understand the atomization mechanism, temporal profiles of bromine signal intensities from ABS-silver compacted samples doped with TBBPA were compared with those from ABS-silver compacted samples doped with KBr. These samples were prepared to yield the same bromine concentration (8% as elemental Br) in both. Although thermal desorption and sputtering can account for bromine atomization in both samples, the extremely low volatility of KBr (especially compared with TBBPA) provides an ideal benchmark by which to compare and contrast the two mechanisms. Under the same glow discharge conditions, it is reasonable to assume the same ionization efficiency for bromine from these two sample types. Therefore, the bromine intensities and temporal profiles can be directly related to atomization processes and the comparison affords the insights to atomization mechanisms.

The experiments were carried out under 0.7 Torr argon, 80 W rf power, and 25% duty cycle. The compacted samples generated much more intense and expansive plasmas than the bulk plastic samples. Correspondingly, the optimum sampling distance for bromine was found farther from the cathode, at about 10 mm. A typical mass spectrum acquired from a compacted sample is shown in Figure 6.6. Significant improvements in both overall ion signal intensity and bromine signal intensity can be seen. The deviation in bromine isotope ratio from natural abundances is caused by the intense $^{80}Ar_2^+$. Silver peaks are identifiable at 107 and 109 amu.

The temporal responses of $^{79}Br^+$ was monitored over 60 min yielding the profiles plotted in Figure 6.7. Distinct temporal variations can be seen for the two sample types. For the KBr sample, $^{79}Br^+$ signal reached a steady value after 15 minutes of discharge conditioning. From 15 to 60 min, it showed excellent long-term stability (4.3% relative standard deviation). The TBBPA compacted sample, on the other hand, showed dramatic variations in the $^{79}Br^+$ signal out to 30 minutes and never reached a steady state. Its initial intensity is very close to the KBr sample, which is not surprising since both samples are of the same bromine concentration and subject to the same glow discharge conditions. However, the bromine signal quickly underwent a dramatic increase, demonstrating the apparent contribution from thermal desorption as the sample temperature rises. The superposition of thermal desorption on top of sputtering results in a much higher Br^+ intensity compared to the KBr sample. We believe this comparison helps elucidate the atomization mechanisms at work for the ABS samples analyzed previously. The predominant bromine signal observed under elevated power is attributed to the additional thermal desorption of bromine. On the other hand, these results also imply sputtering is not a very efficient atomization mechanism for plastic materials.

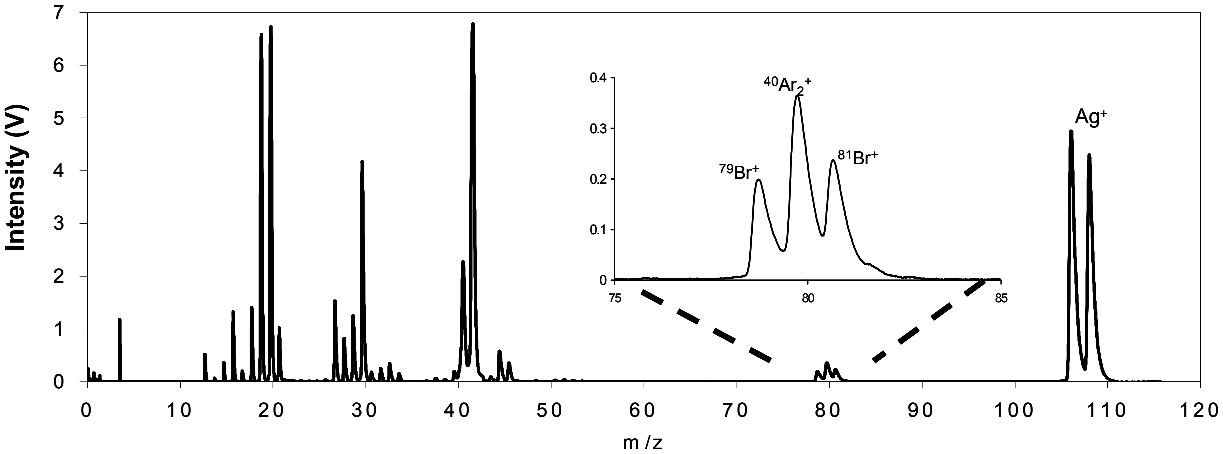

Figure 6.6. Mass spectrum of a compacted sample containing 8% TBBPA (operating power 80 W, 25% duty cycle, and argon pressure 0.7 Torr).

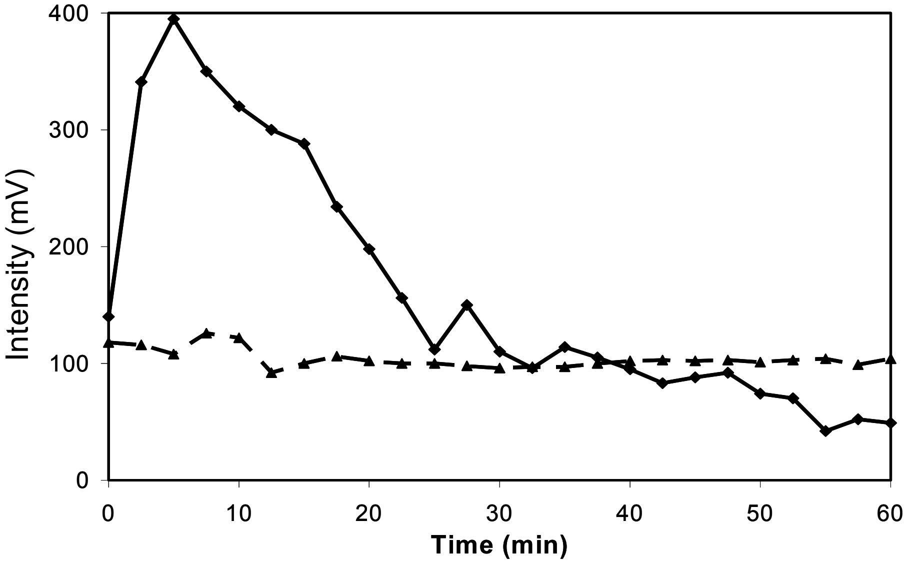

Figure 6.7. Temporal profiles of $^{79}Br^+$ signal from compacted samples containing TBBPA (solid line); and KBr (dashed line).

To further investigate sputter efficiency, weight loss experiments were performed on four different polymers: PTFE, PC, ASA, and ABS. The samples were continuously sputtered under 0.8 Torr, 80 W rf power, and 25% duty cycle for 10 hours and the weight loss measured. No indication of macroscopic thermal degradation was observed in the samples; therefore, weight loss through thermal desorption was assumed to be negligible, and the results can be interpreted as sputter weight loss. The resulting data appear in Table 6.2 along with the major properties of the polymers - sputter rates of PC, ASA, and ABS are extremely low while PTFE is significantly higher. Even with the density difference taken into account, the sputter rate of PTFE is still about 3 times higher than the other polymers.

Table 6.2. Sputter weight loss results and physical properties of PTFE, ASA, PC, and ABS polymers.

	PTFE		ASA		PC		ABS	
	Repre-sentative Value	Range	Repre-sentative Value	Range	Repre-sentative Value	Range	Repre-sentative Value	Range
Specific Gravity	2.17	2.14–2.20	1.07	1.05–1.09	1.20	1.08–1.32	1.18	1.16–1.21
Compressive Strength (Kg/cm^2)	100	80-120	1100	700-1500	850	700-1000	600	500-700
Notched Izod Impact Strength (J/m)	160	150 - 170	525	500 - 550	250	210 - 270	400	160 - 650
Volume Resistivity (Ω•cm)	>10^{18} *		$3\text{x}10^{16}$	$1\text{x}10^{16}$-$5\text{x}10^{16}$	$4.5\text{x}10^{16}$	$4\text{x}10^{16}$ - $5\text{x}10^{16}$	$3\text{x}10^{16}$	$1\text{x}10^{16}$ – $5\text{x}10^{16}$
Melting Temperatures (^{o}C)	327				265		175	
Glass Transition Temperatures (^{o}C)	-97				150			
Resistance to Heat (^{0}C)	260	251-270	82	71-93	120	111-129	94	88 - 99
Thermal Conductivity	6.0	5.0 - 6.0	6.3	4.5 - 8.0	4.8	4.3 - 5.3	6.3	4.5 - 8.0
Weight Loss Rate (mg/hour)	**0.41±0.09**		**0.13±0.02**		**0.11±0.02**		**0.06±0.01**	

The physical property data are taken from reference 41, except those labeled with * from reference 42.

Sputter rate strongly depends on the physical and chemical properties of the sputtered material.[33] The generally low sputter rates of polymers have been attributed to their electrical properties.[34] Electrical resistance causes great rf power losses and lowers the effective power coupled into the plasma; this results in a reduced sputter rate. However, this factor alone cannot completely explain the high sputter rate of PTFE as PTFE has the highest volume resistivity among the polymers tested. Here, we propose polymer molecular structures and intermolecular interactions play a more important role in determining the sputter rate of polymers.

Under the impact of ion bombardment, internal energy can be deposited and quickly randomized into the molecules at or near the sample surface.[35] When the energy localized on a specific bond exceeds the bond energy, bond cleavage will occur and subsequently trigger a series of physicochemical processes leading to molecular fragmentation.[36] Intermolecular interactions have to be overcome for the fragments to escape from the condensed phase. The polymer samples, especially those with low melting points, are labile to heat and, thus, the sample surfaces may be melted under the localized heating. The molecules in the liquid state have much higher flexibility and can absorb more energy into the translational mode, decreasing the portion of bombardment energy deposited into the internal modes. Furthermore, polymer molecules possess a huge number of degrees of freedom and are able to effectively dissipate the deposited internal energy, limiting the bond cleavage damage. Moreover, strong intermolecular interactions, such as N-H hydrogen bonding and strong benzene-benzene interactions in the ABS polymer, may hinder the emission of fragments, especially larger ones, further decreasing sputter rates. Note the strong intermolecular interactions also influence mechanical properties such as impact strength, i.e. the amount of energy required to break the polymer sample. Hence, there appears to be a correlation between mechanical strength and sputter rate. Based on this hypothesis, PTFE's sputter rate can be explained by its relatively higher melting point, molecular structural simplicity, and the lack of strong intermolecular interactions.

In GDMS, ion signal intensity is proportional to the sputtered atom density.[37] This density, in turn, is closely related to sputtering rate.[38] To verify the correlation for polymers, a mass spectrum of PTFE was acquired (Figure 6.8). The peaks therein can be interpreted as fragments of the PTFE polymer molecule and assigned as the general composition $C_mF_n^+$. Two distinct features can be readily observed as compared to the mass spectra of ABS. First, a larger variety of species is observed in the PTFE spectrum, covering an m/z range up to 193 amu. Second, the ion abundances are greater than in the ABS spectrum. The relatively greater ion production capability of PTFE, compared to other polymers, has been reported in several previous accounts.

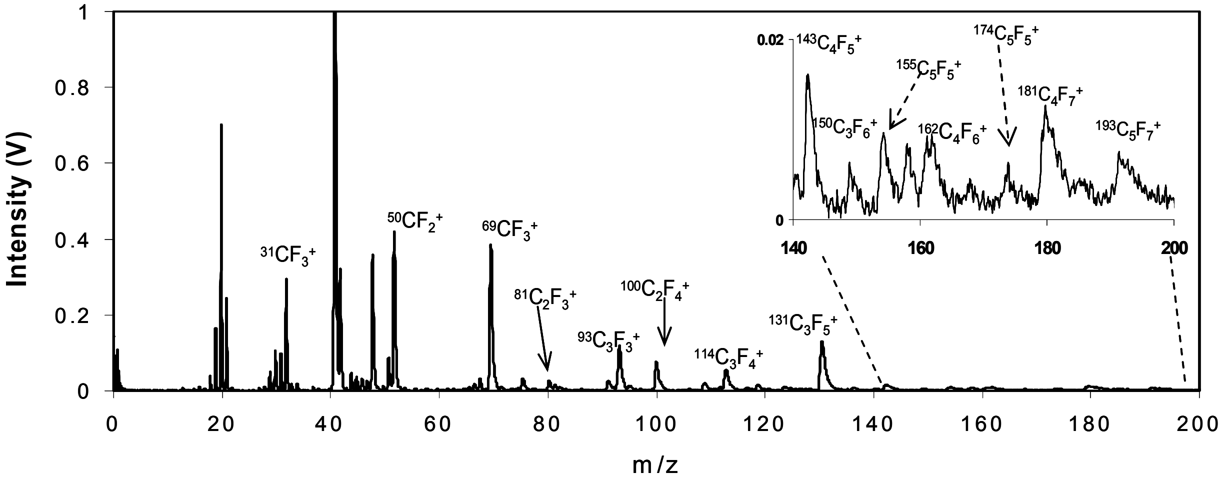

Figure 6.8. Mass spectrum of PTFE obtained from the bulk sample (operating power 80 W, 25% duty cycle, and argon pressure 0.7 Torr).

Coburn compared the glow discharge mass spectrum of a Teflon sample with the spectra of several hydrocarbon polymers such as polyethylene, polystyrene, and nylon.[11] Only the PTFE sample provided a mass spectrum with reasonable intensity, while the hydrocarbon polymer samples suffered from greatly reduced molecular species and broader hydrocarbon interferences from the residual gas. Marcus' group also examined several polymer samples, including PTFE-based plastics[14], bis-(phenoxy)phosphazene polymers[34], and low density polyethylene[17] (LDPE). Although the ion intensities can not be directly compared because of the different experimental conditions, an approximate comparison of the mass spectra therein, which was done by normalizing the total ion intensities of the sputtered species to the corresponding background argon ion intensity, reveals a significantly higher ion production by PTFE. Furthermore, this research group observed the sputtered ion beam current of the PTFE samples was as high as the metal analytes generated by that same source.[14] Here, we conclude the high ion production capability of PTFE can be directly correlated to its high sputter rate, relative to other plastic samples examined.

6.3.3. Quantification of Bromine in Compacted Samples

Quantitative analysis of bulk ABS plastic samples using GDMS faces several obstacles because of the inherent thermal labililty and low sputter yields of these materials. A simple and well-developed alternative approach is to compact the samples into a conductive host matrix as described above. This approach is aimed at increasing the electrical conductivity of the compacted sample.[39] As sample conductivity increases, the power losses in the sample decrease to yield an increase in sputter atomization and ionization efficiency. This increase should lead to more intense analyte signals, as have been observed in the atomization studies described above (Figure 6). At this point the applicability of this methodology for the quantitative determination of bromine was investigated.

Silver powder was selected as the host matrix because of its excellent electrical conductivity, high sputter rate, and absence of potential interferences with bromine. Besides improving sample conductivity, silver may serve a secondary role in facilitating bromine atom transport into the plasma because of its high sputter rate. An optimal mixture of the silver host and analyte, 18:1 silver to plastic powder ratio (mass/mass), was arrived at experimentally based on the following considerations: a) the compatibility of the mixture powders, b) the mechanical strength of the compacted sample, and c) the resultant intensity of the signal from bromine. As previously noted, compacted samples containing TBBPA were prone to overheating in the glow discharge; thereby, yielding poor signal stability. Although this problem could be overcome by decreasing the pulse power, the resultant increase in stability came at the cost of reduced signal intensity. It was determined overheating could be avoided while maintaining, or even increasing, signal intensity by the decreasing the pulse duty cycle. The lower duty cycle limits the heat generation and allows longer "power-off" period for the sample to cool while the instantaneous high power provides a short-lived, intense signal that can be monitored with time gated detection techniques. It was found that a 10% duty cycle provided excellent temporal stability at 80 W rf power and 0.7 Torr argon pressure. A plot of the signal intensity for $^{79}Br^+$ as a function of time obtained under these conditions is presented in Figure 6.9 A. Note both the required pre-burn time (15 min) and temporal variation thereafter (4.1% relative standard deviation) are almost the same as for the KBr sample (discussed above), indicating the effectiveness of this technique for moderating sample overheating effects.

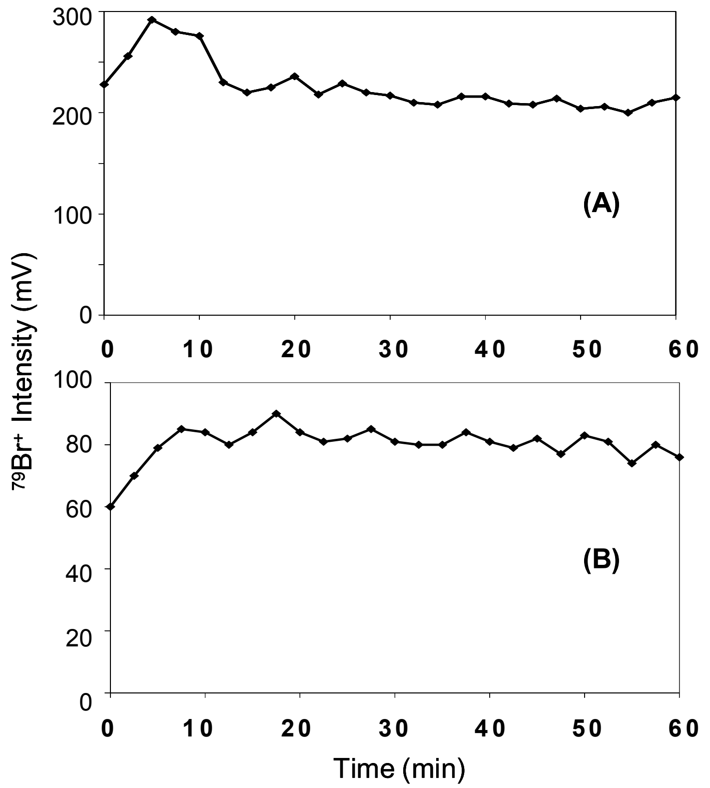

Figure 6.9. Temporal profiles of $^{79}Br^{+}$ signal from TBBPA compacted standards with (A) argon (operating power 80 W, 10% duty cycle, and argon pressure 0.7 Torr); and (B) helium (operating power 90 W, 10% duty cycle, and helium pressure 2.5 Torr).

Table 6.3. Quantitative analysis results of Samples Number 1-4 using rf GDMS.

Sample Number	Calculated Br Conc. (%)	Measured Average Br Conc. (%)		Relative Standard Deviation (%)		Relative Error (%)		Detection Limit (Br%)		Sensitivity mV/Br%	
		Ar [1]	He [2]	Ar	He	Ar	He	Ar	He	Ar	He
1	9.23	8.59	8.93	5.9	6.4	-6.9	-3.2	0.2	0.5	10.3	5.0
2	7.09	7.59	7.56	5.8	7.9	7.0	6.7				
3	4.87	4.97	4.80	5.6	5.8	2.0	-1.4				
4	13.04	12.35	12.59	2.3	4.1	-5.3	-3.4				

1. Results from argon discharge measurements; 2. Results from helium discharge measurements.

A calibration curve for bromine was constructed with the data collected from a series of TBBPA standards mixed with silver. The standards cover the typical concentration range of TBBPA in plastics (0-15% as elemental Br). Three replicate samples were measured for each concentration and the mean and standard deviation were calculated. The resultant calibration curve exhibited excellent linearity (m=10.3 mV/Br%, b=5.5 mV, R^2 =0.9968). The precision of the data was limited by the reproducibility of parameters such as contaminant gas concentration, sampling distances, and sample preparation.

The calibration curve was used in the quantification of bromine in Sample Numbers 1-4. The results of three replicate measurements are presented in Table 6.3. The relative error of the measured averages versus “true” bromine concentration, calculated from the product formula provided by the manufacturer, is on the order of 7% with an average relative standard deviation of 4.9%. This level of accuracy and precision was acceptable for direct solid analysis for the determination of bromine in polymers. It should be noted the ToF used in these studies was not designed for quantitative work and suffers from poor sensitivity; the 3σ detection limit estimated from the background noise is about 0.2% (as elemental bromine).

As mentioned earlier, Penning ionization by metastable argon atoms, which accounts for approximately 40-80% of the total ionization of sputtered species in the steady state argon glow discharges,[40] is not possible for bromine ionization because the ionization potential of bromine atoms exceeds the energy of the metastable argon atoms. On the other hand, metastable helium atoms, with potential energy of 19.82 eV and 20.61 eV, can ionize bromine effectively through the Penning process. As a result, a helium glow discharge should yield greater ionization efficiency than the argon glow discharge for the determination of bromine.

The same series of samples were also analyzed using a helium glow discharge. The glow discharge in these experiments operated at 2.5 Torr helium and 90 W rf power with a 10% duty cycle. A typical mass spectrum generated from the TBBPA standard is presented in Figure 6.10. Compared to the spectrum collected using the argon discharge gas, the silver signal intensity is attenuated by a factor of approximately 50. This dramatic loss can be largely attributed to the lower sputter efficiency of helium compared with argon, a result of its lower mass. However, the bromine ion intensities were only reduced by about ½, suggesting an increase in the ionization efficiency for bromine as expected. The signals for $^{79}Br^+$ and $^{81}Br^+$ were well-resolved and exhibited natural isotope ratios owing to the absence of interferences from Ar_2^+, another advantage of shifting to helium. The temporal response of $^{79}Br^+$ shown in Figure 9 B suggests a 10 min pre-burn period is required. After this pre-burn, the temporal stability of the signal is comparable to that obtained for the argon glow discharge.

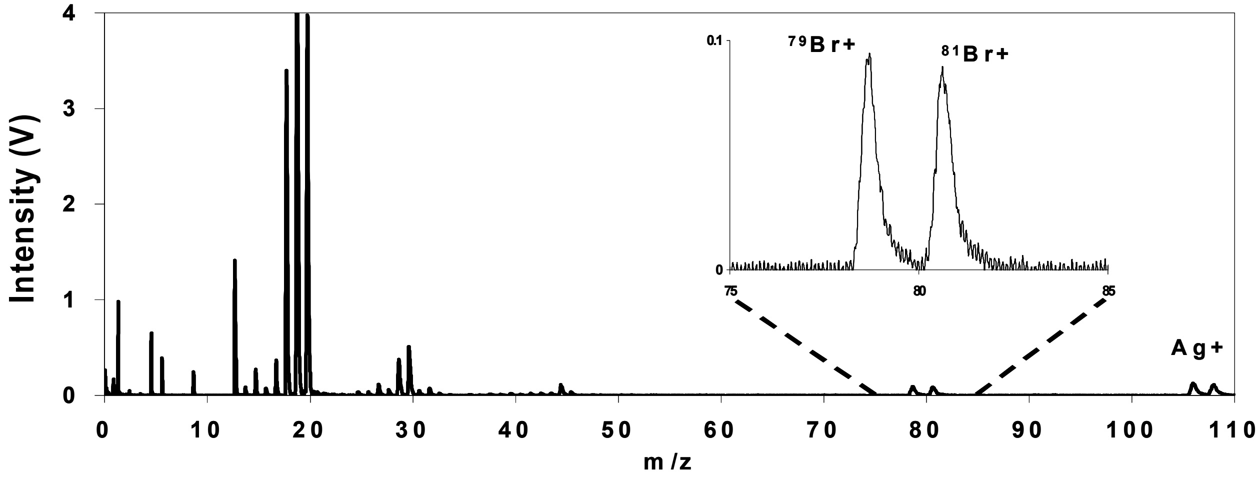

Figure 6.10. Mass spectrum of TBBPA standard with helium as a discharge gas (operating power 90 W, 10% duty cycle, and argon pressure 2.5 Torr).

Following a procedure identical to that described above for the argon glow discharge, a calibration curve was constructed for Br in polymer samples (m=5.0 mV/Br%, b=3.5 mV, R^2 =0.9981). The concentration of Br in Sample Numbers 1-4 was again determined by use of this calibration curve (see Table 6.3). Determinations obtained with the helium glow discharge were comparable to those obtained with the argon glow discharge in terms of both precision and accuracy. Unfortunately, the helium glow discharge provided poorer detection limits than the argon glow discharge. The impact on detection limits clearly illustrates an enhancement in ionization efficiency is not sufficient to compensate for the loss in sputter efficiency resulting from switching discharge gas.

6.4. Conclusions

Direct analysis of bulk plastic samples using rf-GDMS produced both atomic and molecular species, allowing both elemental identification and molecular characterization. However, quantitative results for these species cannot be achieved because they exhibited low signal intensities. The poor ion production capability has been correlated to the reduced sputter rate for some polymers, attributed largely to the inherent physical and chemical properties.

Quantitative analysis was accomplished by compacting powdered plastic samples in a silver host matrix. This method involves minimal sample preparation. The rapid sample introduction and short plasma stabilization time provide an analysis speed of about 30 min per sample. Pulsed operation can effectively alleviate sample overheating without the use of external cooling devices, to provide analyte signal with excellent long-term stability (4% RSD). Quantitative results from compacted samples in argon glow discharges exhibited accuracy of approximately 7% and precision of approximately 8%. This method shows promise as an alternative to the laborious dissolution procedures for routine elemental analysis of plastic samples. Further experiments will focus on the optimization of discharge parameters to improve sensitivity.

6.5. References

(1) Bikales, N.M., Ed. *Characterization of Polymers;* John Wiley and Sons: New York, 1971.
(2) Clark, D.T. *CRC Crit. Rev. Solid State Mater. Sci.* **1978**, *8*, 1-52.

(3) *Chromatographic characterization of polymers*; Provder, T., Barth H.G., Urban M.W, Eds.; Advances in Chemistry Series 247; American Chemical Society: Washington, DC, 1995.
(4) Van Vaeck, L.; Adriaens, A.; Gijbels R. *Mass Spectrom. Rev*. **1999**, *18*, 1-47.
(5) Fairman, B.; Hinds M. W.; Nelms, S. M.; Penny, D. M.; Goodall, P. *J. Anal. At. Spectrom.* **2001**, *16*, 1446-1469.
(6) Marshall, J.; Franks, J.; Abell, I.; Tye, C. *J. Anal. At. Spectrom.* **1991**, *6*, 145-150.
(7) Leis, F.; Bauer, H. E.; Prodan, L.; Niemax, K. *Spectrochim. Acta* **2001**, *56B*, 27-35.
(8) Harrison, W. W.; Barshick, C. M.; Klingler, J. A.; Ratcliff, P. H.; Mei, Y. *Anal. Chem*. **1990**, *62*, 943A-949A.
(9) King, F. L.; Harrison, W. W. *Mass Spectrom. Rev.* **1990**, *9*, 285-317.
(10) Harrison, W. W.; Hess, K. R.; Marcus, R. K.; King, F. L. *Anal. Chem.* **1986**, *58*, 341A-350A.
(11) Coburn, J. W.; Eckstein, E. W.; Kay, E. *J. Vac. Sci. Technol.* **1975**, *12*, 151-154.
(12) Marcus, R. K. *J. Anal. At. Spectrom.* **1996,** *11*, 821-828.
(13) Gibeau, T. E.; Marcus, R. K. *J. Appl. Polym. Sci.* **2000,** *76*, 954-961.
(14) Shick, C. R., Jr.; Depalma, P. A.; Marcus, R. K. *Anal. Chem.* **1996,** *68*, 2113-2121.
(15) Marcus, R. K. *J. Anal. At. Spectrom.* **2000,** *15*, 1271-1277.
(16) Schelles, W.; Van Grieken R. *Anal. Chem.* **1997**, *69*, 2931-2934.
(17) Gibeau, T. E.; Hartenstein, M. L.; Marcus, R. K. *J. Am. Soc. Mass Spectrom.* **1997,** *8*, 1214-1219.
(18) Harrison, W. W.; Yang, C.; Oxley, E. *Anal. Chem*. **2001,** *73***,** 480A-487A.
(19) Klingler, J. A.; Barshick, C. M.; Harrison, W. W. *Anal. Chem*. **1991,** *63*, 2571-2576.
(20) Lewis, C. L.; Oxley, E. S.; Pan, C. K.; Steiner, R. E.; King, F. L. *Anal. Chem*. **1999**, *71*, 230-234.
(21) Steiner, R. E.; Lewis, C. L.; King, F. L. *Anal. Chem*. **1997**, *69*, 1715-1721.
(22) King, F. L.; Harrison, W. W. *Int. J. Mass Spectrom. Ion Proc.* **1989**, *89*, 171-185.
(23) King, F. L.; Pan C. *Anal. Chem*. **1993,** *65*, 735-739.
(24) Lazik, C.; Marcus, R. K. *Spectrochim. Acta* **1993**, *48B*, 1673-1689.
(25) Gibeau, T. E.; Marcus, R. K. *J. Anal. At. Spectrom.* **1998**, *13*, 1303-1311.
(26) King, F. L.; McCormack, A. L.; Harrison, W. W. *J. Anal. At. Spectrom.* **1988**, *3*, 883-886.
(27) Duckworth, D. C.; Marcus, R. K. *J. Anal. At. Spectrom*. **1992**, *7*, 711-715.
(28) Guzowski, J. P., Jr.; Broekaert, J.A.C.; Ray, S. J.; Hieftje, G. M. *J. Anal. At. Spectrom.* **1999**, *14*, 1121-1127.
(29) McLuckey, S. A.; Glish, G. L.; Asano, K. G.; Grant, B. C. *Anal. Chem.* **1988**, *60*, 2220-2227.
(30) Hang, W.; Harrison, W. W. *Anal. Chem*. **1997**, *69*, 4957-4963.
(31) Parker, M.; Marcus, R. K. *Spectrochim. Acta* **1995**, *50B,* 617-638.

(32) Shick, C. R., Jr.; Raith, A.; Marcus, R. K. *J. Anal. At. Spectrom*. **1994**, *9,* 1045-1051.
(33) Carter, G.; Colligon, J. S. *Ion Bombardment of Solids;* Heinemann Educational Books: London, 1968.
(34) Parker, M.; Hartenstein, M. L.; Marcus, R. K. *Anal. Chem*. **1996**, *68*, 4213-4220.
(35) Garrison, B. J. *J. Am. Chem. Soc*. **1980**, *102*, 6553-6555.
(36) Magee, C. W. *Int. J. Mass Spectrom. Ion Phys.* **1983**, *49*, 211-221.
(37) Loving, T. J.; Harrison, W. W. *Anal. Chem*. **1983**, 55, 1523-1526.
(38) Loving, T. J.; Harrison, W. W. *Anal. Chem*. **1983**, *55*, 1526-1530.
(39) Dogan, M.; Laqua, K.; Massman, H. *Spectrochim. Acta* **1972**, *26B*, 631-649.
(40) Smith, R. L.; Serxner, D.; Hess, K. R. *Anal. Chem*. **1989**, *61*, 1103-1108.
(41) The International Technical Information Institute. U*ser's Practical Selection Handbook for Optimum Plastics, Rubbers, and Adhesives*; Tokyo,1976.
(42) Harper, C.A., Ed. *Handbooks of Plastics and Elastomers*; McGraw-Hill: New York, 1975.

Lei Li

EDUCATION

2000 – Present, West Virginia University, Morgantown, WV.

Ph. D. in Analytical Chemistry (Expected July 2004 with 4.0/4.0 GPA).

Dissertation: Molecular Speciation Using Pulsed Glow Discharge Mass Spectrometry

Advisor: Dr. Fred L. King

1989 – 1993, Chongqing University, Chongqing, China.

B. S. in Chemistry, graduated in July 1993 with 3.6/4.0 GPA.

PROFESSIONAL EXPERIENCE

2003 – Present, Graduate Intern, Oak Ridge National Laboratory.

- Investigated fundamental processes related to collision-induced dissociation (CID) in ion trap mass spectrometry in support of US DoE's Office of Basic Energy Sciences.
- Carried out QA/QC and acceptance testing of an inductively coupled plasma time-of-flight mass spectrometer (ICP-ToF-MS) in support of US DoE's Office of Nuclear Nonproliferation Engineering & Research.
- Designed and developed a glow discharge ion source and an octapole ion guide system.

2001 – 2002, Research Assistant, West Virginia University.

- Developed and characterized a pulsed glow discharge ion source using mass spectrometry and various spectroscopic techniques in support of DoE's Office of Basic Energy Sciences.
- Conceived and implemented a new approach to chemical speciation using pulsed glow discharge mass spectrometry (GDMS) for GC effluents.
- Developed a novel technique for quantitative analysis of trace elements in plastic samples using GDMS in collaboration with GE Plastics.
- Operated and maintained a Fourier transform infrared (FT-IR) microscope system.

2000 – 2001, Teaching Assistant, West Virginia University.

- Taught undergraduate General Chemistry and Quantitative Analytical Chemistry lab.

1993 – 1999, Environmental Analyst, Environmental Protection Bureau, Chongqing, China.

- Managed assessment of environmental impact for industrial developments.
- Prepared and analyzed environmental aqueous samples and presented analysis reports.

ACTIVITIES AND HONORS

Awards:

- John H. Trotter Graduate Scholarship in Chemistry, WVU, 2002-2003.
- Bennet Fellowship, Eberly College of Art and Science, WVU, 2001-2002.
- Outstanding Teaching Assistant, Department of Chemistry, WVU, 2000.
- Excellent Employee Award, Chongqing EPB, 1995, 1997, 1998.

Memberships:

- Society for Applied Spectroscopy, 2002, 2003.
- American Chemical Society, 2003.

PUBLICATIONS

- **Lei Li**, Christopher M. Barshick, John T. Millay, Annette V. Welty, Fred L. King; Determination of Bromine in Flame Retardant Plastics Using Pulsed Glow Discharge Mass Spectrometry. ***Anal. Chem***. 75, 3953-3961 (2003).
- **Lei Li,** J. T. Millay, J. P. Turner, and F.L. King; Millisecond Pulsed Radio Frequency Glow Discharge Time of Flight Mass Spectrometry: Temporal and Spatial Variations in Molecular Energetics for $W(CO)_6$. ***J. Am. Soc. Mass Spectrom.*** 15, 87-102 (2004).

- C. Lewis, **Lei Li**, J. Millay, S. Downey, J. Warrick, and Fred L. King; Temporal Emission Characteristics of Millisecond Pulsed Radiofrequency and Direct Current Glow Discharges. ***J. Anal. At. Spectrom.*** 18, 1-7 (2003).
- **Lei Li,** J. T. Millay, J. P. Turner, and F.L. King; Millisecond Pulsed Radio Frequency Glow Discharge Time of Flight Mass Spectrometry: Chemical Speciation of Organic Molecules. ***J. Am. Soc. Mass Spectrom***. (Submitted).

PRESENTATIONS

- **Lei Li**, John T. Millay, John P. Turner, Fred L. King. Chemical Speciation of Organic and Organometallic Compounds Using Pulsed Glow Discharge Time of Flight Mass Spectrometry. The 52nd ASMS Conference on Mass Spectrometry and Allied Topics, Nashville, TN. May 25, 2004.
- **Lei Li**, Jennifer Robertson, Na Zhang, and F.L. King; Spectroscopic Investigation into Nitrogen Containing Glow Discharge Plasma. The 30th Federation of Analytical Chemistry Spectroscopy Societies (FACSS), Fort Lauderdale, FL, October 20, 2003.
- **Lei Li**, Chris Barshick, Tom Millay, and F.L. King; Analysis of Bromine in Flame Retardant Plastics Using Pulsed Glow Discharge Mass Spectrometry. The 30th Federation of Analytical Chemistry Spectroscopy Societies (FACSS), Fort Lauderdale, FL, October 20, 2003.
- **Lei Li**, J. T. Millay, and F.L. King; Temporal and Spatial Ionization of Molecular Species in Millisecond Pulsed Glow Discharge Time-of-Flight Mass Spectrometry. The 29th Federation of Analytical Chemistry Spectroscopy Societies (FACSS), Providence, RI, October 14, 2002.
- **Lei Li**, J. T. Millay, Glen Jackson, J. P. Turner, and F.L. King; Energy Transfer Processes in Pulsed Glow Discharge Mass Spectrometry of Molecular Species. Winter Plasma Conference 2002, Scottsdale, AZ, January 10, 2002.
- **Lei Li**, J. T. Millay, and F.L. King; Molecular Energetics in Pulsed Glow Discharge Plasmas. The 28th Federation of Analytical Chemistry Spectroscopy Societies (FACSS), Detroit, MI, October 12, 2001.

- **Chris Barshick**, J. T. Millay, Lei Li, and F.L. King; Elemental Quantification of Flame Retardant Polymers Using Glow Discharge ToF Mass Spectrometry. The 29th Federation of Analytical Chemistry Spectroscopy Socities (FACSS), Providence, RI, October 13, 2002.
- **Fred King**, Lei Li, J. T. Millay, M. Moser, V. Majidi, and C. Lewis; Ionization and Excitation in a ms Pulsed Glow Discharge Plasma: Implications for Atomic and Molecular Determinations. The 28th Federation of Analytical Chemistry Spectroscopy Socities (FACSS), Detroit, MI, October 8, 2001.
- **Na Zhang**, Jennifer Robertson, Lei Li, and F.L. King; Real-Time Chemical Speciation of Selenium Using Gas Chromatography Coupled with Pulsed Glow Discharge Time-of-Flight Mass Spectrometry. The 30th Federation of Analytical Chemistry Spectroscopy Societies (FACSS), Fort Lauderdale, FL, October 19, 2003.
- **Jennifer Robertson**, Lei Li, Na Zhang, and F.L. King; Investigation of Ionization in a Pulsed Glow Discharge Plasma Using Optical Spectroscopy and Electrostatic Probes. The 30th Federation of Analytical Chemistry Spectroscopy Societies (FACSS), Fort Lauderdale, FL, October 19, 2003.